Australian Government

Bureau of Meteorology

The Centre for Australian Weather and Climate Research

A partnership between CSIRO and the Bureau of Meteorology

CSIRO

Proceedings of the Australian Wind Waves Research Science Symposium, 19-20 May 2010, Gold Coast, Queensland, Australia

CAWCR Technical Report No. 029

Keith A Day. (editor)

July 2010

www.cawcr.gov.au

Proceedings of the Australian Wind Waves Research Science Symposium, 19-20 May 2010, Gold Coast, Queensland, Australia

Keith A Day. (Editor)

Centre for Australian Weather and Climate Research,
GPO Box 1289, Melbourne, VIC 3001, Australia

CAWCR Technical Report No. 029

August 2010

ISSN: 1835-9884

National Library of Australia Cataloguing-in-Publication entry

Author: Australian Wind Waves Research Science Symposium (2010 : Gold Coast, Queensland)

Title: Proceedings of the Australian Wind Waves Research Science Symposium, 19-20 May 2010, Gold Coast, Queensland, Australia / editor Keith. A. Day.

ISBN: 978-1-921605-94-9 (PDF)

Series: CAWCR technical report; No. 29

Notes: Includes index.

Subjects: Meteorology--Research--Congresses. Climatic changes--Research--Congresses.

Other Authors/Contributors: Diana Greenslade, Mark Hemer, Graham Symonds and Peter Craig

Dewey Number: 551.50994

Enquiries should be addressed to:

Keith Day
Centre for Australian Weather and Climate Research:
A partnership between the Bureau of Meteorology and CSIRO
GPO Box 1289
Melbourne VIC 3001
Australia

k.day@bom.gov.au
Phone: 61 3 9669 8311
Fax: 61 3 9669 4660

Copyright and Disclaimer

Contents

FOREWORD

In May 2010, CAWCR hosted the inaugural Australian Wind Waves Research Science Symposium over two days on the Gold Coast, Queensland. The symposium aimed to develop an awareness of related research amongst Australian waves scientists, to unite waves research across sites and organisations, to discuss future directions and current gaps in the Australian waves research, and to provide a forum for the development of possible collaborative activities.

The symposium drew approximately 30 invited Australian public sector researchers, and two international invitees, working on various aspects of surface wave dynamics. Participants came from all over Australia and from a range of disciplines such as Meteorology, Oceanography and Coastal Engineering. Three keynote presentations were given by international leaders in waves research: Professor Rob Holman from Oregon State University; Dr Ralf Weisse from the Institute of Coastal Research, GKSS, Germany; and Professor Ian Young from Swinburne University in Melbourne. The meeting was structured into six sessions as follows:

- Nearshore observations and prediction
- Future projections of wave climate
- Wave climate variability and coastal change
- Wave climatology and historical variability
- Modelling and Forecasting
- Physics and Observations

Four open discussion sessions were held over the two days focussing on research gaps and possible future directions. A summary of the outcomes of these discussions can be found on page 3 of these Proceedings.

The organisers of the symposium would like to thank all the participants for making the symposium a success. Financial support for the symposium was provided through the CSIRO Marine and Atmospheric Research Capability Development Fund, along with additional support from the Wealth for Oceans flagship, the Climate Adaptation flagship and the Bureau of Meteorology. Peter Craig is thanked for his valuable role in moderating the discussion sessions and Val Jemmeson is also thanked for providing excellent administrative support.

The Organising Committee
Diana Greenslade, Mark Hemer, Graham Symonds

Summary of the Australian Wind Waves Research Science Symposium

19-20 May 2010 Gold Coast

Diana Greenslade[1], Mark Hemer[2], Graham Symonds[3] and Peter Craig[2]

[1] *Centre for Australian Weather and Climate Research, GPO Box 1289, Melbourne, VIC 3001, Australia*

[2] *Centre for Australian Weather and Climate Research, GPO Box 1538, Hobart, TAS 7001, Australia*

[3] *Centre for Australian Weather and Climate Research, Underwood Ave, Floreat, WA 6014, Australia*

Introduction

This short paper is a summary of the discussion sessions at the Australian Wind Waves Research Science Symposium, drawing to some extent as well on the presentations and the questions and answers that followed them. While the presentations described the current state of wave research in Australia, at least in public-sector organisations, the discussion aimed to identify both research gaps and possible directions for the future.

For comparison, one of the invited keynote speakers, Prof Rob Holman of Oregon State University, reported on a planning exercise in the US in which the questions addressed were:

a) What are we trying to accomplish with wave research?
b) What are the applications?
c) What is the current capability?
d) What are the existing limitations?

He reported a divergence of opinions, particularly on item (d). However, it is worth noting that the outcome of the US meeting was a recommendation for a long-term observation site, collecting data in which trends could be identified, and against which models and predictions could be tested. The Gold Coast symposium was less formalised, but provides a window at least on questions (a), (c) and (d) as applied to the Australian scene.

The wave-research community in Australia is relatively small, especially given Australia's dependence on its coast. The list of research challenges developed in the symposium's discussion sessions is too long for the current community to address, and would be too expensive to implement within present budgets. This document does not attempt either to prioritise the research imperatives, or to identify funding opportunities. The following sections discuss the research gaps in their context, and the final section, Section 5, presents a summary list of the research questions. Appendix A is a list of participants, and Appendix B is a compilation of the abstracts for the talks.

This was the first gathering of Australian wave researchers for many years. Wave-research projects tend to be locally motivated and implemented, often because they have a coastal focus. There appears to be a clear need for continued communication across the community. Further, Australian coastal researchers, in particular, need to ensure that they remain connected with the international community, even though present funding mechanism do not necessarily encourage international projects and partnerships.

Observations

Remote sensing

At global scales, satellite altimeters provide data on surface-wave variability and trends, but these have limitations and there are data-analysis challenges. With careful analysis, the combined satellite-altimeter dataset can provide several decades of observations but measurements at this time are restricted to significant wave height and to some extent wave period. These provide no information on wave direction which is critical for coastal applications. Directional wave spectra can be extracted from satellite-derived SAR data, but there were no talks or discussion relating to this data stream.

Shore-based radars, both X-band and VHF, are research tools for measuring spatial fields of waves and currents out to a few km offshore. UHF radars (WERA) provide fields of waves and currents to 100 km range, and a number of WERA systems have been deployed, or are in planning stage, on the Australian coast as part of the Integrated Marine Observing System (IMOS) ACORN facility. Two presentations made use of the WERA data, but these data seem largely underutilised at this time.

Shore-based video cameras (Argus systems) are proven technology for measuring waves and beach structure on individual beaches. For both radar and video, inversion calculations give estimates of the (changing) bathymetry. Time-series from radar and video are supplemented by beach surveys and airborne (manned and unmanned) imagery.

In situ

Australia's coastal buoy network is variable in its density around the coast and there are very few directional wave buoys. The network is operated by a number of different state and federal agencies, including the NSW State Government Manly Hydraulics Lab, the WA Department of Transport and the Bureau of Meteorology. Some of these buoys are approaching 20 years of continuous deployment and thus provide a valuable dataset for climate-related studies, local analysis and model verification. In discussion, the point was raised that the funding to support this network of buoys has been under threat for several years.

Proxies

Geological coastal profiles were presented as a method to describe historical wave climate on longer time scales over which instrumental wave records are unavailable. These can be combined with Mean Sea-Level Pressure (MSLP) gradient derived proxies for wave direction.

Data gaps

For coastal management, critical parameters are the shoreline position and the width of the beach. For safe recreational and maritime activity within the surf zone, knowledge of the waves and currents is required.

Australia has few locations of sustained beach measurements, and no consistent measurement approaches. Neither is there a widely available repository for data. There is a clear need for a national set of coastal observatories, following the IMOS model, using standard measurement techniques and supplying data to a centralised data-base. The observatories could, for example, be based on video installations and in-water wave sensors deployed outside the surf zone. They would be located on beaches selected for their representativeness and sensitivity. They would preferably also be inshore of other measurement installations, such as IMOS reference stations, coastal radars or directional waverider buoys, which would provide offshore conditions as context for the shore-based systems. The standard suite of inshore measurements would be supplemented by occasional or regular surveys done by local operational agencies and researchers.

The data would be used to identify variability and trends in the nearshore wave and current regimes, and in the beach structure. Importantly, they would be used to inform and verify models of nearshore and beach process that can be used for application to other beaches, and for prediction.

Offshore wave data are being used for development of source terms in spectral wave models (i.e. wind growth and whitecapping dissipation terms). There was considerable discussion on the need to consider waves in the coupled atmosphere-ocean system. One talk, aiming to quantify the sea-state-dependent surface momentum flux illustrated a lack of data to support this research. Similar data gaps occur in quantifying sea-state dependent mass and heat fluxes. The IMOS Southern Ocean Flux Station mooring has the potential to be developed to support research in this field with the addition of suitable wave measurements at the site. There is some development of wave measurements from the Motion Reference Unit on the IMOS moorings and this has shown some promise, but these require rigorous testing against recognised instrumentation.

As mentioned above, the coastal wave-buoy network is adequate in some areas, such as the NSW coast, but there are considerable gaps in the network, particularly for Victoria, the Northern Territory and the east coast of Tasmania.

A further data gap is in the representation of the coastal bathymetry at high resolution (10's of m). At present, Geoscience Australia maintains a 250 m resolution gridded bathymetry for the Australian region. In some nearshore regions, the bathymetric information does exist at higher resolution and there are a number of applications that would benefit from access to these data.

Wave modelling

Global or basin scale

Australian researchers are using a variety of wave models. At large scales, WAVEWATCH III™ (WW3) is favoured, implemented for operational forecasting at the Bureau of Meteorology (as of June 2010), as well as decadal analysis and climate projections. The possibility of a "community wave model" version of WW3 was raised, potentially to be hosted and maintained by an organisation such as the Bureau. A community model would require dedicated support, but would benefit the community as a reference point for model support and advice on implementation.

Winds for forcing for wave models are sourced from a number of different agencies. It was acknowledged that a knowledge of the errors and biases in surface winds is relevant for wave modelling at all scales.

Regional

At regional scales (10's of kms), SWAN (from Delft) is the most commonly used wave model, but there are one or two applications of MIKE21 (from DHI). WW3 may eventually also prove to be effective at this scale as more shallow water physics are incorporated. In coastal applications, the input data are a more serious problem than the model physics. Offshore boundary conditions are derived from buoys and/or global models, which are not always in exact agreement. The biggest issue is bathymetry. There are data from various high-resolution (10's of metres) hydrographic surveys, LIDAR and/or LADS surveys and hyperspectral flights, but the coverage is sparse, and there is no unified central database. Such surveys do not replace the need for local measurement (see above) within the surf zone, where the bathymetry may change on time scales of hours.

Nearshore

Within the very nearshore region (10's of metres), a number of models such as XBeach, Delft3d (both from Delft), and the NearCOM package (University of Delaware) were all mentioned. The community in general seemed satisfied with these nearshore models. There is active research on wave-current interactions in the nearshore. One application is low-frequency motion driven inside lagoons by waves breaking on reefs. Another is longshore currents driven by waves breaking on a bar. XBeach is still under development and has shown promise, but like other existing nearshore models, it still presents some challenges to modellers in terms of the domain specification and parameter choices. Furthermore, it is only two-dimensional. Three-dimensional models, such as the coupling of SWAN and ROMS, will be more challenging, particularly for verification of model behaviour.

XBeach, Delft3d and NearCOM include morphodynamics. Morphodynamics are often the motivation for coastal model applications, but this component of the models is still very empirical. There is currently little experience with implementation, calibration, verification and correction of such models within Australia. This, and the accompanying data collection, is likely to become a compelling research activity. Carefully designed field programs are likely to advance the process representations in morphodynamic models.

There were no talks on phase-resolving models – that is, models that solve some form of the hydrodynamic equations, rather than invoking the spectral approximation. This appears to be a gap in Australian research. However, there were presentations on specific models, for example, a Lagrangian model of the swash zone, and another using smooth-particle hydrodynamics (SPH), a Lagrangian approach developed in computational fluid dynamics. SPH, in particular, is very different from conventional wave modelling. There appears to be a real research opportunity to use such a model in comparison with more conventional models, given that the former can represent processes such as wave breaking or interactions with structures, which must be parameterised in lower resolution models. One specific process that could benefit from the use of this approach is the role of the wind-water interaction in the surf zone.

Another new research area for nearshore wave models is the incorporation of data assimilation. In atmospheric, ocean or larger scale wave models, data assimilation is used to correct, or improve the initial values of model state variables. In the emerging approaches in coastal wave modelling, the assimilation of radar or video information, for example, can be used to deduce and correct the bathymetry.

Wave Climate

The CSIRO atmospheric model CCAM is being used to downscale Intergovernmental Panel on Climate Change (IPCC) atmospheric models, and drive predictions of wave climate. There is large uncertainty in the projections, which show strong regional variability associated with the forcing scenarios, global climate model biases, and the wave-model error. The wave-climate research aims to explain and quantify this uncertainty. During discussion it was suggested that the wave models may help diagnose problems in the ability of the climate models to adequately describe atmospheric circulation.

There were several presentations and considerable discussion around available products and their ability to characterise present climate. The discussion included existing reanalysis datasets (ERA-40 and C-ERA40, ERA-INTERIM), wave model archives (HI-WAM) and the 23-yr altimeter database. These products can all be used to describe the present wave climate, but all have their problems. There is a perceived need for a high-resolution Australian-region waves reanalysis, combining in situ observations, the long-term altimeter record and a high-resolution model. It is worth noting that the US National Centers for Environmental Prediction (NCEP) are planning to run a 1979-2009 global waves hindcast using WW3 forced with the recently available NCEP Climate Forecast System atmospheric Reanalysis (CFSR). The NCEP CFSR has high spatial (approximately 0.5 degree) and temporal (1-hourly) resolution, and has the potential to be a valuable dataset to describe storm wave systems (99^{th} percentile statistics).

Several speakers noted the IPCC statement that there is little to no ability to predict changes in coastline. This is true on time scales of days, let alone decades. Defining the impact of climate-change on the coastline is a major research challenge.

There was some discussion on the role of waves in the coupled ocean-atmosphere system. At present, waves are represented in climate models only through wind-dependent parameterisation of the surface (momentum, mass and heat) fluxes. There are suggestions that waves may have a more profound impact, particularly on surface ocean mixing, the position of storm tracks, and the oceanic uptake of gases. For example, Eulerian ocean models do not explicitly represent Stokes drift or Langmuir circulation. Atmospheric climate models do not consider sea-state dependent drag on the sea-surface. There are other wave-driven feedbacks in the climate system which need further attention (e.g. storm driven sea-ice dynamics and albedo influences of whitecapping). Over climate time-scales, even subtle effects may be important. The role of these two-way feedbacks in the coupled climate system is a considerable research question.

Summary

The following is a list of research challenges that were identified at the Symposium. These are listed in no particular order:

- establish a coastal observing network
- establish a high-resolution bathymetry for nearshore Australia
- implement and validate inverse techniques for near-shore bathymetry
- improve source-term formulations in conventional spectral models
- resolve differences in global model predictions and coastal buoy measurements
- broaden the Australian wave modelling base to include phase-resolving techniques and new approaches such as smooth-particle hydrodynamics
- nurture skills in the emerging area of nearshore data assimilation, incorporating both measurement and modelling
- expand skills in, and familiarity with, coupled wave-current-morphology modelling
- assess and improve climate-scale wave models by comparison with appropriate time-series (satellite and fixed-point measurements, and model reanalysis)
- develop techniques for climate-time-scale coastal prediction, verified against historical data
- develop theories of wave-current interaction applicable to basin-scale circulation
- encourage the integration of wave models in fully coupled ocean-atmosphere-wave systems over a range of space and time scales.

Acknowledgments

All the participants at the Symposium are thanked for their valuable contributions to this paper.

APPENDIX A: PARTICIPANTS

Back row, L to R: Malek Ghantous, Alessandro Toffoli, Jared Stewart, Ian Young, Murray Rudman, Peter Craig, Jasmine Jaffres, Mal Heron, Russel Morison, Ryan Lowe

Middle row L to R: Chari Pattiaratchi, Tom Durrant, Ian Turner, Jim Gunson, Ian Goodwin, Kristen Splinter, Val Jemmeson, Alex Babanin, Mark Hemer, Tom Baldock

Front row L to R: Diana Greenslade, Julian O'Grady, Grant Smith, Rob Holman, Graham Symonds, James Taylor, Andrew Heap, Ian Coghlan

(not present: Jack Katzfey, Richard Manasseh, Ralph Weiss)

APPENDIX B: ABSTRACTS

Optical data, models and data assimilation for nearshore prediction

Rob Holman
College of Oceanic and Atmospheric Sciences, Oregon State University, Corvallis, Oregon, USA 97331

Background

With rising sea level, increasing storm activity and mounting population pressure, the world's coastlines are becoming a battleground between nature and society. Wise stewardship and effective mitigation strategies will require improved knowledge of how the nearshore works and improved tools to measure and predict the state of coastal health.

Capable nowcasts of nearshore hydrodynamics can be made using any of a number of available numerical models. But these require input data in the form of bathymetry and offshore wave conditions that may not be easily available. In addition, measurements in the domain interior that could allow quality assurance are rarely available, so the adequacy of predictions is unknown.

The best measurements come from in-situ observations of waves and currents and traditional surveys of bathymetry. While these have been used to great advantage for short field experiments, the costs and logistics prohibit such measurements for long duration monitoring. Instead, long-term programs will require low-cost robust methods such as can be provided by remote sensing methods. This paper will discuss available options for nearshore remote sensing with a focus on optical measurements such as the Argus Program.

Optical remote sensing in the nearshore

The nearshore is full of exploitable optical signatures. Waves are clearly visible and an observer can estimate their direction, period and perhaps height. Currents can be seen from tracking drifting foam. The shoreline can easily be located by eye and the shape of the subaerial beach can be estimated from the draping of shadows over the beach contours. Each of these signals can equally well be measured from data collected by visible-band cameras, as long as suitable algorithms can be found, and each has, in fact, been the basis of published and ground-truthed algorithms (See Holman and Stanley 2007 for examples of applications).

In developing algorithms based on optical data, it rapidly becomes clear that the development of robust methods is more difficult than expected. In fact, images of ocean waves are almost always more noisy than expected (Fig. 1) because the reflected radiance depends of sea surface slope, a variable that emphasizes high frequency chop. Most observers do not notice this because the eye is so good at smoothing out this clutter to focus on the underlying swell pattern. But computer algorithms do not have this advantage and care must be taken to use robust signal processing in algorithms.

Fig. 1 Snapshot from Duck, NC, USA showing the wide range of scales of optical variability. Because optics depend on sea surface slope, high frequency chop dominates measured signals and must be mitigated by appropriate signal processing.

Most good algorithms require collection of time series data at each pixel followed by Fourier transform to isolate incident band waves. Cross-spectral arrays then allow robust identification of spatial patterns. A good example of these methods that will be presented is the optical estimation of bathymetry based on the relationship of the measurable celerity of ocean waves to depth through the dispersion relationship. Figure 2 shows an example comparison of bathymetry measured using cross-spectral methods to an excellent in-situ survey.

Bathymetries such as are shown in Fig.2 are a required input to numerical models of the nearshore and the successes of methods such as this are important to the success of sustained observations. However, input wave data are also required to drive the models. To a fair extent, these can be estimated from larger scale ocean wave models such as WWIII or SWAN, provided that inputs can be found for these models. But it would be much preferred to estimate input wave forcing also from the same optical observing system. In fact, algorithms have been published to measure the frequency-direction distribution of incident wave energy at locations in the camera field of view. But it has proved more difficult to measure the actual variance (or wave height). During the talk, recent work on methods to measure sea surface height using optical polarization measurements will also be described that could provide an answer to the model input problem.

Unfortunately, models require wave input at the offshore boundaries while estimates made from camera data are usually centered in the middle of the field of view, well away from the offshore model boundaries. Fusion of data from the interior of the domain into a numerical model can only be done using data assimilation techniques. In other words, inputs must be guessed initially, then the guesses must be corrected in a formal assimilation framework such that model prediction match the available domain data.

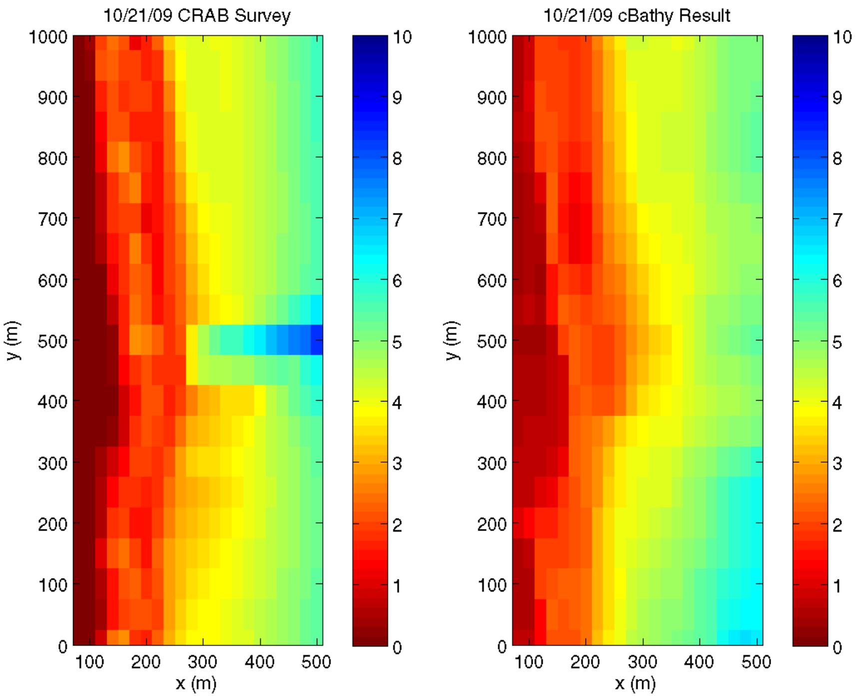

Fig. 2 Comparison of measured bathymetry (left) and bathymetry estimated using optical methods (the cBathy algorithm; right) from Duck, NC, USA for October 21, 2009. The optical algorithm is based on cross-spectral methods of a large spatial array of pixel time series and with a Kalman filter post processing. The blue feature at y=500m in the survey panel is a trench under a pier that is not visible to the cameras.

Initial success has been achieved with correcting nearshore models by assimilation of interior measurements (Wilson et al.) but formal assimilation of optically-derived data has only seen limited exploitation (van Dongeren et al. 2008) and should be the subject of future work.

Other sensors

Standard video cameras are just one example of the available sensors that could be used for nearshore remote sensing. An obvious alternate that will be discussed is X-band radar or even infrared-band optics. Each sees the nearshore with different physics so it is expected that the combination of multi-model sensor combinations could yield important new methods for nearshore remote sensing.

References

Holman, R.A. and J. 2007. Stanley, The history and technical capabilities of Argus. *Coastal Engineering*. **54**: p. 477-91.

van Dongeren, A. et al. 2008. Beach Wizard: Nearshore bathymetry estimation through assimilation of model computations and remote observations. *Coastal Engineering*, 2008. **55**: p. 1016-27.

Wilson, G.W., Özkan-Haller, H.T. and Holman, R.A. Data assimilation and bathymetric inversion in a 2DH surf zone model. *Journal of Geophysical Research*, in review.

Dynamics of infragravity waves in fringing reef systems

Ryan Lowe
School of Earth and Environment, University of Western Australia, WA 6009, Australia
Graham Symonds
CSIRO Marine and Atmospheric Research, Floreat, WA 6014, Australia
Christine Moore
Dept. of Civil and Environmental Engineering, Stanford University, Stanford, CA 94305, USA
Greg Ivey, Chari Pattiaratchi
School of Environmental Systems Engineering,
University of Western Australia, WA 6009, Australia
Ap van Dongeren, Duong Minh Trang and Dano Roelvink
UNESCO-IHE and Deltares, Delft, The Netherlands

Introduction

The majority of the world's coastlines (with some estimates as high as 80% (Emery and Kuhn. 1982) contain submerged reef structures of various types, i.e. tropical coral reefs, relic temperate limestone platforms, and other submerged rock formations. However, surprisingly little research has been conducted on nearshore hydrodynamic processes occurring in reef environments. A good understanding of these processes is important because waves and wave-induced flows ultimately drive sediment transport, nutrient dynamics, as well as the dispersal of larval fish and other organisms; all of which may be significantly impacted by environmental changes (e.g. sea level rise, climate change).

Over the past several decades, considerable advances have been made (both theoretically and numerically) in our ability to predict surface wave dynamics and coupled nearshore currents in coastal systems, however, these studies have largely focused on processes occurring on open-coast sandy beaches. While the physics of nearshore processes on reefs may be largely the same, there are some important differences. These include, among others, wave breaking over the reef resulting in a system-determined partitioning of the momentum fluxes into wave setup and bed shear stress (i.e. onshore flow over the reef) (Lowe et al. 2009), as well as the reef topography being rougher and more spatially-variable, resulting in highly spatially varying frictional effects (e.g. Lowe et al. 2005). Several recent field studies (e.g. (Lowe et al. 2009, Hench et al. 2008) have conducted detailed studies of swell transformation across reefs, and particularly how wave breaking generates *mean* currents via radiation stress forcing. This work has also recently included a detailed field study of the dynamics of the wave-driven *mean* flows within the reef-lagoon system in Ningaloo Reef at Sandy Bay (Taebi et al. 2010).

Although most reef studies have focused on the role of *mean* wave and current dynamics, some studies have highlighted the important contribution of infragravity (IG) waves, with periods ranging from 25 seconds to tens of minutes, to the overall flow variability on coral reef flats (e.g. Lugo-Fernandez et al. 1998, Hardy and Young 1996). Most recently, Péquignet et al. (2009) observed that IG waves dominated the water motion on a narrow (~400 m wide) fringing coral reef flat in Guam. During passage of a tropical storm, wave setup driven by large swell waves generated large IG wave motions on the reef flat that were amplified via resonant wave interactions with the reef morphology. The dynamics of these IG waves could be predicted reasonably well using inviscid shallow water wave theory.

The objective of this present study was to investigate the dynamics IGs on Ningaloo Reef, Western Australia. Ningaloo is Australia's largest fringing reef system, with a morphology very different from Péquignet et al. (2009).

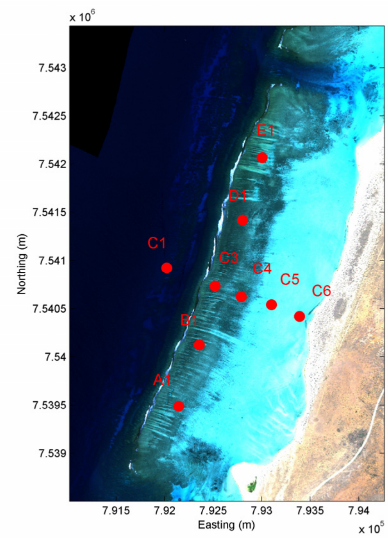

Fig. 1 Instrument array (consisting of a cross-shore and alongshore-transect)

Field study

A three-week field experiment in winter 2009 focused on an ~3 km section of Ningaloo Reef at Sandy Bay (Fig. 1). The reef morphology at this site is typical of many parts of Ningaloo, with a simple configuration of shore-parallel reef sections broken periodically by channels. The fore-reef slope (~1:30) rises to a shallow reef flat (mean depth ~1-2 m) covered by dense assemblages of coral. Waves break on the leading edge of the reef flat (i.e., at the reef crest) located ~1 km from shore. Shoreward of the ~500 m wide reef flat is a somewhat deeper lagoon (mean depth ~2-3 m), comprised mostly of sand and coral rubble.

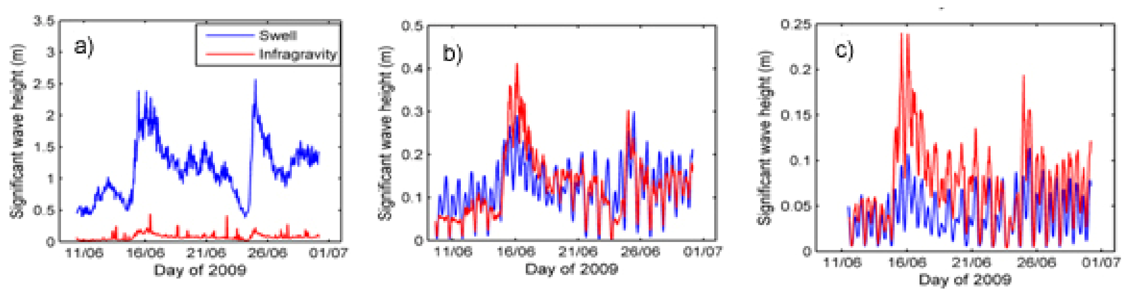

Fig. 2 Spatial variation in wave energy (represented by Hs) for the swell band (1-25 second period) and IG band (25-1000 second period) at a) site C1 offshore, b) site C3 on the reef flat, and c) site C5 inside the lagoon.

A synchronized array of instruments was deployed into both cross- and along-shore transects (Fig. 1). The instruments (all sampling at 1 Hz) consisted of current meters recording 3D velocities and pressure (five Nortek Vector ADVs, one Nortek AWAC, one 2MHz Nortek Aquadopp Profiler, and one 1.2 Mhz RDI ADCP), as well as two pressure-sensor wave gauges

(Seabird SBE26). Pressure and velocity spectra were computed from the raw time series and wave spectra were then inferred from the pressure spectra using linear wave theory. The spectral energy (e.g., used for computing significant wave heights H_s) was partitioned between swell (0.05-0.2 Hz) and IG (0.004-0.05 Hz) bands (Sheremet et al. 2002). Spectral wave energy fluxes were computed from the pressure-velocity co-spectra following Sheremet et al. (2002).

Results

Preliminary results have focused on analysis of the data collected on the cross-shore transect (C1-C6; Fig. 1). During the experiment, a wide range of incident swell conditions were encountered, with H_s varying between ~0.5 and ~2.5 m on the forereef at C1 (Fig. 2a). The swell was largely dissipated at the reef crest, with the IG waves becoming of comparable amplitude on the reef (Fig. 2b). The relative importance of the IG band to the overall wave energy increased towards the lagoon (Fig. 2c). However, unlike in Péquignet et al. (2009) where resonance with the reef drove increases in IG amplitudes towards the coast, the magnitude of the IG waves are significantly damped across the Ningaloo reef flat via bottom friction dissipation (not shown).

The response (amplitudes) of the IG motions on the reef increased with the incident swell, and analysis of the synchronized surface elevation time series on the reef show that shoreward propagating IG are generated by incident swell wave groups (not shown). The computed directional wave energy fluxes suggest the observed IG waves are primarily shoreward propagating progressive waves, i.e. there is little evidence of any significant offshore reflection (not shown).

Overall, the results indicate that IG wave motions are important (and often dominant) sources of hydrodynamic energy on Ningaloo Reef, i.e. on the reef the root-mean-squared velocities associated with IG motions are generally greater than both the swell and the mean wave driven currents. Current work focuses on numerical simulations of these IG waves using XBEACH (Roelvink et al. 2009), which is showing some success in simulating the dynamics of these IG motions.

Acknowledgments

Funding for this project was provided by an Australian Research Council Discovery Grant # DP0770094 to RJL

References

Emery, K. and Kuhn, G. 1982. *Geological Society of America Bulletin* 93 644-54.

Hardy T.A. & Young I.R. 1996. *Journal of Geophysical Research-Oceans* 101(C6) 14311-26.

Hench, J.L., Leichter, J.J. and Monismith, S. 2008. G. *Limnol. Oceanogr*., 53(6) 2681–94.

Lowe, R.J., Falter, J.L., Monismith, S.G. and Atkinson, M.J. 2009. *Journal of Physical Oceanography*, 39(4) 869-89.

Lowe, R.J. et al. 2005. *J of Geophys. Research-Oceans* 110 DOI: 10.1029/2004JC002711.

Lugo-Fernandez, A., Roberts, H.H., Wiseman, W.J. and Carter B.L. 1998. *Coral Reefs*, (17)4 343-9.

Péquignet, A.C.N., Becker, J.M., Merrifield, M.A. and Aucan J. 2009. *Geophys. Res. Letters* 36 L03607.

Roelvink, D. et al. 2009. *Coastal Engineering*, 56(11-12) 1133-52.

Sheremet, A., Guza, R.T., Elgar, S. and Herbers, T.H.C. 2002. *J. Geophys Research - Oceans*, 107 DOI: 10.1029/2001JC000970.

Taebi, S., Lowe, R.J., Pattiaratchi, C.B., Ivey, G.N., Symonds, G. and Brinkman R. 2010. *Journal of Geophysical Research-Oceans*, in review.

Wind wave run-up: swash zone hydrodynamics and sediment transport

Tom. E. Baldock, Matthew P. Barnes, Hannah E. Power
School of Civil Engineering, University of Queensland, St Lucia, QLD 4072

Introduction

This presentation will highlight the importance of swash zone boundary conditions in determining the hydrodynamics of wave run-up on the beach face, and particularly how the boundary conditions influence flow depth and velocity asymmetry. Recent data and modeling is discussed, with application to swash overtopping, sediment transport and bed shear stress.

Applications

Swash zone boundary conditions control overtopping rates over seawalls and dunes, sediment flux into and across the swash zone, and net sediment transport patterns within the swash zone. Recent new solutions to the NLSW equations are discussed with application to overtopping flows and sediment transport. Figure 1 illustrates how the locus of flow reversal, u(x)=0, varies with the strength of the incident bore. Significant differences are apparent, and these influence the overall asymmetry of the swash hydrodynamics.

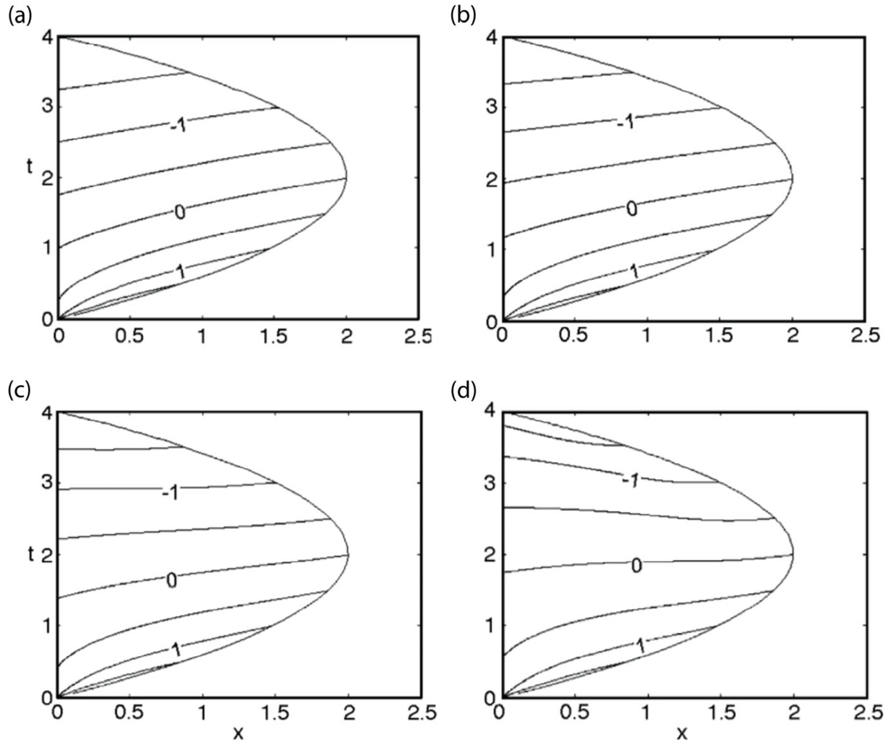

Fig. 1 Contours of flow velocity and the locus of the position of horizontal flow reversal (*u*=0 contour) across the swash zone for (a) *k*=0, (b) *k*=1/3, (c) *k*=2/3, and (d) *k*=1 given by Guard and Baldock (2007).

Verification of this model for field conditions is difficult using single point measurements in an Eulerian reference frame, unless a very extensive instrument array is deployed across the swash zone. However, a novel application of video remote sensing enables both verification of the model and also demonstrates the wide range of swash boundary conditions occurring on natural beaches (Power et al. 2009). Figure 2 shows examples of the locus of flow reversal from natural swash, determined from the streaklines that are visible in time-stack images of wave run-up (e.g. *Stockdon and Holman* 2000).

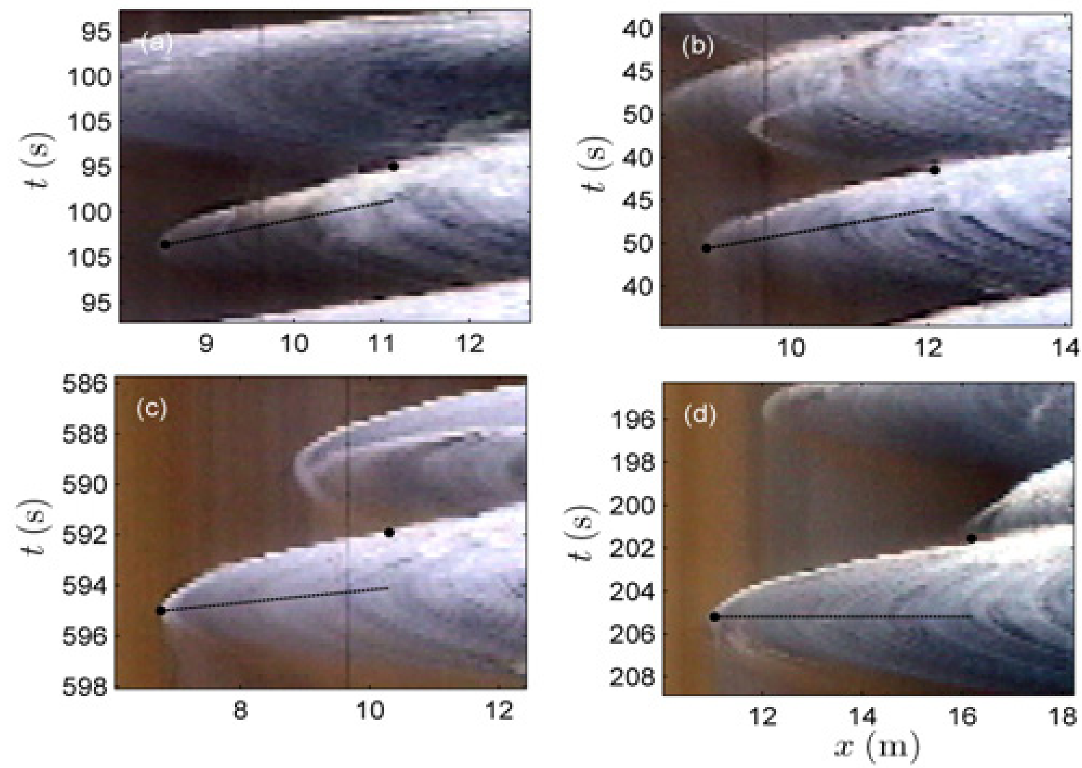

Fig. 2 Example timestacks of waves from Cabarita Beach, NSW, with (a) *k*=-0.38 , (b) *k*=-0.015, (c) *k*=0.71, and (d) *k*=1.15.

The gradient in (x,t) of the locus of flow reversal is easily extracted from the timestack images by a combination of manual and automated processing, from which the values of *k* in the Guard Baldock (2007) model can be determined. Examples from a range of natural beaches will be presented.

The presentation will also discuss direct measurements of bed shear obtained from a shear plate, with application to sediment transport and estimating run-up excursions. The model data is compared to a new Lagrangian boundary layer swash model (Figs 3 and 4). This solves simplified boundary layer equations along the particle trajectories, which enables the model to include the history of the unsteady flow. The model develops an asymmetric bed shear stress without ad hoc parameterisation. Finally, initial results from a field project to measure wind stress over the surf zone are discussed, with application to wave setup.

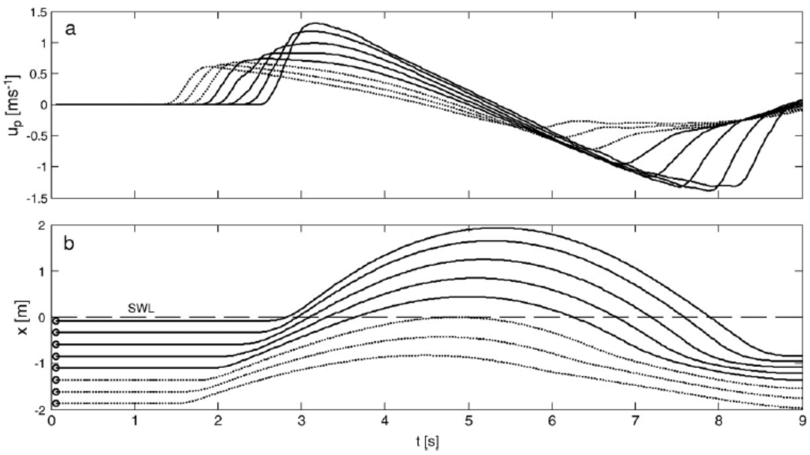

Fig. 3 Particle trajectories (lower panel) and velocity along the trajectories (upper panel) for a swash flow induced by a solitary bore.

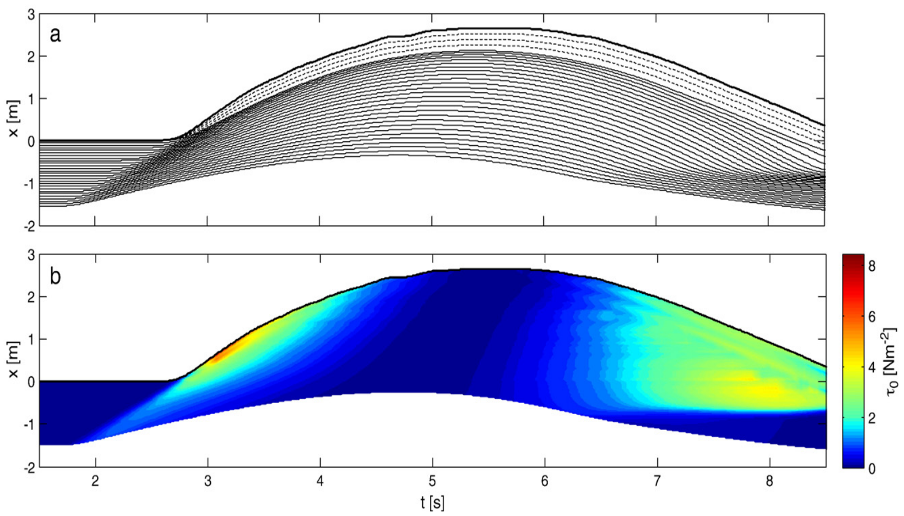

Fig. 4 Particle trajectories (upper panel) and estimated bed shear stress (lower panel) from the Lagrangian swash boundary layer model of Barnes and Baldock (2010).

References

Barnes, M.P. and Baldock, T.E. 2010. A Lagrangian model for boundary layer growth and bed shear stress in the swash zone, *Coastal Engineering*, *57*(4), 385-96.

Guard, P.A. and Baldock, T.E. 2007. The influence of seaward boundary conditions on swash zone hydrodynamics, *Coastal Engineering*, *54*(4), 321-31.

Power, H. E. et al. 2009. Remote sensing of swash zone boundary conditions using video and Argus, in *Coastal Dynamics 2009*, ASCE, Tokyo.

Stockdon, H.F. and Holman, R.A. 2000. Estimation of wave phase speed and nearshore bathymetry from video imagery, *Journal of Geophysical Research*, *105(C9)*.

Wind and wave driven flow in a temperate reef environment

Graham Symonds and Liejun Zhong
CSIRO Marine and Atmospheric Research,
Underwood Ave, Floreat, WA 6014, Australia

Introduction

A feature of the coastal zone of South West Western Australia is a series of limestone reefs scattered along approximately 700 km of coast, 3-10km offshore, which occasionally break the surface or are shallow enough for waves to break forcing currents across the reef. Unlike coral reefs these temperate reefs have a very patchy distribution, the length scales of individual reefs being of O(100m), gaps of O(100-1000m). How far the influence of wave forcing over such patchy reefs extends beyond the immediate vicinity of the reefs is not well known but, during periods of high waves, wave forced transport of water, particles and kelp wrack through these reef environments may be significant and is thought to be important in maintaining unusually high benthic biomass. In Mulligan et al. (2007) hurricane waves breaking over an isolated reef near the entrance to Lunenberg Bay, Nova Scotia, Canada, affected circulation across the bay which is approximately 8km long and 4km wide.

Observations

In situ measurements of waves, currents and water properties were made on and around a series of reefs off Perth, Western Australia. The top of the reefs are typically 1-2m below the sea surface, and between the reefs and shore the average depth is about 10m.

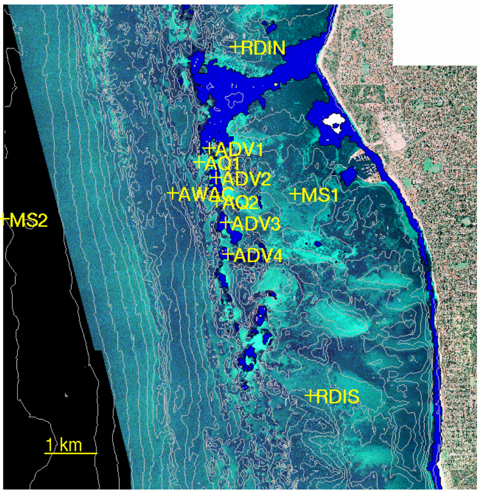

Fig. 1 Aerial photograph of measurement location. Depths less than 4m are shown as filled blue areas and the current meter sites are labeled in yellow.

The aim of the project was to examine the role of wave forcing with moorings centred on the main line of reefs about 3km offshore as shown in Fig. 1. Nortek Vector current meters were deployed on the back of several reefs (ADV sites) and Nortek Aquadopps in the channels between the reefs (AQ sites). A Nortek AWAC was deployed just seawards of the reef line and RDI ADCP's were deployed at sites RDIN and RDIS. Multi-sensors measuring temperature, salinity, oxygen, PAR and fluorescence, were deployed at sites MS1 and MS2 in Fig. 1. The moorings were deployed four times between July 2007 and May 2008, each deployment being 6-8 weeks duration.

Time series plots of current vectors at the RDIN, RDIS and AWAC sites from the first deployment (July 6 to September 5, 2007) are shown in Fig. 2. At the AWAC and RDIS sites the currents are predominantly towards the south, and are generally stronger inside the reef line at RDIS. At RDIN the currents are generally weaker and more variable than RDIS, with more periods of northward flow.

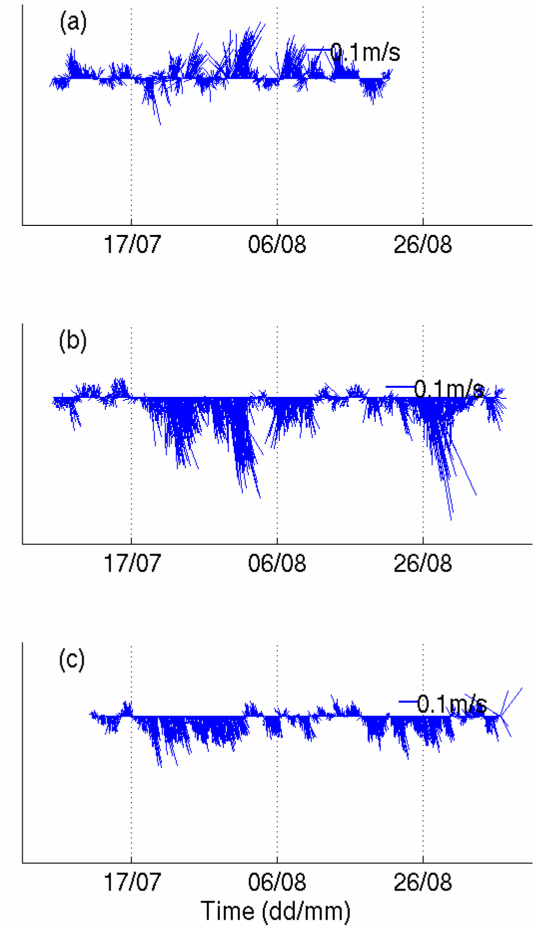

Fig. 2 Current vectors from deployment 1 at (a) RDIN, (b) RDIS and (c) AWAC sites.

Previous studies in this region have concluded the nearshore alongshore currents are wind driven and the current speed is reasonably predicted using 2% of the wind speed. In Fig. 3 the alongshore currents from all four deployments are plotted against the alongshore wind seawards of the reef line at the AWAC (Fig. 3a) and shorewards of the reef line at RDIS (Fig. 3b). At the AWAC the alongshore currents are correlated with the alongshore wind consistent with previous work. However at RDIS there is considerably more scatter. The red and black points in Fig. 3 correspond to times when the root mean square wave height (Hrms) measured at the AWAC is greater than 1.5m and less than 1.5m respectively. At RDIS (Fig. 3b) much of the scatter is associated with the larger waves, the strongest currents are towards the south when Hrms>1.5m (red dots), often occurring when the wind speed is small, and at times are opposed to the wind.

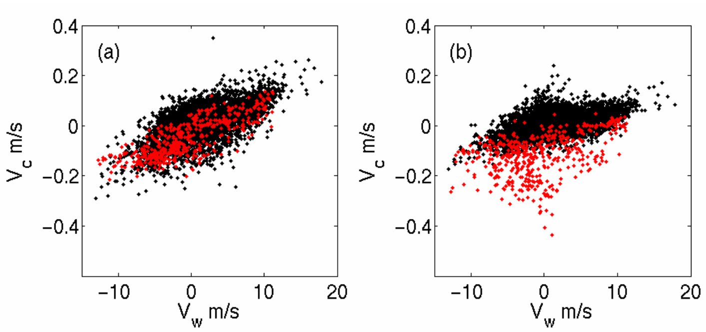

Fig. 3 Alongshore current (V_c) versus alongshore wind (V_w) at (a) AWAC and (b) RDIS, positive values northward. Black dots at times when Hrms<1.5m and red dots when Hrms>1.5m.

A scatter plot of current speed at RDIS and Hrms at the AWAC is shown in Fig. 4. With low waves there is little correlation but when AWAC Hrms exceeds about 1.5m the current speed shows a significant correlation with the offshore wave height.

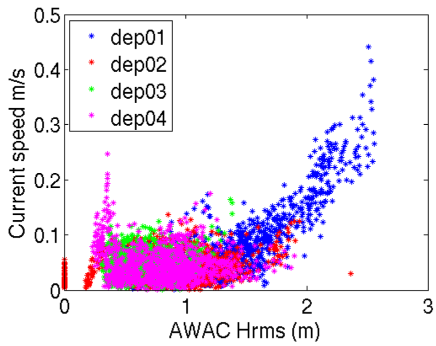

Fig. 4 Current speed at RDIS versus Hrms at the AWAC.

Significant wave driven currents across the reefs will not occur until the waves are big enough to break. A measure of the wave height at the onset of breaking is obtained by comparing the wave height seawards of the reefs at the AWAC with wave heights measured at the back reef locations, sites ADV1…4. In Fig. 5 when the waves are small Hrms at the ADV sites is similar to Hrms at the AWAC. However, as the offshore wave height increases we begin to see a reduction in wave height at the ADV sites relative to the AWAC which can be attributed to dissipation associated with depth induced breaking over the reefs. The onset of breaking differs slightly between reefs but on average occurs when Hrms at the AWAC is about 1.5m, similar to when we begin to see a correlation between the AWAC Hrms and current speed at RDIS (see Fig. 4).

Modelling

The numerical model XBeach (Roelvink et al. 2009) has been used to simulate the wave driven circulation on and around the reefs. The model grid size is 30x30m and the domain size is 268x439 grid cells. An example of XBeach output is shown in Fig. 6 for a case when the Hrms at the offshore boundary is 2.2m. The current vectors show a lot of spatial variability in the vicinity of the reefs with onshore flow over the reef crests, offshore flow between the reefs and southward flow in the southern part of the model domain between the reef line and the shore.

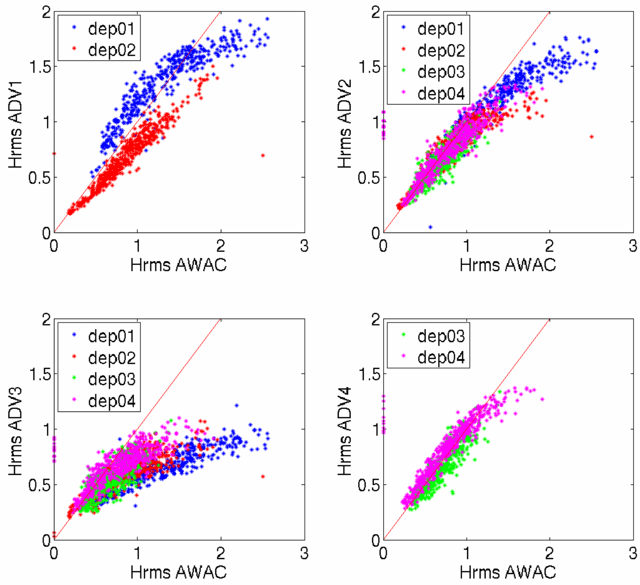

Fig. 5 Hrms at the ADV sites versus Hrms at the AWAC for the four deployments.

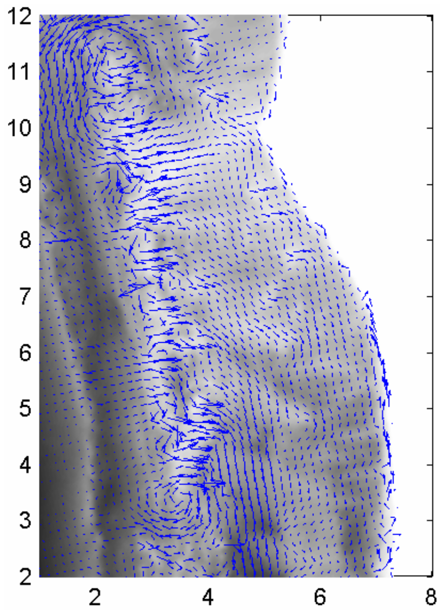

Fig. 6 XBeach output showing current vectors over bathymetry in grey. Model forced with Hrms=2.2m, T=14s and dir=266^{o} at the offshore boundary.

Qualitatively the model is consistent with the observations but some quantitative differences remain.

References

Mulligan, R.P., Hay, A.E. and Bowen, A.J. 2008. *J. Geophys. Res.,* 113, doi:10.1029/2007JC004500.

Roelvink, D., Reniers, A., Van Dongeren, A., van Thiel de Vries, J., McCall R. and Lescinski, J. 2009. *Coastal Eng*., 56, 1133-52.

Wave-driven currents on a barred beach during a sea-breeze cycle

Jim Gunson and Graham Symonds
Centre for Australian Weather and Climate Research,
Underwood Ave, Floreat, WA 6014, Australia

Introduction

Bluelink II is a joint project between CSIRO, the Bureau of Meteorology and the Royal Australian Navy to develop ocean forecasting capability in the Australian region. Part of this project is to develop a Littoral Ocean Modelling System (LOMS), a computer software system that will provide users with real-time forecasts of wave and current conditions in the nearshore region. Another element of Bluelink II is a field experiment designed to measure wave and current conditions on a barred beach during the sea-breeze cycle and hence provide observations to compare with model simulations.

This paper presents results from the implementation of the nearshore hydrodynamic model XBeach, and its application at Secret Harbour. First the background of LOMS is described, then the Secret Harbour field experiment. The model XBeach is described and its simulations compared to the observations. Finally some conclusions are drawn on the performance of XBeach.

LOMS

In order to provide forecasts of nearshore conditions, the LOMS has the following requirements: high resolution (5-10m mesh), relocatable (various shoreline profiles), forced by waves and wind. Also the hydrodynamic model should be state-of-the-art, in wide use, and be run in reasonable computing time. Knowledge of the bathymetry is one of the most important factors in making a realistic simulation.

Various hydrodynamic models were considered for inclusion in LOMS. The primary challenge to successful implementation is the numerical treatment of wave and flow conditions at the open boundaries of the model domain. The model XBeach proved to be effective in its treatment of boundary conditions, compared to other models.

Secret Harbour field experiment

The aim of this experiment was to measure wave-driven alongshore currents and compare the observations to numerical simulations. Previous studies (Ruessink et al. 2001) of alongshore currents have focused on steady conditions. The strong sea breeze cycle along Perth’s metropolitan beaches provides an opportunity to measure the temporal growth and decay of the wave driven flows.

A quite straight and alongshore uniform beach with sandbar at Secret Harbour was selected. Several instruments were deployed in a line spanning the surf zone out to 10 metres depth, measuring water velocities, pressure and wave height (see Fig. 1). Measurements were taken continuously during February 2009

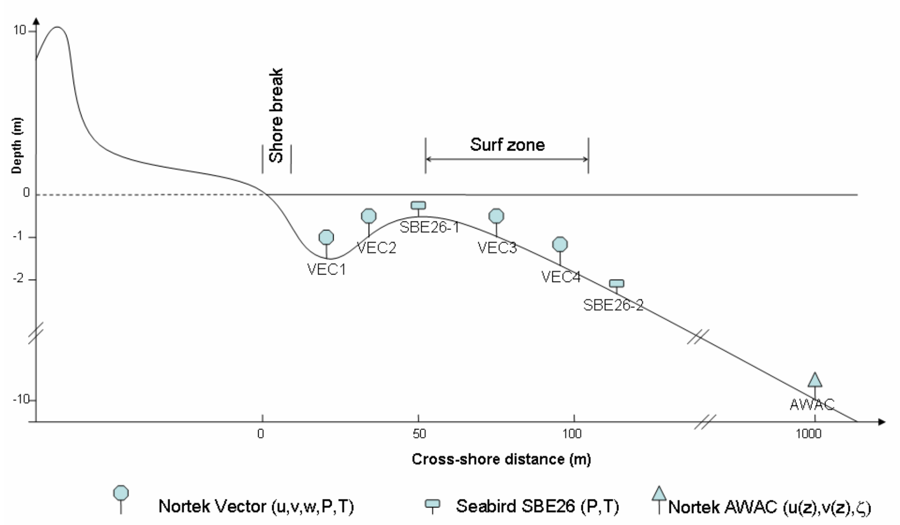

Fig. 1 Schematic of the cross-shore instrument array at Secret Harbour.

XBeach

The XBeach model (Roelvink 2009) was developed at TU Delft and Deltares and consists of a wave module coupled to a circulation module. The physics employed are conservation of wave action and the vertically-averaged conservation of momentum. As waves enter shallower water they eventually break and the resultant gradients in radiation stress (excess momentum due to the waves) cause setup of mean sea level and nearshore currents. XBeach also includes a morphology module that allows evolution of the seabed in response to water movement. This is an area of future research.

Figure 2 shows the XBeach model domain for the field site and the predicted wave height and currents at the height of a typical sea-breeze. The model is forced by hourly values of wave height, period and direction taken from the AWACS (see Fig. 1) which is situated on the southwest boundary of the model domain.

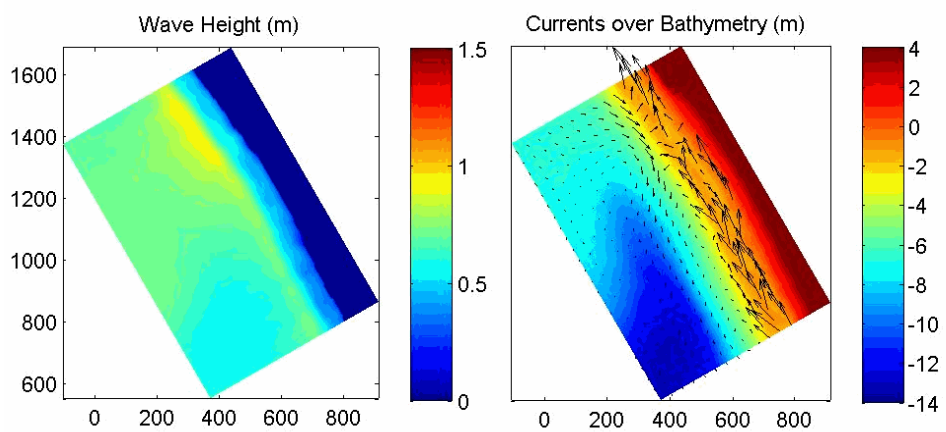

Fig. 2 The Xbeach model domain for Secret Harbour, showing wave height and currents.

Model/data comparison

From the observations, the sea-breeze cycles over 17-19 February, 2009 were used to compare with the model simulations. Figure 3 shows comparisons of XBeach with the observations from VEC1, VEC2 and VEC3 (see Fig. 1).

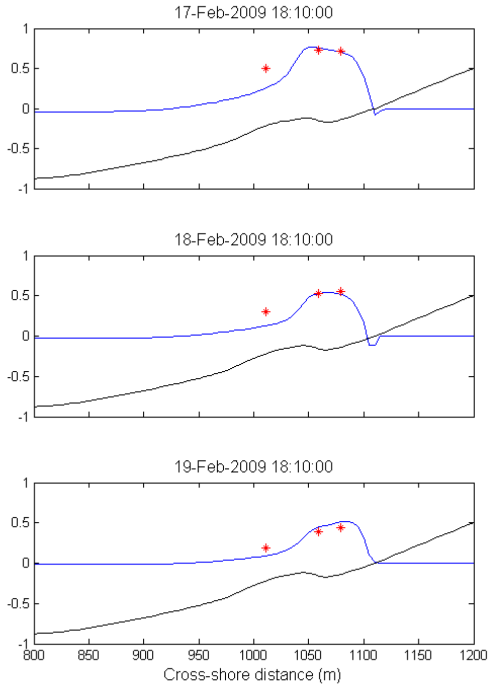

Fig. 3 Cross-shore profiles of alongshore current speeds (m/s) from Xbeach (blue) and observations (red) from VEC1, VEC2 and VEC3 at the height of the sea-breeze on the 17, 18 and 19 February. The black line represents the bathymetry (m/10).

The time series of observed and modeled alongshore current speed at the locations of VEC1, VEC2 and VEC3 are shown in Fig. 4. Although the alongshore current is somewhat underestimated at VEC3, in general the agreement is good.

Discussion

Preliminary results are presented illustrating the performance of the hydrodynamic model XBeach against observations from the Secret Harbour field experiment. The agreement is quite good at the vector current meter locations.

Further comparisons with the other instruments are underway. Hourly wind forcing also needs to be implemented. As was known *a priori,* knowledge of the bathymetry is crucial to an accurate simulation. The sensitivity of the model to the bathymetry needs to be assessed, and will be performed by a perturbation analysis.

The XBeach model displays sufficient ability to capture the wave-driven currents during the sea-breeze cycle. Not only does XBeach meet the requirements for LOMS in Bluelink II, it also shows good potential to study morphological changes in future research.

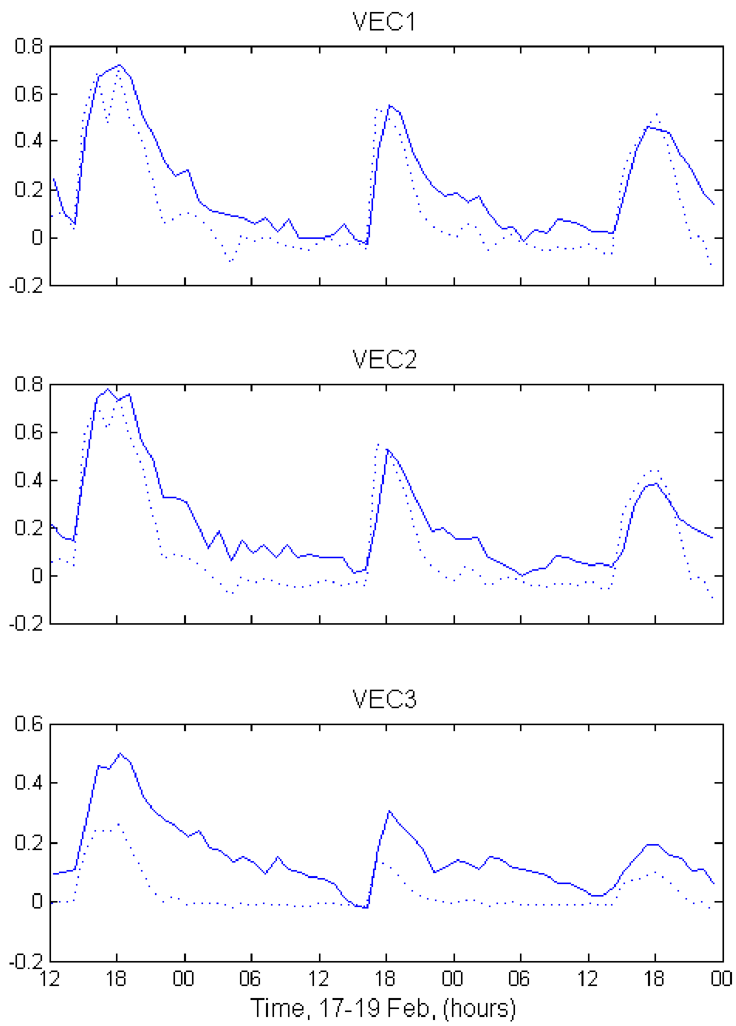

Fig. 4 Observed (solid) and modeled (dotted) time series of alongshore current speed during 17-19 February 2009, at the locations of VEC1, VEC2 and VEC3.

References

Roelvink, D., Reniers, A., van Dongeren, A., de Vries, J.V., McCall, R. and Lescinki, J. 2009. *Coastal Eng.*, **56**, 1133-52.

Ruessink, B.G., Miles, J.R., Feddersen, F., Guza R.T. and Elgar S. 2001. *J. Geophys. Res.*, **106**, C10, 22451-63.

Gold Coast Seaway: ocean surface, wave setup and TC Roger

Jared Stewart
KBR (Kellogg Brown & Root Pty Ltd), GPO Box 633, Brisbane, QLD 4001, Australia
Dr David Callaghan and Behnam Shabani
Coastal Engineering Group, University of Queensland, St Lucia, QLD 4072, Australia

Introduction

There have been numerous storm surge events recorded along the southern Queensland and northern New South Wales coastlines in past decades which have resulted in flooding and inundation of coastal areas. Many such events have resulted from large but less intense Tropical Cyclones or East Coast Low (ECL) pressure systems that didn't cross the coastline (e.g. TC Dina in 1967, TC Pam in 1974, TC Roger in 1993 and ECL in February 1996). The recorded storm surges during these events have been compared with planning guidelines which classify many of the recorded events as being rare (i.e. >100 year return period).

In order to resolve the large discrepancy between predictions for storm surges contained in the planning guidelines and recorded events a number of investigations have been undertaken. These investigations have been principally undertaken at the Gold Coast Spit site and have included wave set-up measurements and wind profile measurements. In addition, a hydrodynamic model has been established and simulated for recorded storm surge events.

Storm surge modelling

A storm surge model was established in the DHI software MIKE 21FM, which solves the depth averaged continuity and momentum equations using a cell- centered finite volume solution technique. The model has been simulated using hindcast wind and pressure data for the TC Roger and February 1996 ECL events. The effect of wave radiation stresses and tides on the modelled surge was also investigated, together with numerous sensitivity analyses.

The NCEP-DOE reanalysed meteorological dataset was used as the basis for the spatially varying wind and pressure fields in the model. The wind stress coefficient (CD) proposed by Wu (1982) was adopted.

The simulation results for both of the events showed that the model under-predicted the surge by between 35-70% at the standard tide stations and approximately 30% at offshore tide stations. A better agreement between the simulated and recorded surges was obtained using a wind stress coefficient of approximately double that proposed by Wu as illustrated in Fig 1. The inclusion of wave radiation stresses in the model also resulted in improvements between the simulated and recorded surges

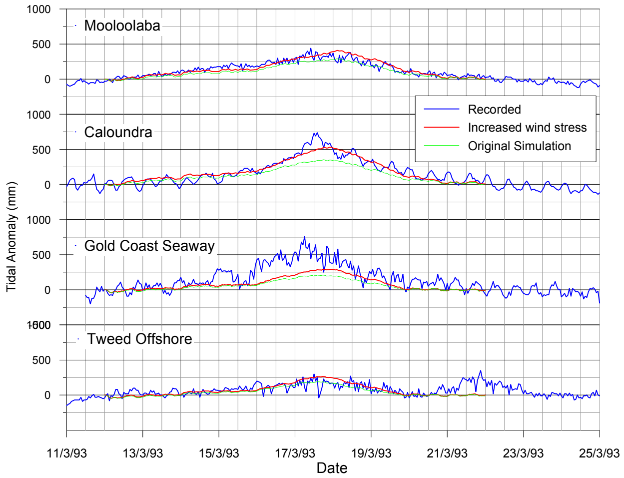

Fig. 1 Comparisons between recorded and simulated storm surge during TC Roger in 1993 at four locations for Wu (1982) CD and increased CD.

Wave setup

In order to investigate whether the oceanic surge is enhanced by wave setup or if there is another physical process that amplifies the storm surge in the nearshore, field measurements (Fig 2) were obtained during the passage of the May 2009 ECL using the Coastal Field Research Facility, The Spit, Gold Coast, Australia (see Cartwright et al. 2009). The research site has, amongst other things, 10 tubes from 60 m to 500 m offshore which are able to measure mean water level at ±0.5 cm. The tidal anomaly within the Broadwater (difference between ─✕─ and ─⊟─) was calculated to be 0.5m on Thursday 21 May 2009 around noon. The offshore significant wave height was Hm0 ≈ 5 m. The mean water levels in the Broadwater and 500 m offshore were different by approximately ±20 cm (─┼─ and ─▲─). This water level difference is most likely wind driven seiches in the Broadwater (tidal gradients water level differences of ±5 cm have been estimated from other field measurements that exclude wind and wave forcing). The average shoreline setup during the measurement period was 1.64m or $\eta(h = 0)/H_{rms} \approx 0.46$. The average still water line setup was measured at 0.70m or $\eta_{SWL}/H_{rms} \approx 0.2$.

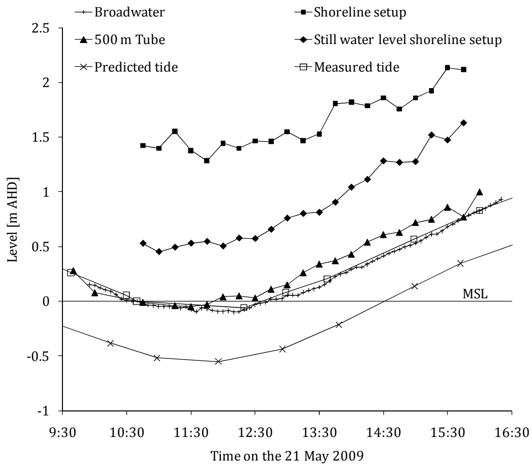

Fig. 2 Measured mean water levels on 21 May 2009 in the Broadwater (─┼─) and nearby exposed coast (the shoreline ─■─, the still water shoreline ─◆─ and 500 m offshore ─▲─) at the Spit, Gold Coast. For reference, the predicted (─✕─) and measured (─⊟─) tide in the Broadwater measured by Queensland Transport are also shown.

The results also demonstrated that wave setup dramatically increases when water depth is much less than 1 m, which has been previously demonstrated at Brunswick Heads by Hanslow et al. (1996). The measurements indicate that the wave setup at the shoreline (—■—) or the still water line (—◆—) has no influence on the Broadwater surge. Figure 3 suggests Broadwater setup will be controlled by setup at the water depth equal to that over the offshore bar of 6 m. That is, the mismatch between the observed surge (TCs Dinah, Pam and Roger) and Broadwater predictions is in no significant part due to wave setup. The Broadwater mean water level is similar to that 500 m offshore where wave setup is minimal.

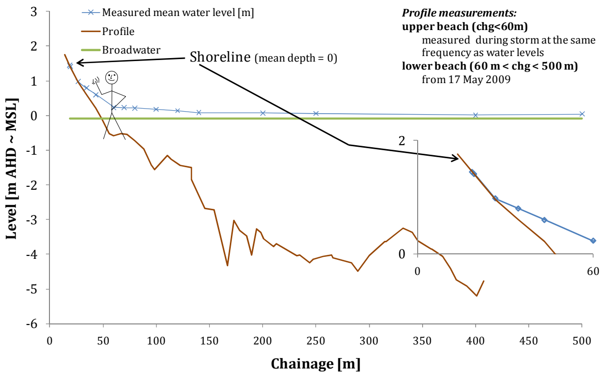

Fig. 3 Measured mean water levels in the Broadwater (▬) and nearby exposed coast (—×—) at the Spit, Gold Coast. The beach profile (▬) and a 2 m tall person is shown for scale. Inset on right shows setup above MSL.

Ocean surface

There have been few or no field studies on the problem of wind stress over the surf zone and its potential importance in forecasting wind setup. For this reason a field investigation into the surf zone aerodynamic roughness and its parameterization is being undertaken. The wind stress over the surf zone is being investigated through the study of wind profiles at the shoreline.

Wind profiles have been measured using a 10m mast with anemometers installed at 10 points along the mast. Measurement points have been selected to be spaced evenly in the logarithmic scale. The lowest and highest anemometers are respectively deployed at used at z = 0.80 and z = 10 above the mast base.

Preliminary results based upon data collected during the May 2009 ECL suggest that the wind stress coefficient (CD) is approximately double that suggested by the earliest work by Charnock (1955) as shown in Fig 4.

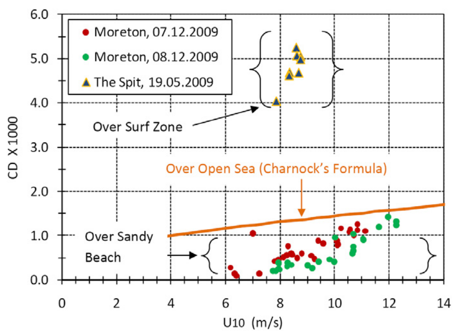

Fig. 4 Comparison of inferred wind stress coefficient (CD) from preliminary measurements at the Spit Coastal Field Research Facility together with Charnock's (1955) formula.

References

Cartwright, N., Callaghan, D.P. and Nielsen, P. 2009. Coastal field research facility: The Spit, Gold Coast, Australia, *Civil Engineering Bulletin* 25, The University of Queensland, Brisbane.

Charnock, H. 1955. 'Wind stress on a water surface', *Quarterly Journal of the Royal Meteorological Society,* vol. 81, pp. 639-40.

Hanslow, D., Nielsen, P. and Hibbert, K. 1996. Wave setup at river entrances. In: B.L. Edge (Editor), *Proceedings of the 25th International Conference on Coastal Engineering*. ASCE, Orlando, Florida, pp. 1335-48.

Wu, J. 1982. 'Wind-stress coefficients over sea surface from breeze to hurricane', *Journal of Geophysical Research*, vol. 87, pp. 9704-6.

Introduction of a new friction routine into the SWAN model that evaluates roughness due to bedform and sediment size changes

Grant Smith, Alexander V. Babanin, Ian R. Young
Swinburne University of Technology, Melbourne, Victoria 3122 Australia
Peter Riedel
Coastal Engineering Solutions, 600 Burwood Road, Hawthorn East, VIC, 3123, Australia
Stephen Oliver and Graeme Hubbert
Global Environmental Modelling Systems,
PO Box 149, Warrandyte Victoria, 3113, Australia

Introduction

The interaction between wave energy and the seabed results in a dissipation of energy that is due to bottom friction. Work is also done on bedforms both solid and mobile (cohesive and noncohesive sediments) such as sand ripples, on suspending and moving sediment, due to percolation (Komen et al. 1994), and due to excessive breaking caused by shoaling (e.g. Babanin et al. 2001). For a relatively flat granular seabed, the magnitude of the roughness that contributes to dissipation is determined by the grain size of the sediment, and dependence of the wave-motion friction on this grain size is one of the subjects of this paper. However, the bedform of a mobile seabed can be altered due to the action of waves and currents. Experimental analysis of flow in the boundary layer found, for example, eddies moving the sediment in an orbital trajectory that results in parallel ridges (or ripples). Their formation and size is determined by the dimension of the eddies (Melnikhova amd Volkov 2000).

A bottom-friction routine, based on the Nielsen algorithm (Nielsen 1981), was introduced into the SWAN model (Booij et al. 1999) which makes the bottom friction for waves dependent on presence/absence of ripples if the sea bed is mobile, and on grain size of the sediment. The routine is suitable for spectral models of wave evolution, and in the present study it was tested by means of the SWAN model by hindcasting waves at two finite-depth field sites.

The first location for validation and testing of the new friction subroutine is Lake George, Australia. Lake George is located in the state of New South Wales. It covers an area of about 65km2 and has a maximum depth of 2.1 metres. The advantage of using a shallow lake for investigating the impact of bedforms on wave evolution is that all developed waves will exhibit finite depth characteristics (Young and Babanin 2006). Also, the Lake George bed is flat which makes the bottom topography simple and results will not be affected by a complex bathymetry. Sediment from this lake has been utilised in laboratory measurements to evaluate the interaction of the lake bed and waves (Babanin et al. 2005).

Observed data exists for eight stations located at various intervals spanning the length of the lake. The data timescale is an 18 month period from the 6th of March 1992 to 7th October 1993. This data was collected during an investigation on finite-depth spectral evolution as described in Young and Verhagen (1996) and Young et al. (1996).

Initial modelling of Lake George, Australia, using the default friction configuration in the SWAN model showed that the significant wave height was overestimated at most time steps (in some locations the predicted wave height was more than double the observed data). This discrepancy supports the hypothesis that in shallow depths when friction dissipation is the dominating dissipation term, overestimation of wave energy will occur when conditions and sediment characteristics are likely to produce sand ripples.

The results from the Lake George SWAN model using the ripple friction algorithm case are very promising as shown in Fig. 1 (the water depth is approximately two metres across the lake). In some locations model agreement with observed data was excellent. There was an overall improvement in model prediction for significant wave height, and a small yet identifiable improvement on the peak period.

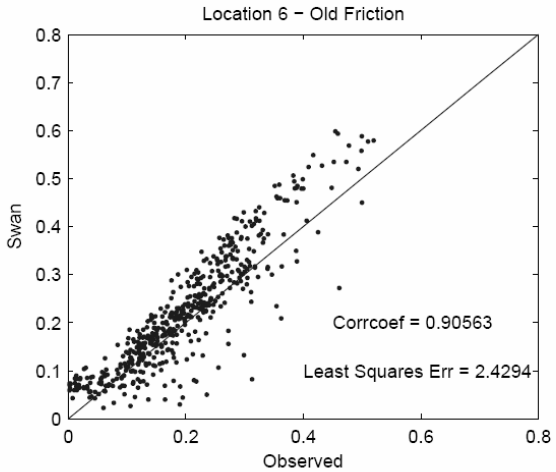

Fig. 1a Scatter plot showing correlation between the default SWAN friction routine and the observed data at Lake George

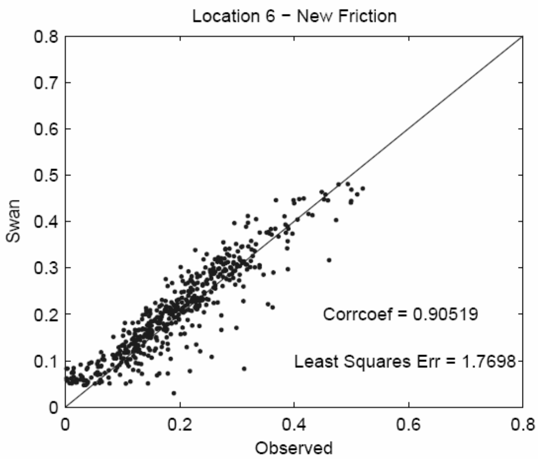

Fig. 1b Scatter plot showing correlation between the new Nielsen algorithm friction routine and the observed data at Lake George.

The algorithm that determines the occurrence of sediment mobility and the evolution of bed-forms was also validated to emulate the expected behaviour found in laboratory experiments using a sediment sample from Lake George (Babanin 2005). The near bed orbital velocity exceeded the uni-directional velocity found in laboratory experiments (that was deemed to be the threshold to initiate sediment mobility) at similar time steps as the Shields parameter

threshold predicted. The maximum roughness coefficient calculated by the algorithm for the month of October 1992 was 19.1mm, which is similar to the maximum value of 20mm expected to occur for sediment at Lake George (Babanin 2005).
An overestimation of the presence of fully developed ripples was amended by implementing an averaging process that remembers the history of the roughness at each grid cell. The final roughness factor at any given time step and location was derived from this array.

Further testing was done for an offshore coastal location at Lakes Entrance at a depth of 16.3 metres. The original SWAN Model showed quite acceptable results. At the particular output point in question, there were no ripples found to exist based on the bed-form algorithm. The roughness coefficient was therefore solely based on the grain size diameter. Results from the new friction algorithm showed that there was a very slight improvement on the original model results. The results from both models are comparable as they both utilised a constant value for roughness over the model run due to the absence of bed-forms. Since the Lakes Entrance sand size (0.41mm) is very different from the Lakes George silt size (0.13mm) this outcome provides a support to the grain-size dependence of the new bottom-friction routine (Babanin et al. 2001).

References

Babanin, A.V., Young, I.R. and Banner, M.L. 2001. Breaking Probabilities For Dominant Surface Waves On Water of Constant Depth. *Journal of Geophysical Research*, 106(C6) (2001) p. 11659-76.

Babanin, A.V., Young, I.R. and Mirfenderesk, H. 2005. Field and Laboratory Measurements of Wave-Bottom Interaction, in Coasts and Ports: Coastal Living - Living Coast. Institution of Engineers, Australia Adelaide, Australia

Booij, N., Ris, R.C. and Holthuijsen, L.H. 1999. A third-generation wave model for coastal regions, 1, Model description and validation. *J. Geophys. Res*., 104 (C4) p. 7649-66.

Komen, G.J. et al. 1994. *Dynamics and Modelling of Ocean Waves*, Cambridge: Cambridge University Press.

Melnikhova, O.N. and Volkov, P.Y. 2000. Sediment transport by eddies formed in the boundary layer of open flows. *New Trends in Water and Environmental Engineering for Safety and Life*, p.

Nielsen, P. 1981. Dynamics & Geometry of Wave-Generated Ripples. *Journal of Geo-physical Research*, 86(C7) p. 6467-72.

Young, I.R. and Babanin, A.V. 2006. The form of the asymptotic depth-limited wind wave frequency spectrum. *J. Geophys. Res*., 111(C06031) p. doi:10.1029/2005JC003398, 15p.

Young, I.R. and Verhagen, L.A. 1996. *The growth of fetch limited waves in water of finite depth*. Part 1. Total energy and peak frequency. Coastal Engineering, V(29) p. 101-21.

Young, I.R., Verhagen, L.A. and Khatri, S.K. 1996. *The growth of fetch limited waves in water of finite depth*. Part III: Directional spectra. Coastal Eng, (29) p. 101-21.

Wind, wave and storm surge reanalyses and projections at the GKSS Institute for Coastal Research and their use in practical applications

Ralf Weisse
GKSS Research Center, Institute for Coastal Research,
Max-Planck-Str. 1, 21502 Geesthacht, Germany

Introduction

Coastal and offshore applications require appropriate planning and design. For most of them, statistics of extreme wind, wind waves and storm surges are of central importance. To obtain such statistics long and homogeneous time series are needed which are often unavailable. To complement the limited observational record, consistent meteorological-oceanographic data sets derived from regional reanalyses and climate change projections have proven to be particularly useful. In the following a set of coastal and offshore hindcasts complemented with climate change projections commonly referred to as coastDat is presented. Subsequently some representative examples in which coastDat data were applied to practical applications will be given. It turns out that wind waves are of interest for the majority of applications.

The coastDAT data set

The coastDat data set comprises a number of consistent meteorological-oceanographic hindcasts for the past decades of years and climate change projections for the future.

Hindcasts are generally based on the NCEP/NCAR global reanalysis (Kalnay et al 1996). The global reanalysis first was used in combination with spectral nudging (von Storch et al. 2000) to drive a regional atmosphere model covering most of Europe and adjacent seas (Feser et al. 2001) over an extended period from 1948-2007. Using data from this regional atmosphere hindcast, subsequently a number of regional marine hindcasts were provided comprising for example tide-surges (Weisse & Pluess 2006), wind waves (Weisse & Günther 2007) or thermodynamic conditions (Meyer et al 2010) in the North Sea.

Climate change projections were derived in a similar way based on existing climate change simulations with atmospheric regional climate models. So far, these are limited to an ensemble of tide-surge (Woth 2005, Woth et al. 2006) and wind wave (Grabemann and Weisse 2008) simulations for the North Sea.

A more detailed description and broader overview can be found in Weisse et al. (2009).

Coastal and offshore applications

Consistent meteorological-oceanographic data sets can be used for a variety of purposes. Most common are assessments of climate, trends or variability. Moreover such data sets may provide a useful tool for a number of practical and/or commercial applications that are not that common. In the following a few examples will be illustrated.

Optimization of ship operations profiles and design

Operation profiles of RoRo vessels operating on fixed routes in the North Sea were simulated over decades of years using environmental conditions provided by coastDat (Friedhoff and Abdel-Maksoud 2005). Operation profiles (such as velocity or power) were varied under the constraint, that operations are time critical, that is, the individual trips need to be finished within a given time window, as long as permitted by safety requirements (weather conditions). Results for a 200m RoRo vessel operating on a 332 nm round trip between Zeebrügge, Belgium and Immingham, UK are provided in Friedhoff and Abdel-Maksoud (2005) indicating that operation profiles may be optimized compared to conventional approaches minimizing operation costs and delay.

Response of a ship to design modifications is usually determined by direct simulations taking various sea states into account (Cramer et al. 2002). In case operation area and schedule are known in advance, this information may be used during the design phase to simulate the ship's behavior in environmental conditions to be expected in the area over the vessels lifetime and to optimize the design with respect to the intended operational profile. To do so, detailed wind- and wind wave information over decades of years as required which may be provided by data sets such as coastDat.

Offshore wind farms and energy use

Considerable efforts are presently underway to implement a substantial number of offshore wind farms within the German exclusive economic zone in the North Sea. For design, detailed knowledge of prevailing wind, wave, current, etc. conditions is required but often unavailable. Data bases such as coastDat provide a useful tool to derive required information such as joint probability distributions or return values of wind speed, wave heights and periods, etc. Also statistics of weather windows with wind speed and/or wave heights remaining below specified thresholds needed for planning construction phases or maintenance schemes may be determined.

When sufficiently large numbers of offshore wind farms are built they may have consequences on cost-effectiveness of conventional power plans. In Weise (2008) coastDat is used to simulate the impact of Germanys offshore wind plans on the operating efficiency and profitability of future coal-burning power plans in Northern Germany that are presently in planning phases. Provided that all presently planned offshore wind farms are finally build and the legal framework remains unchanged, (Weise 2008) concluded that there may be more effective alternatives compared to present plans of implementing future coal-burning power plans in Northern Germany.

Assessment of chronic oil pollution

The coastDat data set in combination with a Lagrangian transport model including an oil chemistry module was used to simulate and assess long-term trends in chronic oil pollution (Chrastansky et al. 2009). Chronic oil pollution predominantly results from illegal oil dumping, represents a major threat for the marine environment, but is difficult to quantify. Often the number of oil-contaminated beached birds is used as an indirect indicator. In Chrastansky et al. (2009) it is demonstrated that the latter may be misleading and that variations and trends in the number of corpses registered during beached bird surveys at the German coast primarily reflects inter-annual variability of prevailing weather conditions.

Marine energy assessment

Marine energy provided by ocean waves, tides, currents, and temperature and salinity gradients is considered to represent a significant source for renewable energy. Using coastDat an assessment was made for the German exclusive economic zone in the North Sea with strong emphasize given to wave energy (Marx 2010). Considering the high density of economic uses (shipping, fisheries, offshore wind etc.) and naturally protected areas together with technical constraints there presently remains only limited potential for marine energy uses in the German exclusive economic zone in the North Sea.

Other applications

There are a number of other applications not discussed in detail here. Examples comprise application to coastal protection, oil risk modeling, the assessment of policy regulation, interpretation of measurement data, or water quality studies. Details can be found in Weisse et al. (2009).

Summary

Apart from assessing climate, climate change and variability consistent meteorological-oceanographic reanalyses and climate change projections provide a useful tool for many practical and/or commercial applications in coastal and offshore areas. Examples comprise the use in ship and offshore wind design and planning, the assessment of chronic oil pollution and risk, or the assessment of marine energy resources. Based on the experiences with more than 40 users and commercial clients Table 1 provides an overview of the parameter most frequently requested and analyzed in major applications of the coastDat data set. It can be inferred that wind wavs are of central importance and represent the backbone of the data set when practical applications are considered. Summarizing and in addition to the analysis of existing observational data it is believed that comprehensive model-based regional climate data sets such as coastDat may provide a valuable source of information for the analysis of regional changes and the identification of options for actions especially in data sparse coastal or offshore regions.

Table 1. Parameter most frequently requested and analyzed in most frequent types of applications

Application	Wind	Wind waves	Tide-Surge	Currents	Other
Ship Design	X	X	X	X	
Offshore Wind	X	X	X	X	
Chronic Oil Pollution	X	X	X	X	
Oil Risk Assessment	X	X		X	
Marine Energy Use		X	X	X	
Coastal Protection		X	X		
Water Quality Studies				X	Temperature, Salinity
Safety of Navigation		X			

Acknowledgments

The manuscript represents an overview of the work from numerous colleagues at the GKSS Institute for Coastal Research and at different research labs and companies. Where publications were available these are referenced accordingly. Moreover I specifically wish to mention and to thank the following colleagues who substantially contributed to the success of coastDat: H. von Storch, U. Callies, A. Chrastansky, F. Feser, H. Günther, J. Marx & I. Grabemann (all GKSS Institute for Coastal Research), A. Pluess (Federal Waterways Res. and Eng. Institute), J. Tellkamp (DNV Germany), T. Stoye (Flensburger Schiffbau-Ges. mbH & Co. KG), A. Mitzlaff (IMS Ingenieursges.), D. Schrader (Federal Maritime Office), & J. Winterfeldt (now at GE Energy).

References

Chrastansky, A. et al. 2009. Environ. Pollution, **157**.

Cramer, H. et al. 2002. Final Rep. BMBF ROLL-S.

Feser, F. et al. 2001. *EOS Transactions*, **82**.

Friedhoff, B. and Abdel-Maksoud, M. 2005. *Forum Forschung*, **8**.

Grabemann, I. and Weisse R. 2008. *Ocean Dynamics*, **58**.

Kalnay, E.M. et al. 1996. *Bull. Am. Meteorol. Soc.*, **77**.

Marx, J. 2010. Masterth

Meyer, E. et al. 2010. Marine Systems, submitted.

von Storch, H. et al. 2000. *Mon. Wea. Rev.*, **128**.

Wiese, F. 2008. Masterthesis, Univ. Flensburg.

Weisse, R. et al. 2009. *Bull. Am. Met. Soc.*, **90**.

Weisse, R. and Günther, H. 2007. *Ocean Dynamics*, **57**.

Weisse, R. and Pluess, A. 2006. *Ocean Dynamics*, **56**.

Woth, K. 2005. *Geophys. Res. Lett.*, **32**.

Woth, K. et al. 2006. *Ocean Dynamics*, **56**.

Towards and empirical model of wave set up for extreme sea level assessments

Julian O'Grady ***and*** **Kathleen McInnes**
Centre for Australian Weather and Climate Research,
PMB#1 Aspendale, VIC 3195, Australia

Introduction

Global mean sea level rise and ocean based inundation from storm events are two impacts of climate change that threaten low-lying coastlines. Rising mean sea levels interact with hydrodynamic agents such as storm surge and waves to exacerbate coastal inundation. For example, McInnes et al. (2009) found with a projection of 0.47m mean sea-level rise by 2070, a one in one hundred year sea level could occur every one to three years along the Victorian coastline based on modelling of extreme sea levels due to storm surges and tides.

Wave setup can also contribute to coastal sea levels during storm surge events. Wave setup refers to the slope on the ocean surface at the coast arising from the shoreward transport of momentum from breaking waves in the surf zone. The magnitude of the setup is related not only to the incident wave height but also to the incident direction of waves relative to the coast (Hsu et al. 2006).

The relationship of extreme waves and storm surge was investigated by O'Grady and McInnes (unpublished) who found that for the southeast facing coastline of the Ninety Mile Beach in eastern Victoria, the most favourable wind conditions for storm surges were generally least favourable for high waves and wave setup at the coast and vice versa along this coastline. A preliminary modelling study (McInnes et al. 2009), in which wave and hydrodynamic models were coupled to simulate the wave setup along parts of this coastline, additionally highlighted the high resolution requirements for both data and models to simulate wave setup. They noted that such requirements would be prohibitive for large scale coastal assessments and proposed the need for simpler approaches in these circumstances.

The present paper reports on progress towards the development of an empirical wave setup model. The next section evaluates the suitability of the Simulating WAves Nearshore (SWAN) spectral wave model for simulating wave setup. It also outlines an approach to developing an empirical model for wave setup. Section 3 presents preliminary results. Conclusions and further work are discussed in the final section.

Methodology

Swan model validation

In the absence of detailed coastal measurements against which to assess the suitability of the SWAN model to simulate wave setup, the approach of Péchon et. al. (1997) is adopted in which the SWAN simulated variables are compared to laboratory results for wave transformation around a detached breakwater presented in Mory and Hamm (1997).

The SWAN model version 40.72AB was set up over the idealized region illustrated in Fig. 1 on a 30m x 30m grid. Wave setup in SWAN is estimated from the divergence of the driving force field i.e. the rotation-free part of the radiation stress gradients. The SWAN simulated wave setup, shown in Fig. 1, agrees well with the laboratory measurements (see Fig 6 of Mory and Hamm 1997). For example, at a point at the coast approximately 4 m from the breakwater the SWAN model simulates 0.0071m of setup compared to the observed setup of ~0.0075m. This close agreement occurs despite the caution by Holthuijsen (2007), that wave setup in SWAN is computed as an approximation for slow variations in the current field and therefore may not produce valid results near sharp features in the coastline or obstacles such as headlands or breakwaters.

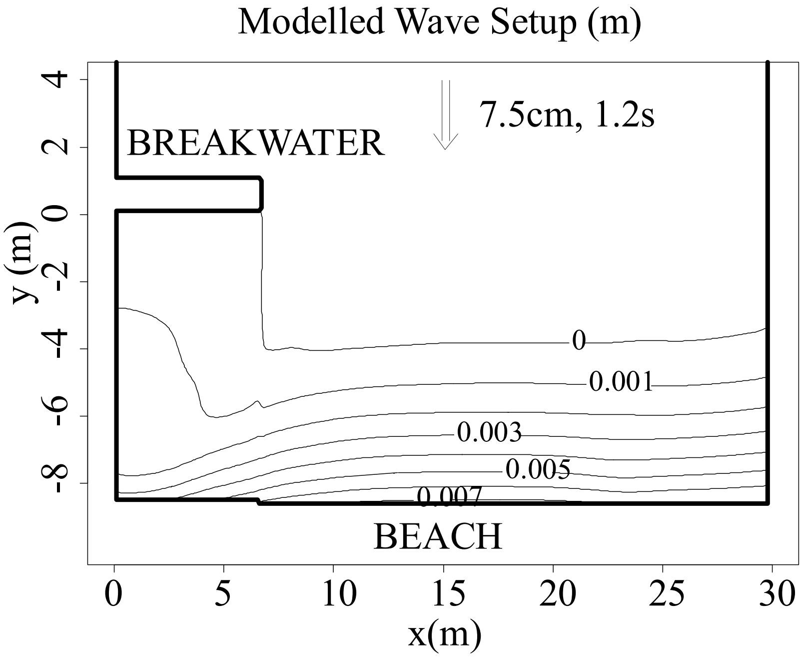

Fig. 1 Computed setup contour line (in m) – SWAN. Wave setup forced by 7.5cm, 1.2s waves from the top boundary.

Wind/wave direction experiments

In this part of the study the relationship between the magnitude of coastal wave setup to incident wind/wave direction relative to coastline orientation is investigated. An example is presented for eastern Bass Strait including the Ninety Mile Beach at 1km resolution (Fig. 2). As the waves impacting the coast are comprised of remotely generated swell as well as local wind waves, swell was specified on the lateral boundary of the outer grid. Wave measurements from the King Fish B (KFB) Oil Platform were compared to the simulated wave heights (Hs) and periods (Tp) for a range of swell conditions applied at the lateral boundary of the model grid. Simulations were conducted for four constant wind speeds (3.5, 9.5, 15.5 and 21.5 m/s) and eight directions at 45° (i.e. a total of 32 simulations) and the simulated wave heights and periods at KFB compared to observed wave heights and periods binned according to the same wind speed and direction criteria. Closest agreement between modelled and observed waves at KFB was found using values of Hs=1m and Tp= 9s on the boundary. The simulated results at KFB when weighted for the number of observations differed by an average of 4% from the observed Hs or Tp. The simulated coastal wave setup from this set of 32 runs with these boundary conditions for swell was then extracted to examine wave setup.

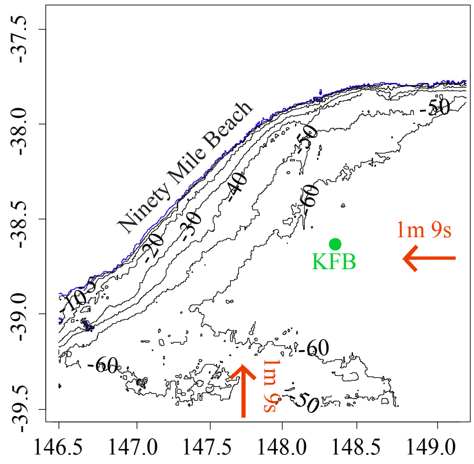

Fig. 2 Model Domain with 10m depth contours. Forced by 1m 9s swell on the boundaries

Preliminary results

Figure 3 shows the wave setup at a number of coastal points along the 2m contour of Ninety Mile Beach (grey solid lines) for all simulations undertaken with a 21.5 m/s wind. The wave setup is highest for the onshore winds (wind direction relative to the normal of coast line is 0 deg), reduces as the winds increase in angle to the shore (±90 deg) and approaches zero for off-shore wind direction (±180 deg). The coarse 250m resolution computational grid used in these simulations means that the coastline exhibits stepwise change in directions along its length. Using a coarse 1km bathymetry dataset (the highest resolution dataset available at the time of running these experiments) the model does not sample the precise coastline orientation for each grid cell leading to a spread in the simulated setup for a chosen wind direction seen in Fig. 3. The mean of all points was taken for each wind direction (dashed red line Fig. 3). This was found to be well represented by the fitting of a Gaussian distribution (dashed black line)

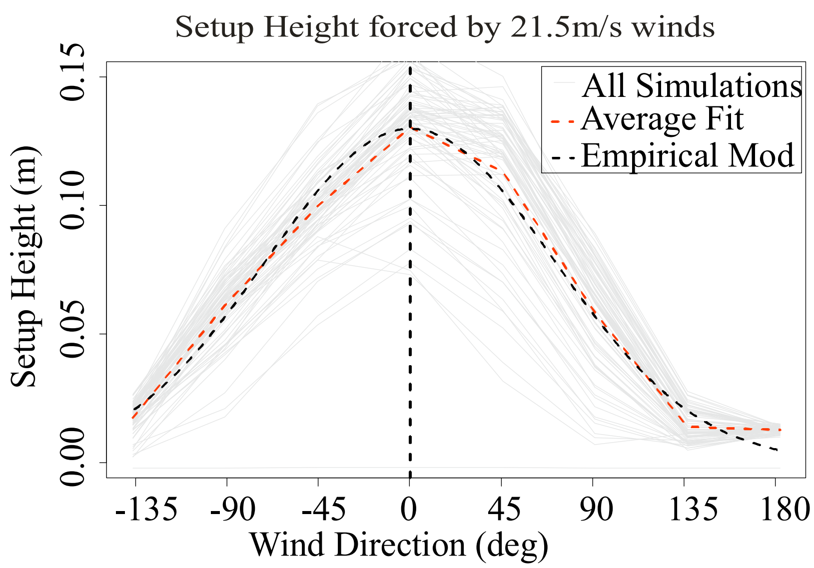

Fig. 3 Wave setup plotted against wind direction relative to the coastline orientation, 0 deg is onshore wind and ±90 deg are longshore winds.

Discussion and further work

Results presented here suggest that a simple relationship can be obtained for wave setup at the coast under a prescribed wind direction relative to the shoreline orientation. However, several features warrant further investigation. The first is that the results are based solely on parametrisations for setup within SWAN that do not account for the effect of longshore currents. These could reduce the magnitude of wave setup for obliquely incident waves which may result in a narrowing of the Gaussian distribution. An alternative approach is to couple the SWAN model to a hydrodynamic model as was done in McInnes et al, (2009). Wave setup is also sensitive to the bathymetric profile in the nearshore region which has not been adequately resolved in the experiments presented here. A new nearshore bathymetry dataset developed from a LiDAR survey of of the entire Victorian coast as part of the State Government of Victoria's 'Future Coasts Program' will be used in future modelling efforts.

References

Holthuijsen, L. H. 2007. Cambridge: Cambridge University Press. 387 pp.

Hsu T., Hsu J. R., Weng W., Wang S and Ou S. 2006. *Coastal. Eng*. 53,pp 865-877.

McInnes, K.L., Macadam, I., Hubbert, G.D. and O'Grady, J.G. 2009a. *Natural Hazards* 51 115–37. DOI 10.1007/s11069-009-9383-2.

McInnes, K.L., O'Grady, J.G. and Hubbert, G.D. 2009b. *J. Coastal Res*. SI56 1005-1009.

Mory, M. and Hamm, L. 1997. *Coastal Eng*. **31**, pp. 77–96.

Péchon, P., Rivero, F., Johnson, H., Chesher, T., O'Conner, B., Tanguy, J.-M., Karambas, T., Mory, M. and Hamm, L. 1997. *Coastal Eng*. 31, pp. 199–215

Projected future wave climate along Australia's eastern margin

Mark Hemer
Centre for Australian Weather and Climate Research,
GPO Box 1538, Hobart, TAS 7001, Australia
Kathleen McInnes
Centre for Australian Weather and Climate Research,
PMB#1 Aspendale, VIC 3195, Australia
Roshanka Ranasinghe
UNESCO-IHE, PO Box 3015, 2601 DA Delft, The Netherlands

Introduction

Sea level rise, and to a lesser extent the contribution of storm surges driven by changing storm patterns, associated with projected climate change has received increased attention along the Australian coast over recent years (Church et al. 2006). However, to date only minimal consideration has been given to how the surface wave climate will respond to projected climate conditions. The aim of this study is to provide projections of the surface ocean wave climate along the eastern Australian continental margin, to provide a suitable dataset which will aid assessment of the possible effects of climate change on coastal erosion in the region.

Methodology

Regional downscaling of global climate change projections

The Coupled Model Intercomparison Project produces large numbers of global climate model (GCM) runs which provide projections of future global climate. These models provide relatively consistent projections of global mean parameters, but at a regional scale they provide highly variable results, attributed to the coarse model resolution. Wave models require suitable surface winds as forcing, and consequently the regional flow patterns must be well represented. We take an opportunistic approach, making use of regional model runs carried out for the Climate Futures Tasmania (CFT) project (Grose 2010). Here, a variable resolution global climate model (Conformal Cubic Atmospheric Model; CCAM, McGregor and Dix 2008) is used to dynamically downscale results from the GCM's. The CFT runs dynamically downscale a number of GCM's from bias-adjusted sea-surface temperatures (SSTs) and sea-ice directly (i.e. no atmospheric forcings; Katzfey et al. 2009). CCAM is employed in a stretched mode with a resolution of ~60km over the Australian region, and much coarser on the opposite face of the globe.

In this study, an ensemble of six climate change realisations for the period 1960-2100 are taken from the 60km CFT CCAM runs. Three ensemble members with forcing from CSIRO Mk3.5, GFDLCM2.0, and GFDLCM2.1 were included under two emission scenarios (SRES A2 and SRES B1, representing high and low range emission scenarios, respectively). No perturbed physics are represented in the ensemble. We use the near-surface marine wind fields at 10m height, archived at six hourly intervals, from three 20 year time-slices (1981-2000; 2031-2050; and 2081-2100) to force the wave model.

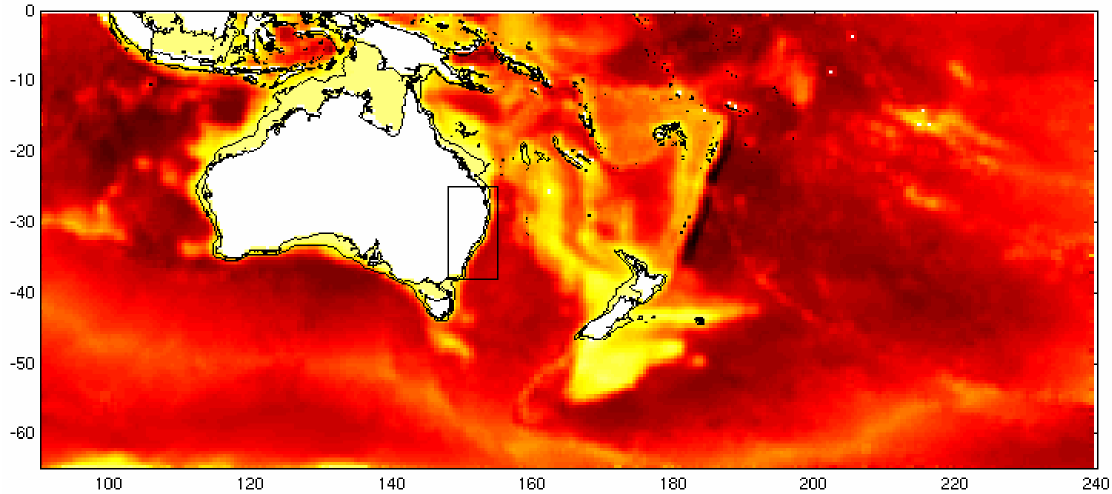

Fig. 1 Wave model grids. 0.5° WaveWatch3 model is run over whole domain. Nested 0.1° SWAN model is run over boxed domain). Colours represent bathymetry.

Surface wind bias adjustment

Surface winds derived from the CCAM model under present climate conditions are found to differ significantly from observed and re-analysis derived surface winds. Adequate wave hindcasts have been derived previously using NCEP re-analysis (NRA) surface winds (e.g. Swail et al. 1988). To ensure a wind field consistent with present climate , CCAM surface winds are bias adjusted using a quantile adjustment procedure, by mapping the joint probability distribution of eastward (u) and northward (v) wind components of the 1981-2000 CCAM winds onto the distribution of the 1981-2000 NRA winds, at each grid cell. To obtain adjusted projected winds, future CCAM wind distributions are adjusted according to the same bias adjustment matrix as for the present climate (i.e. the bias adjustment is assumed to be stationary).

Wave model

The response of the wave climate to projected climate change scenarios is investigated using numerical wave models. The WaveWatch 3 model (version 2.2; Tolman 2002) was implemented on a 0.5° x 0.5° lat-lon grid over the domain 90° - 240°E, 65° - 0°S, spanning the Australia and South-West Pacific region. The wind fields from the climate simulations were bi-linearly interpolated onto this grid. Nested within this was a 0.1° x 0.1° resolution SWAN model (Booij et al. 1999) spanning 150° - 155°E, 38° - 25°S as the region of interest along the NSW coast (Fig. 1). Wave spectra were calculated with a directional resolution of 15° and at 25 frequencies ranging non-linearly from 0.04 Hz to 0.5 Hz. Seasonally varying sea-ice conditions were derived from the National Snow and Ice Data Center climatology and were assumed to remain constant for each time-slice. A benchmark model run was initially carried out, forced with NRA 10-m surface winds for the 1981-2000 period. Best model to buoy wave height and period comparisons in the SWAN model were obtained using the white- capping parameterisation described by Rogers et al (2002). Else, default parameters were defined for each model.

Results

As each GCM realization is as likely as another, we derive ensemble means from each of the following 3-member ensembles, as representative of the wave climate for the given scenario. These ensemble sets are:

- NRA benchmark run (1981-2000).
- Present climate (1981-2000). 3 members.
- Mid century (2031-2050), B1 scenario. 3 members.
- Mid century (2031-2050), A2 scenario. 3 members.
- End century (2081-2100), B1 scenario. 3 members.
- End century (2081-2100), A2 scenario. 3 members.

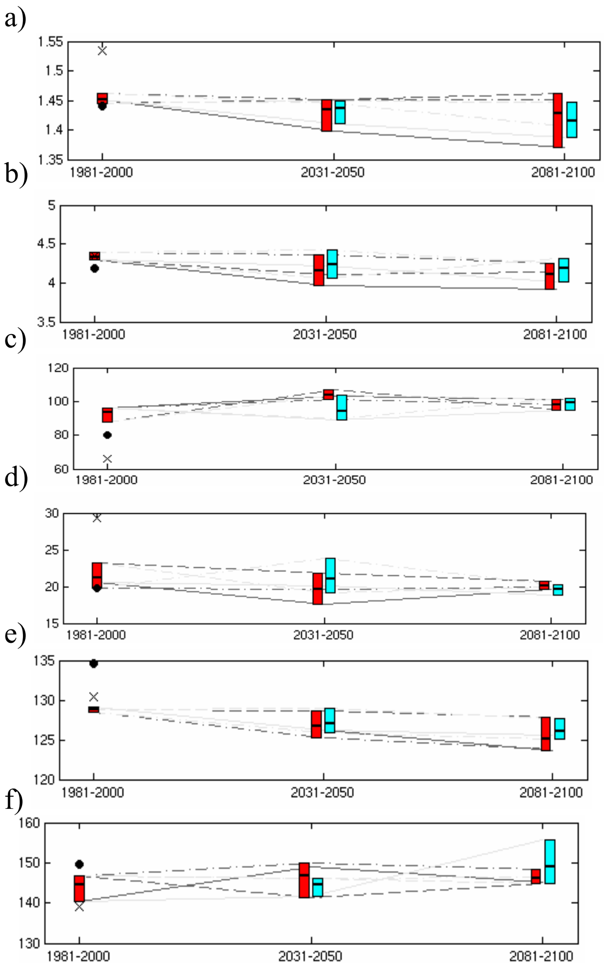

Fig. 2 Sydney projected wave climate: a) 50th percentile of Hs (m); b) 99th percentile of Hs (Hs99, m); c) Number of exceedances of Hs99; d) DUR (hrs); e) mean WDir (°N); f) mean WDir of large wave events (°N). Red (blue) bars indicate A2 (B1) scenario ensembles; Horizontal line represents ensemble mean, Cross - benchmark model, solid circle - buoy data.

Wave model height and direction parameters derived from these ensembles were compared with buoy derived parameters at seven sites (Gold Coast, Byron Bay, Coffs Harbour, Crowdy Head, Sydney, Port Kembla and Batemans Bay). Analysis was limited to significant wave height (Hs), wave direction (Dir), and number (N), duration (DUR) and intensity (I) of large wave events (defined as when Hs exceeds the 99th percentile). Projections of the Sydney wave climate are shown in Fig. 2; these are qualitatively consistent with other sites along the NSW coast.

Discussion and concluding remarks

Projected change in the high emission A2 scenario projections are larger than for the low emission B1 scenario. The ensemble mean projects robust change of Hs decrease, and anti-clockwise rotation of wave direction. However, the magnitude of Hs change of less than 5cm, and of mean and large wave Dir of approximately 5° at these offshore locations (~100m depth) is likely too small to influence the coastal environment. The CSIRO Mk3.5 model (shown by the solid line in Fig. 2) leads to largest projected change. Projected wave climate determined from this regional study is qualitatively consistent with available global wave climate projections in this region (Wang and Swail 2006). To avoid substantial effort for individual regional studies, we propose effort be placed in global projections. Both statistical and dynamical projection methods should be used to produce an increased number of wave projection ensembles that correspond to climate projections from different GCMs for different emission scenarios, allowing an assessment of all three levels of uncertainty (associated with forcing, GCMs, and wave projections, respectively) (Hemer et al. 2010).

References

Booij, N., Ris, R.C. and Holthuijsen, L.H. 1999. *JGR-Oceans*, **104**, C4, 7649-66.

Church, J.A., Hunter, J.R., McInnes K.M. and White N.J. 2006. *Aust. Met. Mag.,* **55**, 253-60.

Grose, M. 2010. *ACECRC Technical Report, Hobart, Tas*., 36pp.

Hemer, M.A., Wang, X.L., Church, J.A. and Swail, V.R. 2010. *BAMS,* **91**.

Katzfey, J.J., McGregor, J., Nguyen, K. & Thatcher, M. 2009. *Proc. 18th World IMACS/MODSIM Congress, Cairns*, 3942-7.

McGregor, J.L. and Dix, M. 2008. *In K. Hamilton & W. Ohfuchi (eds), Springer*, 51-76.

Rogers, W.E., Hwang, P.A. and Wang, D.W. 2002. *J. Phys. Oceanog.,* **33**, 2, 366-89.

Swail, V.R., Cardone, V.J. and Cox, A.T. 1988. *5th Int. Workshop Wave hindcasting and forecasting*.

Tolman, H. 2002. *NOAA/NWS/NCEP/MMAB Technical Note* **222**, 133pp.

Wang, X.L. and Swail, V.R. 2006. *Climate Dyn.* **26**, 109-26.

Observations and modelling of waves along the southwest WA coast

Charitha Pattiaratchi and Cyprien Bosserrele
*School of Environmental Systems Engineering and The UWA Oceans Institute,
The University of Western Australia, 35 Stiring Highway,Crawley WA 6009*

Introduction

Global wave climate results from the action of wind and storm activity. Thus any changes in the ocean wind climate and storm activity (number and severity) will have influences on the wave climate which in coastal regions are the dominant forcing mechanism of beach sediment transport and thus beach stability. To examine long-term (e.g. decadal) changes we require sustained long period observations. Along the West Australian coastline, although wave measurements have been sporadically since the mid 70's, long-term measurements were only available since 1993 (Rottnest Island), a period of less than 20 years. With the availability of re-analysis atmospheric datasets (e.f. NCEP, ERA-40) it is possible to extend the periods of these data records through the use of numerical modeling.

The offshore wave climate in the region is dominated by moderate energy swell from the south to southwest, and a variable wind wave climate is superimposed on the background swell (Masselink and Pattiaratchi 1999). Sea breezes have a strong influence on the offshore wave conditions during summer, therefore the prevailing wave direction is south to southwest. Offshore waves during summer have predominantly low period (less than 8 s) in the range of 1-2 m (Lemm et al. 1999). Northwesterly to southwesterly storm waves occur during the winter months, and the offshore wave climate is characterised by high period (more than 8 s) swell and storm waves of 1.5-2.5 m (Lemm et al. 1999). Hence, for the study area, there is a distinctive offshore wave climatic shift from moderate, locally generated seas in summer to higher, distantly generated swell in winter. A background swell above 0.5 m was found to be present all year round (Lemm et al. 1999). The wave climate also exhibits strong inter-annual variability.

Hemer et al. investigated seasonal and inter-annual and historical trends in waves around Australia. For South Australia, a strong positive correlation between the Southern Annular Mode index and storm activity associated with an anticlockwise shift in wave direction (i.e. more southerly) was found. This correlation is a result of the intensification of the Southern Ocean storm belt associated with SAM index (Marshall 2003). The shift southward of the storm belt also reduces the exposure to waves of the region located further north (e.g. Rottnest). Some IPCC climate models are predicting a positive trend in SAM index that could lead to an increase in activity on the storm belt and more southerly waves can be expected for Western Australia.

To examine the long-term variability in wave climate and its influence on beach stability a series of models are being developed which includes simulating the southern Indian Ocean using WaveWatch3 (WW3) and higher resolution models using SWAN and XBEACH.

Methods

WAVEWATCH III (Tolman 2009) and SWAN (Booij et al. 1996) wave models are be used to simulate the offshore and inshore wave climate. WAVEWATCH III is the operational ocean wave prediction model for the National Oceanic and Atmospheric Administration (NOAA). It is a third generation wave model that solves the random phase spectral action density balance equation for wavenumber-direction spectra (Tolman 2002). Although WW3 can simulate wave in the inshore, the Simulating Waves iNshore (SWAN) (Booij et al., 1999) model provides a more suitable alternative for the coastal zone. Based on the same principles as WW3, SWAN provides focus more on inshore wave process, such as wave setup and diffraction. SWAN can also be run on an unstructured grid which allows areas of interest to be modelled in high resolution, without compromising run times.

WAVEWATCH III grids used in the current study is shown on Fig. 1. A series of 4 model grids are used with different resolution: (1) One degree resolution grid covers the entire southern Indian Ocean; (2) 30’ in the southern ocean where we receive majority of the storms;i.e. the generating region (3) 30’ in the along the outer WA coast; and (4) 10’ grid encompasses the WA coast (Fig. 1).

The model is forced by NCEP winds at 6 hourly intervals have a resolution of 2.5^{o}.

Results

The WAVEWATCH III model has been run for the period 1990 to 1998 (and ongoing) and this period overlaps with the measured data off Rottnest Island (off the south-western Australia) located in 50m of water. Comparison between the observed and predicted time series is shown on Fig. 2. At this initial stage a very good correspondence has been achieved with the WAVEWATCH III model predicting the majority of the major storms observed at the Rottnest wave rider buoy.

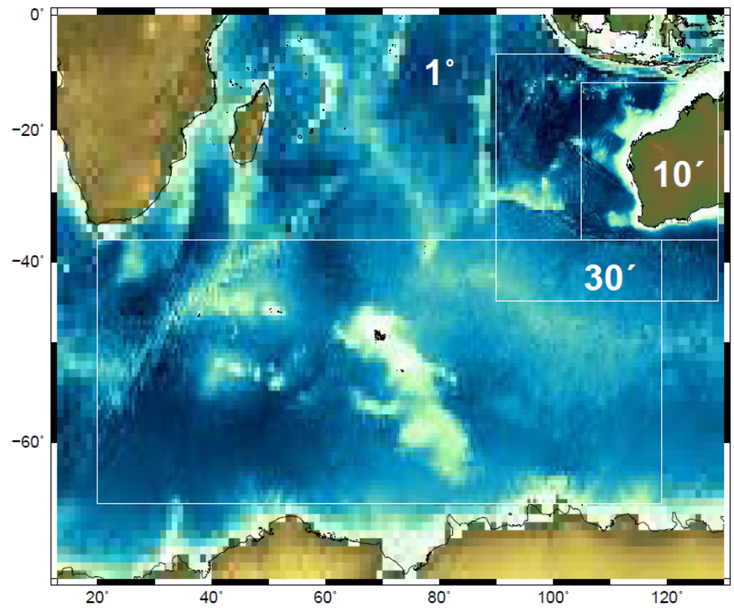

Fig. 1 WAVEWATCH III grids:

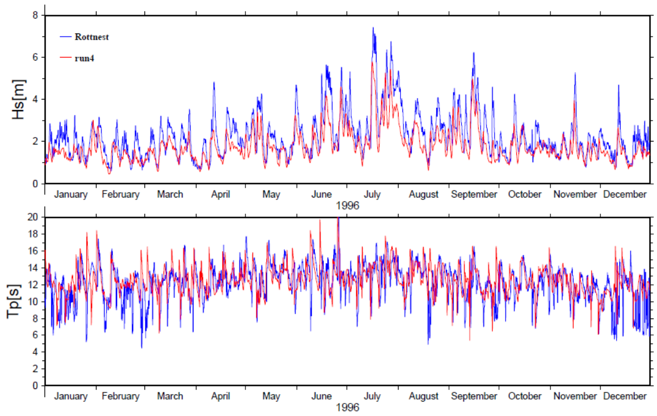

Fig. 2 Time series of observed (blue) and predicted (red) wave heights and periods at the Rottnest Island.

In the past 20 years, 1996 has been generally recognised as being one of the stormiest with a series of large storms impacting on the coast. With a view of examining the generation of large wave heights (to 8m at Rottnest), the WAVEWATCH III model was used to simulate the storm events (Fig. 3). Initially (0000 22/07/1996), the storm was generated in the middle of the Indian Ocean (Fig. 3a) and begins to propagate westward (0300 23/07/1996), increasing in size and the wave heights at the centre of the storm exceeding 10m (Fig. 3b). Subsequently (1800 23/07/1996), although the storm is still propagating westward it decreases in size and the swell generated by the storm approaches the WA coast (Fig. 3c). The South West Coast of WA is impacted by large waves (0600 24/07/1996), while the storm losses most of it's energy. (Fig. 3d) and then (1800 24/07/1996), storm is too weak to generate more waves but a significant residual swell affect most of WA's coast (Fig. 3f).

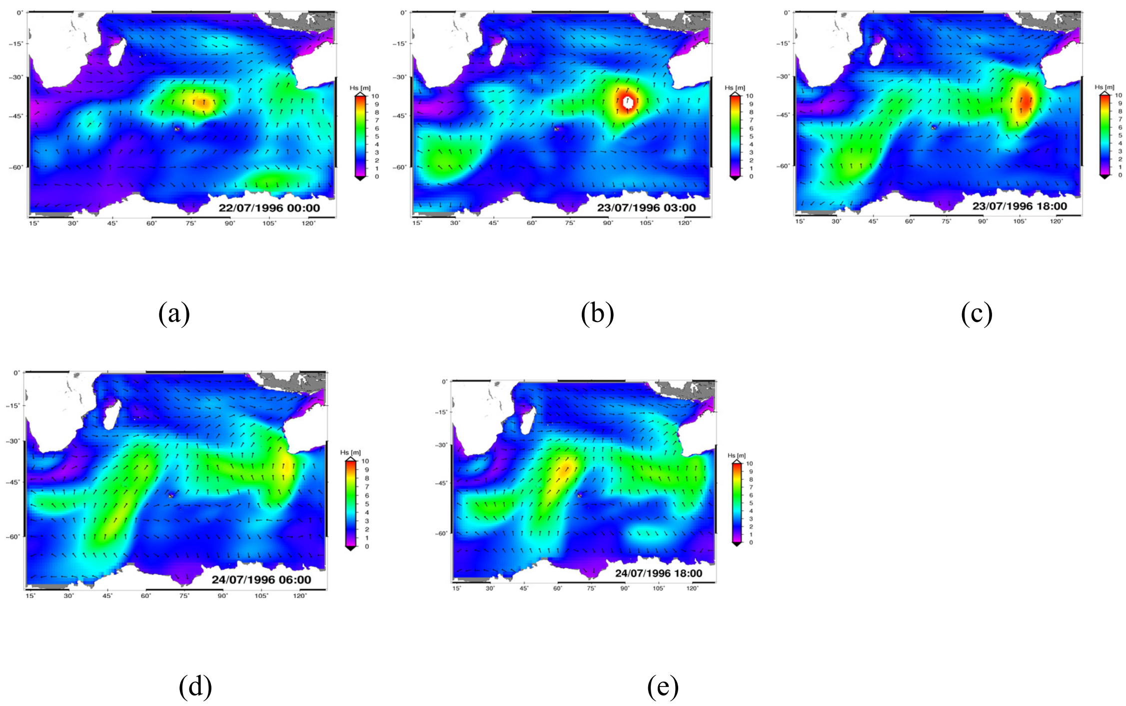

Fig. 3 Timeseries of storm generation 22-24 July 1996

References

Booij, N., Ris, R.C. and Holthuijsen, L.H. 1996. *J. Geophysical Research*, **104**, 7649-66.

Hemer, M., McInnes, K., Church, J., O'Grady, J. and Hunter, J. *Final report for Dept. of climate change.*

Lemm, A., Hegge, B. and Masselink, G. 1999. *Marine and Freshwater Research*, **50**, 92–102.

Marshall, G. 2003. *J. of Climate,* **16,** 4134-43.

Masselink & Pattiaratchi. 2001. *Marine Geology*, **146**, 115–35.

Tolman, H. L. 2002. NOAA / NWS / NCEP / OMB Technical Note Nr. **213**.

Tolman, H.L. 2009. NOAA / NWS / NCEP / MMAB Technical Note **276**, 194 pp.

Dynamical downscaling of waves in the Pacific

Jack Katzfey
Centre for Australian Weather and Climate Research,
CMAR, PMB No.1, Aspendale, VIC 3195, Australia

Introduction

The Pacific Climate Change Science Program (PCCSP) is a component of the $150 million International Climate Change Adaptation Initiative, managed by the Department of Climate Change (DCC) and AusAID. The PCCSP will provide the climate science needed for adaptation to climate change in the Pacific. The program will be complemented by a vulnerability assessment program also being undertaken under the ICCA.

A component of the PCCSP is to downscale six global climate models (GCMs) from the IPCC CMIP3 using the Cubic Conformal Atmospheric Model (CCAM) at 60 km horizontal resolution. Output from these runs is then being used to drive the Wave Watch 3.14 wave model (WW3) in order to assess possible changes to the wave climatology for the region. This paper describes the methodology used to downscale and some preliminary results.

These higher resolution simulations will provide a more detailed depiction of current and projected future climate in the region. As well as feeding into impact and adaptation assessment directly, the output of the high resolution modeling will be used for tropical cyclone assessment, and in more detailed studies of changes to wave climate, with production of additional very high-resolution runs focussed on individual islands in the region.

Model description and experimental design

CCAM (McGregor and Dix 2008) is a semi-Lagrangian, semi-implicit primitive equations atmospheric model that includes a fairly complete set of physical parameterizations.

The main criterion for choice of GCM to initialise CCAM was that it have credible interannual variability and suitable seasonality over Australia. Smith and Chandler (2010) carried out analyses of the GCMs included in the Intergovernmental Panel on Climate Change (IPCC) Fourth Assessment Report (Meehl et al. 2007), assessing their performance in reproducing a range of metrics over the Australian continent. The Geophysical Fluid Dynamics Laboratory (GFDL) CM2.1 model performed well and is used in this study. Runs with other GCMs are planned for the future.

The next choice is the grid spacing and resolution of the downscaling model (CCAM). Due to the large area of interest for the PCCSP and the requirement to have the region at approximately 60km resolution, CCAM was run with a quasi-uniform global grid shown in Fig. 1.

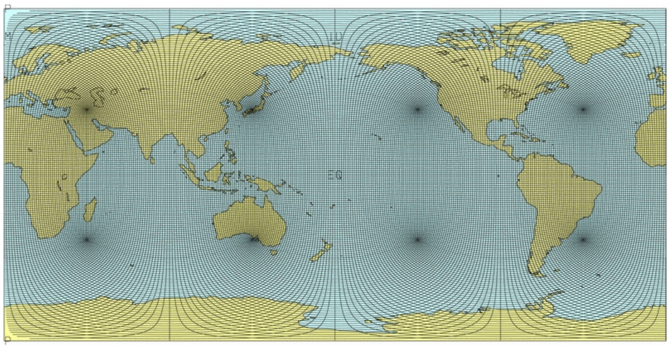

Fig. 1 Sample of grid used in CCAM simulations.

The CCAM simulation was driven by interpolated monthly SSTs and sea-ice cover provided by the GCM. Since GCMs tend to have biases in SSTs relative to observed climatologies, see especially in the tropics, the next step was to correct these biases, using a technique based on that of Reynolds (1988) (see Fig. 2), first, the monthly climatologies of the GCM SSTs were computed for the current climate (1961-2000). For each month, the GCM SST bias relative to the observed SST was computed. Then, the monthly bias was subtracted from the GCM SST field for each month before using the values in the downscaled simulation. Using this technique, the monthly climatology of the SSTs for the current climate in the downscaled simulation are the same as observed, while the inter- and intra-annual variability is the same as the host GCM. Since the monthly bias correction is unchanged throughout the run, both the interannual variability and climate change signal of the GCM SSTs are not altered.

The wave model used in this study is the NOAA Wave Watch model, version 3.14 (Tolman 2009). Winds and ocean depths from the CCAM 60 km model were interpolated to a .5° longitude-latitude grid every 6 hours to drive the wave model. The observational dataset used is the corrected ERA40 wave reanalysis (CERA) for the period 1981-2000 (Sterl and Caires 2005)(Caires and Sterl 2005).

Preliminary results

A regional climate simulation using the above configuration has been completed for the period 1961-2100. Winds from this simulation were used to drive the WW3 wave model for the periods 1970-1999 and 2080-2099. Results of the comparison of the simulated wave climatology for the period 1970-1999 with the climatology of the CERA dataset for 1981-2000 are given in Fig. 3. The annual mean significant wave height shows that some larger waves in mid-latitudes in the CERA dataset are captured to some extent by the simulation. However, there appear to be significant boundary effects (reduced wave heights along the edges of the field, especially at the eastern boundary).

However, if one compares the maximum 99-percentile significant wave height, the pattern and magnitudes look more similar, though there is still some degradation along the eastern boundary.

The preliminary climate change results for the annual mean significant wave height and the maximum 99-percentile significant wave height are presented in Fig. 4. Decreases in wave height are evident over most of the simulated Pacific basin. However, the 99-percentile extreme significant wave heights do show some increases over the eastern portion of the domain.

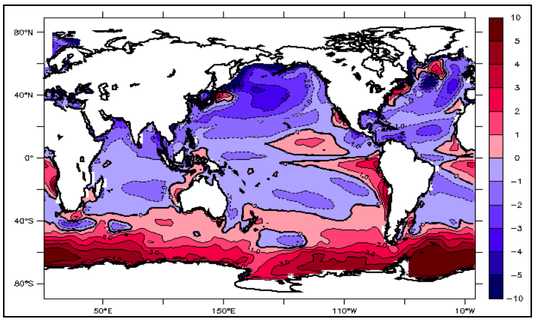

Fig. 2 January sea surface temperature bias for GFDLCM2.1 global coupled model (K).

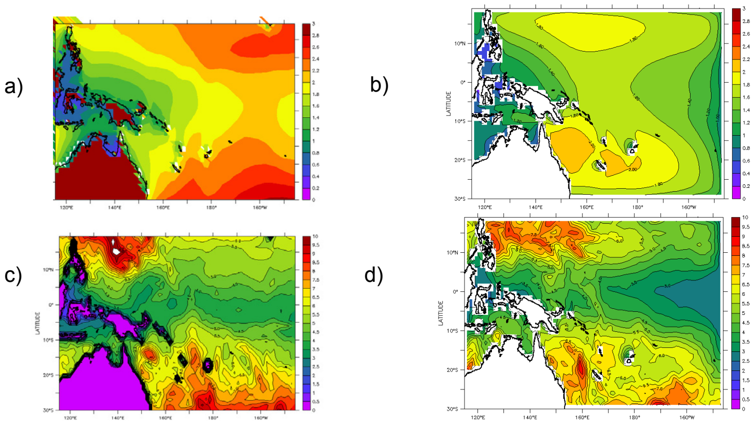

Fig. 3 Annual mean significant wave height (m, scale from 0 to 3 m) from a) CERA dataset and b) CCAM simulation for 1970-1999. Annual maximum 99 percentile significant wave height (m, scale from 0 to 10 m) for c) CERA dataset and d) CCAM simulation.

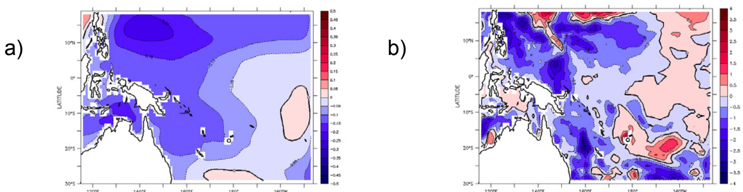

Fig. 4 Changes (2080-2099 minus 1970-1999) in CCAM simulated a) annual mean significant wave height (m, scale from -.5 to .5 m); b) maximum 99 percentile significant wave height (m, scale from -4 to 4 m).

Summary

This paper presents preliminary results of using a regional climate model to drive a wave model to assess the possible changes in waves in the Pacific due to climate change. Initial runs suggest a larger domain needs to be considered, but results are promising. Initial climate change results show possible decreases in wave heights, though some increase in extreme waves are possible in the eastern portion of the equatorial Pacific. A more thorough analysis will be presented at the workshop.

Acknowledgments

Author acknowledged the financial support of the Department of Climate Change and Energy Efficiency and AusAID. Thanks also to Mark Hemer for help with setting up the wave model

References

Caires, S. and Sterl, A. 2005. A new non-parametric method to correct model data: Application to significant wave height from the ERA-40 reanalysis. *J. Atmospheric and Oceanic Tech.*, **22**(4), 443-59.

McGregor, J. L. and Dix, M. R. 2008. An updated description of the Conformal-Cubic Atmospheric Model. In *High Resolution Simulation of the Atmosphere and Ocean*, eds. K. Hamilton and W. Ohfuchi, Springer, 51-76.

Meehl, G. A., Stocker, T.F., Collins, W.D., Friedlingstein, P., Gaye, A.T., Gregory, J.M., Kitoh, A., Knutti, R., Murphy, J.M., Noda, A., Raper, S.C.B., Watterson, I.G., Weaver, A.J. and Zhao, Z.-C. 2007. Global Climate Projections. In: *Climate Change 2007: The Physical Science Basis*. Contribution of Working Group I to the Fourth Assessment Report of the Intergovernmental Panel on Climate Change [Solomon, S.,D. Qin, M. Manning, Z. Chen, M. Marquis, K.B. Averyt, M. Tignor and H.L. Miller (eds.)]. Cambridge University Press, Cambridge, United Kingdom and New York, NY, USA.

Reynolds, R. W. 1988. A real-time global sea surface temperature analysis. *J. Climate*, **1**, 75-86

Smith, I. and Chandler, E. 2010. Refining rainfall projections for the Murray Darling Basin of south-east Australia-the effect of sampling model results based on performance, *Climatic Change*, in press.

Sterl, A. and Caires, S. 2005. Climatology, Variability and Extrema of Ocean Waves - The Web-based KNMI/ERA-40 Wave Atlas. *Int. J. Climatol.*, **25**(7), 963-77, doi: 10.1002/joc.1175.

Tolman, H. L. 2009. User manual and system documentation of WAVEWATCH III™ version 3.14. NOAA / NWS / NCEP / MMAB Technical Note 276, 194 pp + Appendices.

Decadal wave climate variability and implications for interpreting New South Wales Coastal Behaviour

Ian D. Goodwin and Rhaelene Freeman
Environmental Science and Climate Futures at Macquarie, Macquarie University, 2109, NSW, Australia

Karen Blackmore
Environmental Science, Macquarie University, 2109, NSW, Australia

Introduction

Decadal to multi-decadal trends in shoreline recession or progradation are apparent in observed shoreline and dune scarp position time series on the New South Wales Coast over the past century. In a broad context, these trends have been associated with the Interdecadal Pacific Oscillation (IPO)(Goodwin 2005) which also modulates sea-level anomalies (Holbrook et al. 2010). Modal wave climate on all time scales comprises both a 'storm-wave' component and a 'mean-state component' and the relative contributions of these components on shoreline stability, cross-shore and longshore sand transport (Fig. 1) requires resolution for understanding coastal processes and for model development.

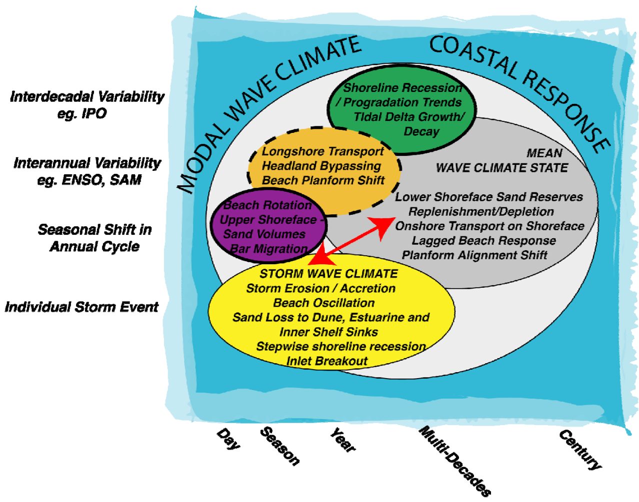

Fig. 1 Conceptual diagram linking the components of modal wave climate and different time scales with the associated coastal behavior responses.

Directional waverider buoy data along the NSW and south-east Queensland coast spans only one of the recent IPO phases (El Nino-like phase from 1977 – 2007). Hence, the shelf and shoreface wave climate during the prior La Nina-like phase from 1946 to 1976 is poorly defined.

This paper investigates the modal wave climate change between IPO phases by using an approach based on synoptic typing of monthly sea-level pressure (SLP) NOAA-NCAR Reanalysis (NNR) data, calibrated to directional wave climate data from the Sydney and Byron Bay buoys.

Wave climate hindcasting

Numerical reanalyses of the meteorological archive data back to 1948 have been applied to force global wave models to generate monthly wave statistics (Sterle and Caires 2005). These global wave model data, and recent satellite altimeter-derived wave data, have been used to establish a wave climatology for the past half century in the Australian region (Hemer et al.) have also used global wave data for the Tasman Sea region derived from ERA-40 reanalyses to investigate the wave-forcing of temporal coastal behaviour at Narrabeen-Collaroy in Sydney. They found significant biases in the offshore wave model data when compared to mid-shelf-located, buoy data.

Previously (Blackmore and Goodwin 2008) and in this study we have used an alternative approach to provide hindcast wave climate based on the variability of synoptic sea-level pressure (SLP) types in the Tasman Sea region. (Goodwin 2005) hindcast mean wave direction (MWD) for the Sydney mid-shelf location back to 1878 and found that southerly/easterly MWD is significantly correlated to sea-surface temperature (SST) anomalies in the southwest Pacific, and that the MWD variability is modulated by phases of the IPO. For the western Tasman Sea region, the IPO preferentially reinforces La Nina (El Nino) wave climate during IPO –ve (La Nina-like) and +ve (El Nino-like) climate phases. More recently, (Hemer et al.,Hemer et al. 2009) have supported these findings that the Tasman Sea wave climate is sensitive to variability in the ENSO signal, in addition to the rotation of the Southern Ocean generated swell associated with variability in the Southern Annular Mode (SAM).

We used synoptic typing of monthly NNR SLP data, calibrated to monthly mean statistics from the buoy data, to develop multi-decadal time series based on the recent IPO phases (Folland et al.). We calculated the annual wave climate cycle for MWD, Hsig and Hmax for each IPO phase, using the frequency of ST's per month. The annual cycle in Sydney MWD for the two IPO phases is shown in Fig. 2. A second approach was to generate randomized time series for the wave climate parameters, by drawing on the probability distribution of instrumental wave climate parameters for each ST.

Available historic data was sampled in order to generate a historic monthly mean wave direction (MWD) time series for the period from January 1948 to December 2007. This task was completed using seasonal probability distributions and the frequency of occurrence of synoptic types (STs). Firstly, probability distributions for each season (JFM, AMJ, JAS, OND) for each of the twelve (12) identified STs were created. In all, 48 distributions were created.

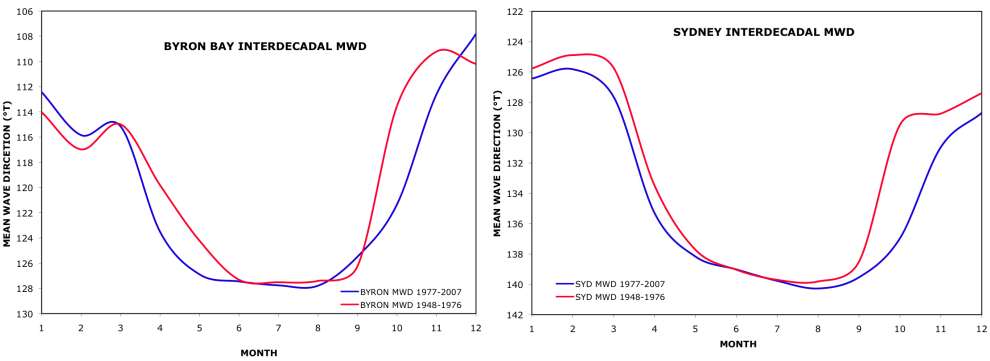

Fig. 2 Mean interdecadal MWD plots showing the different annual cycles for the two IPO phases (1948-1976, 1977-2007) at Sydney and Byron Bay. These were hindcast using the synoptic typing approach and mean monthly buoy statistics.

The time series of monthly STs for the period from January 1948 to December 2007 was then populated with a MWD value drawn from the associated probability distribution. For example, the mean ST for January 1948 was ST10. Thus, a value was randomly drawn from the probability distribution for ST10 occurring in summer (JFM).

In some cases, sample data was not available for STs in all seasons. If an ST in the time series occurred in a month with no sample probability distribution to draw from, a value was randomly selected from all possible values for that ST. In this way, all months in the 1948-2007 time series were populated with a MWD value.

The above process was arbitrarily repeated 100 times for validation purposes. This ensures that the generated time series is not affected by random permutations.

Mean multi-decadal wave climate variability

The annual cycle in MWD at both Sydney and Byron Bay is most variable between IPO phases during Spring where interdecadal MWD varies by up to 8°. This is forced by synoptic variability between anticyclonic intensification forcing a more easterly component, and southern Tasman Lows forcing a more southerly component.

Coastal response to multi-decadal wave direction variability

Historical shoreline change in northern NSW indicates that shoreline planform alignment and curvature responds on an interannual to interdecadal time scale in phase with the IPO driven MWD variability. In contrast, historical bathymetric change on the shoreface at the same sites in northern NSW indicates that trends in sand volume replenishment and depletion may lag the IPO driven MWD, longshore sand transport and headland bypassing variability.

Conclusions

The hindcasting of mean wave climate parameters using a synoptic typing approach, that is supervised for each location using the probability density distributions from buoy data, can be used to determine the magnitude and seasonality of wave climate change between multi-decadal climate phases. The approach has been used to investigate shifts in the mean wave climate state, but further work is required to investigate the coupled storm wave climate variability, such that the forcing of coastal process variability can be explored.

References

Blackmore, K. and Goodwin, I.D. 2008. *Newcastle Innovation Technical Report*, 91.

Folland, C.K., Renwick, J.A., Salinger, M.J. and Mullan, A. B. *Geophys. Res. Letters* **29**/13, 21-1-21-4 doi: 10.1029/2001GL014201.

Goodwin, I. D. 2005. *Int. J. Climatol*.,**25** 1715-29.

Harley, M.D., Turner, I.L., Short, A.D. and Ranasinghe, R. 2009. Int J. Climatol., 10.1002/joc.1962.

Hemer, M.A., Church, J.A. and Hunter, J.R. *J. Coastal Res.,* **50**, 432-7.

Hemer, M.A., Church, J.A. and Hunter, J.R. 2009. *Int. J. Climatol.* DOI: 10.1002/joc.1900.

Holbrook, N.J., Goodwin, I.D., McGregor, S., Molina E. and Power, S.B. 2010. *Deep-Sea Res*., (in press).

Sterle, A. and Caires, S. 2005. *Int. J. Climatol*., **25**/7, 963-77.

Development of a wave classification scheme to examine climate variability and nearshore response

Kristen D. Splinter and Aliasghar Golshani
Griffith Centre for Coastal Management,
Griffith University, Gold Coast Campus, Southport, QLD 4216, Australia

Introduction

Nearshore response to changing wave conditions, both at the short-term (storm) and long-term (climate) time scales, can be observed through temporal variations in shoreline position and orientation. Approximately 500,000 m^3/yr of sand is estimated to travel northwards past the Gold Coast, however, several studies (Delft Hydraulics Laboratory 1992, Patterson 2007) have shown this can vary considerably along the coast and from year to year. Gradients in longshore transport (both spatially and temporally) can play a significant role in temporal variations of the shoreline, thus understanding the driving mechanisms (breaking wave characteristics) and their variability are key to predicting future shoreline change.

The roughly east-facing coast is exposed to energetic wave conditions throughout the year. South-East ground swell is the predominant wave signature, however, isolated events such as East-Coast Lows (ECL) and tropical cyclones (TC) also contribute to the large longshore drift. Wave models, such as NOAA's Wave Watch III (WWIII) and ECMWF's ERA reanalysis provide offshore wave data at roughly 6-hr intervals and can be used as offshore boundary conditions in nearshore spectral models to estimate wave breaking conditions. However, running spectral wave models in near real time requires large computational costs and in most cases is redundant given that offshore wave conditions are often repeatable and can be grouped based on similarities in wave properties, thus reducing the number of individual model runs drastically.

Here we first develop a method to classify the yearly offshore wave climate into distinct bins (classes) describing the various forcing mechanisms. Compared to joint pdf methods, the classification scheme considers the three parameters (wave height, H_s, wave period, T_p, and mean wave direction, θ) as a single entity and provides a succinct way of describing a yearly wave climate (composed of 100s of observations) into a much more manageable number of approximately 10 classes.

Methodology

Yearly offshore wave climates from 1958-2009 are calculated using the C-ERA-40 (1958-2001) (Caires and Sterl. 2005) and ERA-Interim (1989-present) data sets. Caires and Sterl (2005) noted that the original ERA-40 model (1958 – 2001) under-estimated large waves compared to measured data and applied a correction factor to the ERA-40 wave heights resulting in a corrected data set known as the C-ERA-40. To extend the data set beyond 2001, over-lapping time series (n = 18992) between the initiation of the ERA-Interim reanalysis and the C-ERA-40 data sets were used to determine a non-linear correction factor for the ERA-Interim wave heights using a Generalized Additive Model (GAM) technique (Fig. 1).

(a) (b)

Fig. 1 Nonlinear correction for ERA-Interim data based on comparison of 18992 data points using GAM model. Solid line idicates nonlinear correction coefficient and dashed lines are the 95% confidence intervals. Vertical hash marks along the x-axis indicate data values used in fit; b) Comparison of C-ERA H_S and C-ERA-Interim Hs based on nonlinear correction. R^2=0.92.

Wave classes for each year are determined using the method of Bagirov (2008), whereby a collection of data is clustered into unique subgroups based on similar properties using a modified global *k*-means algorithm. The clustering method assumes that each cluster, or class, can be identified by its centroid, $x^j(H_s,T_p,\theta)$. The minimization problem is based on the distance between the centroid and all data points within that year:

$$\psi_k\left(X,w\right)=\frac{1}{m}\sum_{i=1}^{m}\sum_{j=1}^{k}w_{ij}\left\|x^j-a^i\right\|^2, \tag{1}$$

where $X = (x^1, x^2, \ldots, x^k)$ is the family of all cluster centroids. a^i represents the i^{th} data point (H,T,θ) and w_{ij} is a weighting function equal to 1 when a^i is within the j^{th} cluster and 0 elsewhere. As wave energy and power are both a function of H^2 and large waves have a substantially larger impact on nearshore processes, Bertin et al. (2008) suggest the distance minimization equation should be modified such that (x^j, a^i) =f (H^2, T, θ).

The solution is initially seeded with the global mean, $y^1=\left(\bar{H}_s,\bar{T}_p,\bar{\theta}\right)$ so all data belongs to this initial cluster. We assume every data point as an initial guess at the next centroid, y^2. Through an iterative process, data points are assigned to clusters based on minimization of the distance matrix. New estimated centroids for $Y = (y^1,\ldots,y^k)$ are calculated based on the updated clusters and the process repeated until no more data points move between clusters. We then set X=Y, increase k = k+1 and repeat the process until our stopping criteria is met:

$$\frac{f^{k-1}-f^k}{f^1}<\varepsilon \tag{2}$$

Where

$$f^k(x^1,\ldots,x^k)=\frac{1}{m}\sum_{i=1}^{m}\min_{j=1,\ldots,k}\left\|x^j-a^i\right\|^2. \tag{3}$$

The final result is a set of *k* wave classes per year. Each class is then shoaled and refracted into the nearshore using MIKE21 SW. Breaking conditions at 8 locations along the Gold Coast (Fig. 2) are used to estimate longshore transport potential and describe the spatial and temporal variability.

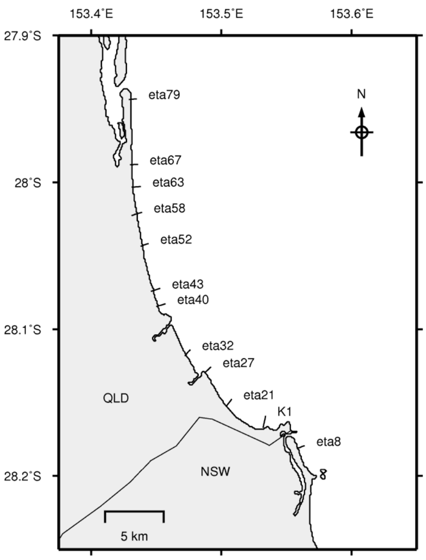

Fig. 2 Layout of selected transcects where breaking wave heights are estimated.

Results

An example wave class result is given in Table 1. For 2008, the data was divided into 10 wave classes describing the offshore wave climate. We see that ground swell from the SE was the dominant signal (67%). During the spring and summer, wind events drive a southerly longshore transport and two classes describe the ECL and mid-latitude storms out of the S-SE.

The resulting nearshore waves (Fig. 3) show considerable variability in direction along the coast. This is due to the curved shoreline and wave refraction. At the exposed north end (ETA79) breaking wave heights are larger and from the E-ESE, while by comparison at Palm Beach (ETA 32) near the southern end of the coast, the dominant S-SE waves are reduced considerably due to wave shadowing and shoreline orientation. Using the formulation of Bayram et al. (2007), variability in estimated longshore transport between the two sites is considerable, with Q_y(ETA79) = -7.44 * 10^5 m^3/yr and Q_y(ETA32) = -4.14 * 10^5 m^3/yr.

Table 1. Example offshore wave classification results for 2008.

Class	% time	H_s (m)	T_p (s)	MWD (^{0}N)	Comments (GS = ground swell, WS = wind swell)
1	23	1.76	8.76	135	Yr round, GS
2	20	2.18	8.87	141	Yr round, GS
3	13	1.32	8.49	148	Winter GS
4	11	2.80	9.05	150	Fall GS
5	11	1.32	7.45	95	Summer WS
6	7	1.41	6.54	31	Spring – summer WS
7	5	3.61	9.37	152	ECL and mid-lat storms
8	5	1.84	6.80	26	Spring WS
9	4	1.72	6.68	298	Summer, WS, offshore
10	2	4.86	10.32	160	ECL and mid-latitude storms

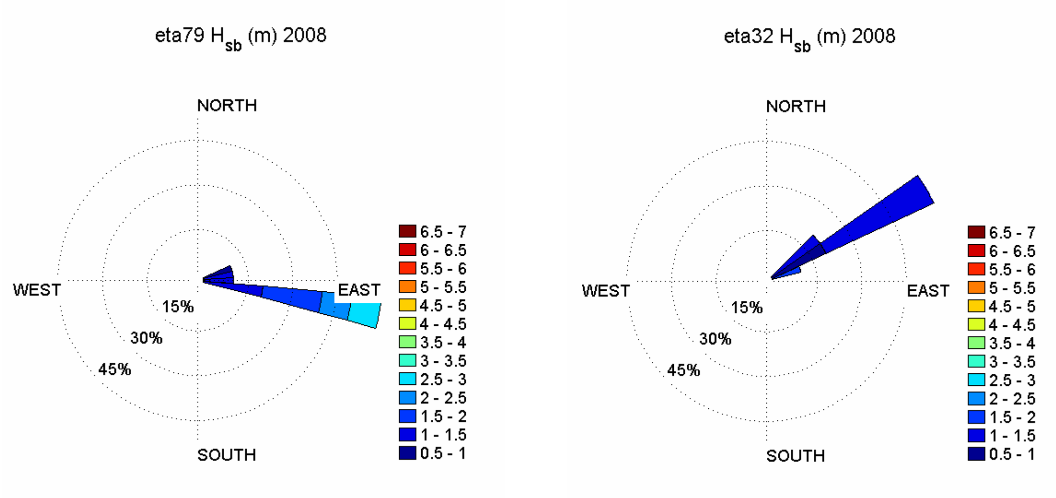

(a) (b)

Fig. 3 Estimated breaking wave height roses for 2008. a) ETA 79 (the Spit). b) ETA 32 (Palm Beach)

Acknowledgments

The authors would like to extend their appreciation to Russell Richards for his help with GAM models, Kathryn Jackson for her insight into offshore wave climates, and to Andreas Sterl (KNMI) for providing the C-ERA-40 data set. This work was funded under The Future Coastlines project by Griffith University and Queensland Smart State Innovation.

References

Bagirov, A.M. 2008. *Modified Global K-Means Algorithm for Minimum Sum-of-Squares Clustering Problems.* Pattern Recognition. **41** 3192-9

Bayram, A., Larson, M. and Hanson H. 2007. *A New Formula for the Total Longshore Transport Sediment Transport Rate.* Coastal Engineering. **54** 700-10

Bertin, X. et al. 2008. *Longshore Transport Estimation and Inter-Annual Variability at a High-Energy Dissipative Beach: St. Trojan Beach, SW Oleron Island, France.* Continental Shelf Research. **28** 1316-32

Caires, S. and Sterl, A. 2005. *A New Nonparametric Method to Correct Model Data: Application to Significant Wave Height from the ERA-40 Re-Analysis.* Journal of Atmospheric and Oceanic Technology. **22** 443-59

Delft Hydraulics Laboratory. 1992. *Southern Gold Coast Littoral Sand Supply.* Delft Hydraulics Laboratory. **H85**

Patterson, D.C. 2007. *Sand Transport and Shoreline Evolution, Northern Gold Coast, Australia*. in *9th International Coastal Symposium*. Australia: Journal of Coastal Research. **SI 50**. 147-51.

Wave climate variability and coastal change - the value of sustained coastal monitoring around Australia's coastline

Ian L. Turner & Mitchell D. Harley
Water Research Laboratory, School of Civil and Environmental Engineering
University of New South Wales, King Street, Manly Vale, NSW 2093, Australia

Introduction

Wind-waves are the primary driver of coastal variability and change (beach erosion/accretion) around much of the Australian coastline. At the site of the *SE Australia Climate Change Coastal Reference Station* (*CC-CRS*) located within the Narrabeen-Collaroy embayment in NSW – presently the only location around the entire continent where a combination of automated and manual methods are being used to extend a high resolution and multi-decadal record of coastal change – episodic storms result in significant damage to public & private infrastructure and loss of beach amenity (Fig. 1).

Fig. 1 Historical and contemporary beach erosion at the site of the SE Aus CC-CRS: (a) 'The Great Storm' of 1920 [Hs > 6 m]; 'Pasha Bulker Storm', 2007 [Hs ~ 7m].

The *CC-CRS* dataset now spans more than 3 decades, and is one of just seven sites world-wide where the results of multi-decadal, high-resolution coastal monitoring programs are currently available. Recent analyses using this *CC-CRS* dataset illustrate the importance of both the regional and local characteristics of the inshore wind-wave climate, as the primary driver of complex and variable beach response. As Australians plans for projected changes to regional wave climates and sea-level rise in coming decades, expanded coastal monitoring via the establishment of a *National Coastal Observatory* is now a requirement. Encompassing all key regions of the Australian coastline, sustained monitoring of the physical coastal environment would compliment and add value to existing wind-wave and water-level monitoring networks, and provide the fundamental information that is needed to quantify and project present and future coastal change.

SE Australia Climate Change Coastal Reference Station (CC-CRS)

A survey program comprising monthly 2D cross-shore profiles at five locations along the Narrabeen-Collaroy embayment was initiated and maintained by Professor Andy Short of the Coastal Studies Unit, University of Sydney, commencing in 1976 and continuing through to 2006. A total of 335 surveys were completed during this 30-year period. In 2004 and 2005 respectively, this conventional rod-and-tape survey program was significantly expanded by the introduction of daily 'virtual' surveys of the beachface bathymetry achieved by the deployment of a 5-camera Argus coastal imaging station, and monthly fully-3D RTK-GPS surveys of the entire 3.6 km subaerial beach (see Fig. 1). By the careful integration of these various survey data sources (Harley et al., Harley and Turner 2008),the *CC-CRS* now span some 35 years, and growing.

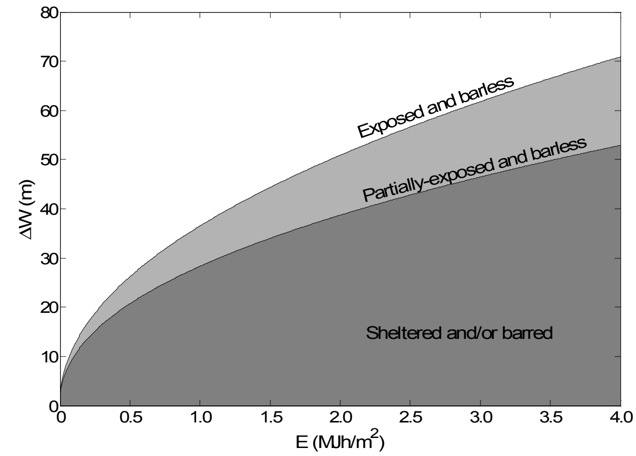

Fig. 2 Empirical model of beach response ΔW (reduction is beach width) as a function of cumulative storm energy (E), embayment exposure and nearshore sandbar conditions. Source: Harley et al. 2009

The collocation of the *CC-CRS* with the Sydney directional wave-rider buoy, extended by use of regional ERA-40 wave data, plus detailed numerical modelling to transform the offshore to inshore wave conditions, provides the basis to investigate and quantify the role of wind-wave forcing as the key driver of observed daily to decadal coastal variability and change.

The *CC-CRS* datatset has enabled the magnitude of observed shoreline recession on a storm-by-storm basis to be quantified for many individual events. Based upon this analysis, Fig. 2 summarises the results of a new empirical model that provides a practical engineering approach to determine the anticipated shoreline recession (and hence set-back required) as a function of cumulative storm wave energy, prevailing nearshore conditions, and the local degree of wave sheltering by adjacent headlands (Harley et al. 2009). Further testing to establish the broader applicability of this model to other regions around the Australian coastline requires additional datasets of suitable coastal observations.

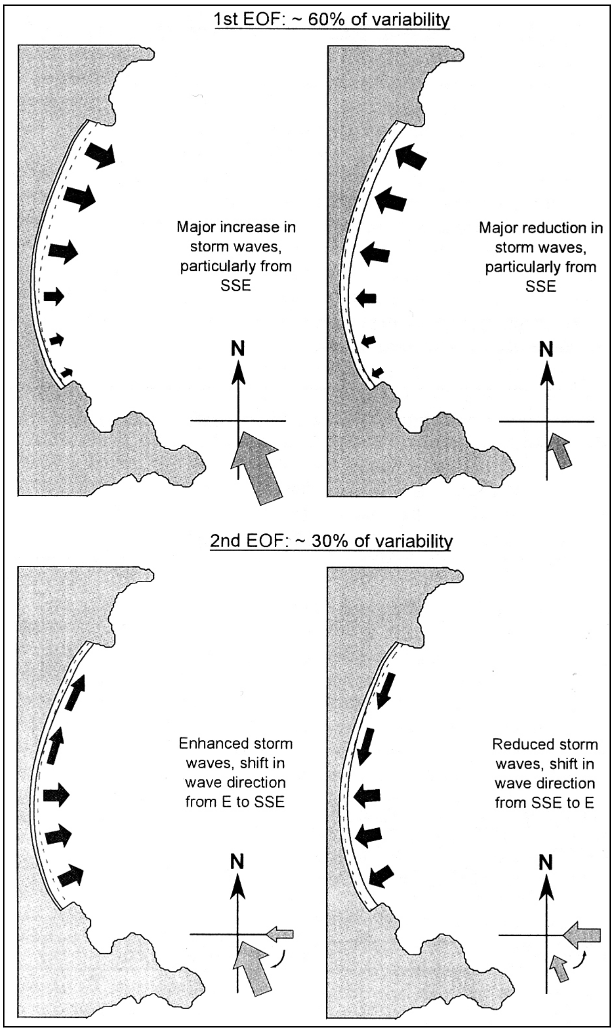

Fig. 3 Conceptual model beach oscillation and rotation on the SE Australian coastline. Source: Harley et. al. "what causes beach oscillation and rotation on the SE Australia coastline".

Three decades of *CC-CRS* coastal monitoring exhibits nil long-term net erosion trend to the present time. Instead, these data reveal that beach width variability in this region of the Australian coastline is dominated by inter-annual cycles (period two – seven years) of shore-normal beach oscillation and shore-parallel beach rotation. These cycles appear to be related to ENSO, with El Nino/La Nina periods coinciding with an overall accretion/erosion clockwise/counter-clockwise rotation of the beach (Harley et al. 2008). Prior research in Australia and internationally has hypothesised that cyclic and regional-scale shifts in prevailing wind-wave direction is likely to be the primary forcing of observed beach rotation. A new EOF analysis of the *CC-CRS* dataset (Harley et al. 2010) has established the counter conclusion that 60% of the apparent embayment rotation can be attributed to the interaction of inter-annual changes in wave energy (rather than wave direction), modulated by the alongshore variation in the degree of sheltering provided by adjacent headlands. Counter to previous conceptions, just 30% of the total beach width variability can be attributed at the *CC-CRS* site to the alongshore transfer of sediment within the embayment associated with shifting wave direction. The broader conclusion that this is similarly the case for other regions around the Australian coastline again requires suitable and expanded coastal monitoring.

Proposal for the establishment of a "National Coastal Observatory"

In mid 2009, 20 representatives from the coastal geoscience & engineering research communities (Universities & CSIRO) plus key personnel from state governments, met to workshop the establishment of a *National Coastal Observatory*, with the objective to provide baseline monitoring of the physical coastal environment at key representative sites by region around the Australian coastline. The existing *SE Australia CC-CRS* provides a useful template toward this objective. The clear need emerged from this workshop for a sustained and ongoing national coastal monitoring network, to compliment other important monitoring initiatives (incl. wind-waves and water-levels) that are already underway. The *CC-CRS* dataset clearly demonstrates the present and future value to Australian coastal management & research of sustained coastal monitoring. The challenge is to now identify and secure a suitable funding model.

References

Harley, M.D., Turner, I.L., Short, A.D. and Ranasinghe, R. Assessment of conventional, RTK-GPS and image-derived beach survey methods for daily to decadal coastal monitoring. *Coastal Engineering* (in press).

Harley, M.D. and Turner, I.L. 2008. A simple data transformation technique for processing survey data at embayed beaches. *Coastal Engineering*, 55, 63-68.

Harley, M.D., Turner, I.L., Short, A.D. and Ranasinghe, R. 2009. An Empirical model of beach response to storms – SE Australia. *19th Australasian Conference on Coastal and Ocean Engineering*, Engineers Australia, Wellington NZ.

Harley, M.A., Turner, I.L., Short, A.D. and Ranasinghe, R. 2008. Rotation and oscillation of an embayed beach. *31st International Conference on Coastal Engineering.* American Society of Civil Engineers, Hamburg.

Harley, M.D., Turner, I.L., Short, A.D. and Ranasinghe, R. 2010. What causes beach oscillation and rotation on the SE Australia coastline? *Journal of Geophysical Research – Earth Surface* (in review).

Global trends in wind speed and wave height over the past 25 years

Ian Young, Stefan Zieger and Alexander Babanin
Swinburne University of Technology, Hawthorn, Victoria

Introduction

Studies of climate change typically consider measurements of temperature change over extended period of time. Climate, however, is much more than temperature. Over the oceans, changes in wind speed and the surface gravity waves, generated by such winds, play an important role. In addition to being themselves an indicator of climate change, winds and waves play important roles in the design and operation of offshore shipping and structures, as well as controlling the flux of energy from the atmosphere to the ocean and potentially upper ocean mixing. Thus, they significantly influence the mechanisms of air-sea interaction.

This presentation investigates changes in global wind speed and wave height over the past 25 years, using a consistently calibrated and validated altimeter data base for this period.

Altimeter database

Zieger et al (2009) have considered observations of significant wave height and radar cross-section (wind speed) from all altimeter missions in the period 1985-2008. Each mission was calibrated against insitu buoy data over this period. Each data set from the various missions was then cross-validated against other satellites operating at the same time. In this way, periods of altimeter drift or discontinuities were identified and corrected. The resulting data set represents a high quality data set with global coverage over an extended period of time.

Trend determination

Our aim is to determine the linear trend in the data set for the mean, 90th and 99th percentile values of both wind speed and wave height. The determination of trend has been extensively considered in the literature, the aim being to determine the linear increase/decrease in the mean of the time series in the presence of seasonal variation and data gaps. Five different methods were considered, each was tested against synthetic data sets and their error characteristics determined. Ultimately, the Seasonal Kendall Test (Hirsh et al. 1982) was adopted.

Data accuracy

Altimeter data has been previously used to determine mean wind and wave climatology. However, as we intend to consider extreme values at the 90th and 99th percentile, it is necessary to demonstrate that the altimeter can accurately measure such value. Fig. 1 shows a percentile-percentile (Q-Q) plot comparing buoy and altimeter for both wind speed and wave height. Excellent agreement is demonstrated at all values up to the 99th percentile (most extreme value in the plot).

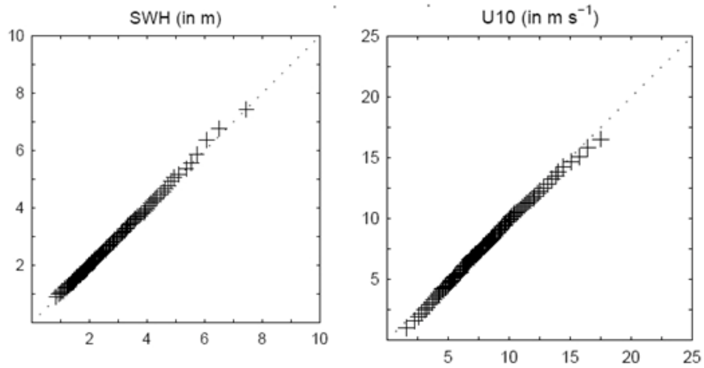

Fig. 1 Percentile-percentile plot between buoy (vertical axis) and altimeter (horizontal axis) at NDBC buoy 46005. Significant wave height is shown as the top panel and wind speed as the lower panel.

Such comparisons were conducted at all NDBC buoy locations. In each case, the altimeter data was capable of accurately determining 90th and 99th percentile values.

Global trends

The data was binned into 2 degree by 2 degree regions and the trend analysis applied to each bin. This process was repeated for each of wind speed and wave height at the mean, 90th and 99th percentile levels. The mean values show a weak global trend of increasing values of both wind speed and wave height. This positive trend becomes progressively stronger at the 90th and 99th percentile. Fig. 2 shows the trend values, expressed as a percentage increase/decrease per year for the 99th percentile. The positive trend is clear.

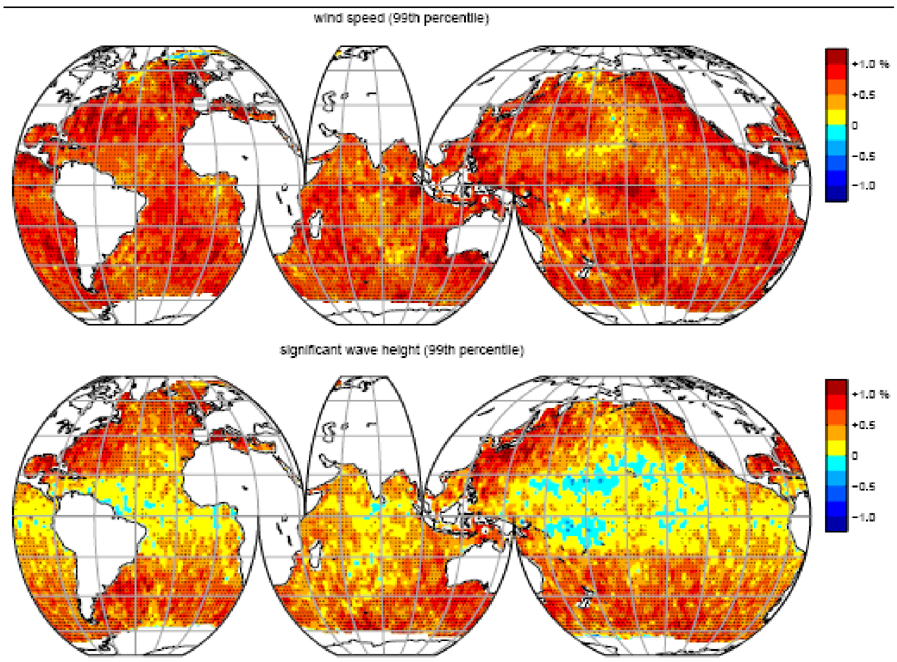

Fig. 2 Trend (percentage increase/decrease per year) for wind speed (top) and significant wave height (bottom) at the 99th percentile. Both quantities show an overall global increase, with a stronger trend for wind speed.

References

Hirsh, R.M., Slack, J.R. & Smith, R.A. 1982. Techniques of trend analysis for monthly water quality data. Water Resour. Res., 18, 107-121.

Zieger, S., Vinoth, J. and Young, I.R. 2009. Joint calibration of multi-platform altimeter measurements of wind speed and wave height over the past 20years. J. Atmos. & Ocean. Tech., 26, 2549-64.

Modelled wave climatology around Australia: Engineering design and vessel operations

Ian Coghlan and William Peirson
Water Research Laboratory, University of New South Wales,
110 King Street, Manly Vale, NSW 2093, Australia

Diana Greenslade
Centre for Australian Weather and Climate Research,
GPO Box 1289, Melbourne, VIC 3001, Australia

Introduction

The Australian Bureau of Meteorology predicts coastal and offshore wave conditions using a version of the third generation ocean wave prediction model, WAM (WAve Model) (WAMDI Group 1988, Komen et al. 1994, Bender 1996). A high-resolution form of the model, known as "HI-WAM", was developed for the purposes of examining of sediment mobility on the Australian continental shelf (Porter-Smith et al. 2004). HI-WAM is the most detailed (and computationally intensive) wave model of the Australian coastline developed by BoM but its output has not been publically available. During a recent collaboration between BoM and the Water Research Laboratory, the skill of HI-WAM has been benchmarked against recorded wave measurements (Coghlan 2010). There are three primary interests in wave model data:

1. Climate (modelling to fit overall nature trends)
2. Design (engineers designing a coastal structure)
3. Operational (ports day-to-day decision making).

Specifications of the HI-WAM model

The HI-WAM model has a spatial resolution of 0.1 ° and a domain spanning longitudes from 110°E to 156°E and latitudes ranging from 7°S to 46°S and is nested inside a coarser resolution WAM model. Surface wind velocity estimates generated by BoM's Meso Limited Area Prediction System provide the wind input to the model. The HI-WAM model outputs of significant wave height (H_S), mean wave period (T_1) and mean wave direction (*Drn*) were archived at six-hourly intervals for a duration of 11 years (1997 to 2008).

An additional source term is included in HI-WAM; representing the dissipation of energy due to bottom friction. Other finite depth effects, such as depth-limited wave breaking and triad non-linear interactions, are not included in the model. For this reason, water depths of 20 to 30 m were considered to be the shallowest depths to which the model could be run successfully (Booij et al. 1999). The bathymetric dataset for defining water depths in HI-WAM had a grid spacing of $1/12^{th}$ °.

Wave measurement records

In order to validate the performance of the HI-WAM model, 18 long term datasets recorded in 15 to 100 m water depth from around the Australian coastline were used (Fig. 1). The record duration is sufficient for several major storms to be recorded at most locations.

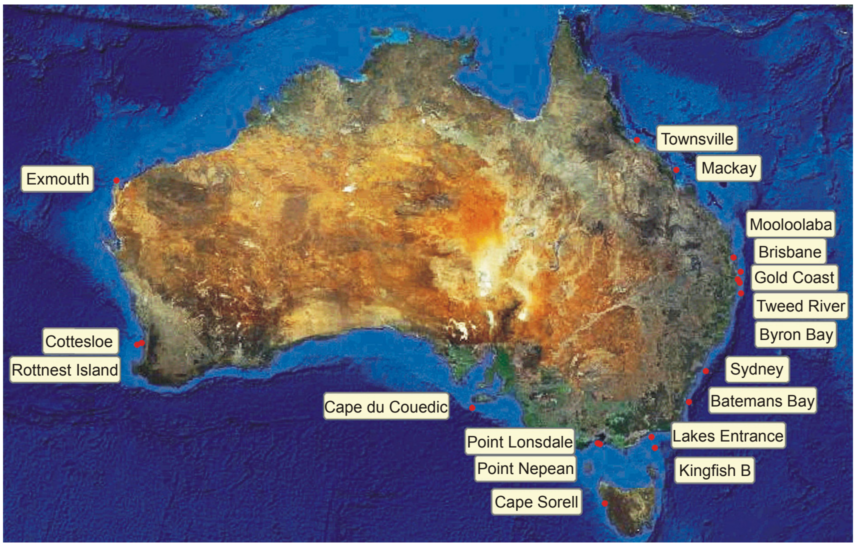

Fig. 1 Wave measurement datasets from 18 locations.

Data preperation

To assess the skill of HI-WAM for engineering design purposes, significant data manipulation was required to transform the wave measurement records into a common format for comparison with the model. These operations included adjustments for time zone, local magnetic declination and temporal smoothing. Output from adjacent model grid points was interpolated to the co-ordinates of each wave measurement location.

Model validation

Several standard statistical measures of model skill were calculated for each parameter as shown in Table 1.

Table 1. Model Skill Statistics: *Bias* (predicted – measured values), *R* (Linear Correlation Coefficient), RMSE (Root-Mean-Square Error), *SI* (Scatter Index), $\hat{p}_T$ (Circular Correlation) and $\hat{k}$ (Concentration Statistic).

Wave Parameter	Standard Statistical Measures of Model Skill			
H_S	*Bias*	*R*	*RMSE*	*SI*
T_1	*Bias*	*R*	*RMSE*	*SI*
Drn	*Bias*	$\hat{p}_T$	*RMSE*	$\hat{k}$

HI-WAM correctly reproduced the overall natural variability of the sea state. For any Australian location within the range of depths tested, HI-WAM predictions had a general accuracy (based on *RMSE*) as follows:

- Significant wave height predictions within ± 0.4 m
- Mean wave period predictions within ± 0.9 s
- Wave direction predictions within ± 10 ° ($H_S \geq 1$ m).

Time series plots comparing measured and predicted values for one site for one month are shown in Fig. 2.

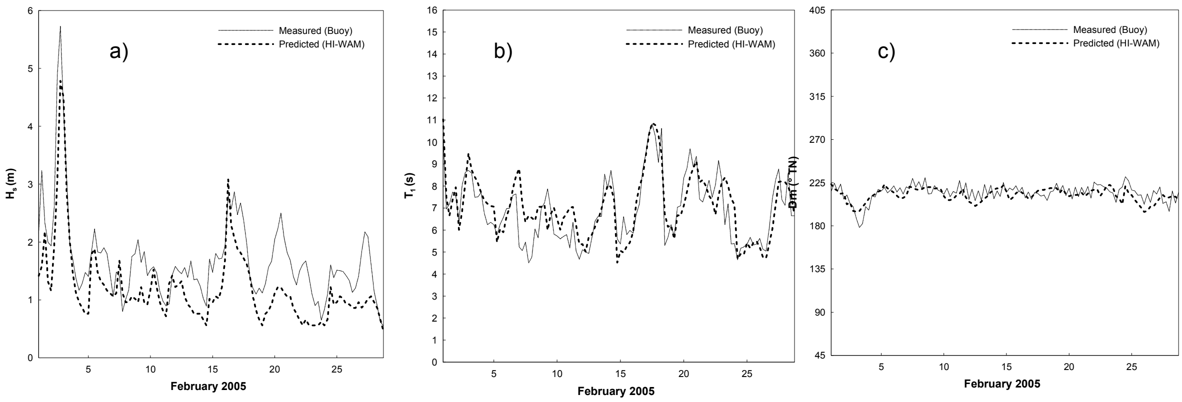

Fig. 2 Comparison of Measured and Predicted Values for Point Nepean (Victoria) during February, 2005

(a) Significant wave height, H_S (m)
(b) Mean wave period, T_1 (s)
(c) Mean wave direction, D_{rn} (° TN)

Variation of model skill with depth

The model skill parameters *R* and *SI* (which are both independent of mean wave climate) were plotted as a function of water depth. It was observed that, in general, model skill for H_S and T_1 reduces with depth (*R* decreasing and *SI* increasing). Although it is acknowledged that there was considerable scatter in the data, HI-WAM was shown to produce effective results in water depths of 20 to 30 m and even as shallow as 15 m (H_S: $R \approx 0.90$, $SI \approx 0.23$ and T_1: $R \approx 0.73$, $SI \approx 0.16$).

Design and operational implications

The interests of climate modelling are satisfied by the skill demonstrated by HI-WAM to predict overall natural trends. From an operational perspective, HI-WAM wave model data would also be considered acceptable for day-to-day risk management in ports facilities. However, since model skill during extreme wave conditions is of most importance to engineering design, additional analysis of HI-WAM performance was required. To examine model skill under these conditions, *Bias* and *RMSE* for predicted H_S and T_1 were calculated in 1.0 m bins of measured H_S for all locations. Although only a limited number of extreme events occurred during this period, it was found that wave energy (both H_S and T_1) was vastly over predicted at one site, Sydney (NSW), for extreme wave heights but, conversely, energy was under predicted for those sites exposed to full swell in Victoria, Tasmania (Cape Sorrell), South Australia and Western Australia.

Example model *Bias* during extremes is shown below:

- Sydney H_S 7 - 8 m: $H_S \approx + 2.5$ m, $T_1 \approx + 2.8$ s
- Cape Sorrell H_S 9 - 10 m: $H_S \approx - 3.0$ m, $T_1 \approx - 1.3$ s.

Summary

This study is the first national assessment of the performance of BoM's HI-WAM wave model. Its overall skill was validated and its variation with water depth observed, but its performance during extreme wave events indicates some limitations for engineering design purposes.

Acknowledgments

The authors acknowledge the use of data supplied by BoM, Queensland Government Hydraulics Laboratory (DERM), Manly Hydraulics Laboratory (NSW Public Works) on behalf of NSW DECCW, Gippsland Ports, Esso Australia, the Port of Melbourne, Fremantle Ports, and the WA Department of Transport.

References

Bender, L.C. 1996. "Modification of the Physics and Numerics in a Third-Generation Ocean Wave Model", *Atmos. & Ocean. Tech.,* **13**, 726-50.

Booij, N. et al. 1999. "A Third-Generation Wave Model for Coastal Regions", Model Description and Validation, *Geophys. Res.,* **104**, 7649-66.

Coghlan, I. 2010. "Validation of Australian Bureau of Meteorology High Resolution Wave Model (HI-WAM)", *WRL Research Report*.

Komen, G.J. et al. 1994. *Dynamics and Modelling of Ocean Waves,* Cambridge University Press.

Porter-Smith, R. et al. 2004. "Classification of the Australian Continental Shelf based on Predicted Sediment Threshold Exceedance from Tidal Currents and Swell Waves", *Marine Geol.*, **211**, 1-20.

WAMDI Group. 1988. "The WAM model – A Third Generation Wave Prediction Model", *Physical Oceanography,* **18** (1988), 1775-1810.

National-scale wave energy resource assessment for Australia^

Michael G. Hughes* and Andrew D. Heap

**Australian Hydrographic Service, R.A.N., Locked Bag 8801, Wollongong, NSW 2500, Australia*

Geoscience Australia, GPO Box 378, Canberra, ACT 2601, Australia

Introduction

Wave energy is a largely untapped renewable energy resource, with the advantage of having the highest energy density among all the renewable energies (Clement et al. 2002). There are currently more than twenty wave energy projects around the world, but in almost all cases they are still in the pilot stage serving as research and development or proof of concept (World Energy Council 2007). Few are contributing electricity to local grids and none are contributing significantly to national electricity production. Nevertheless, there is a continuing trend of rapid technological development in wave energy converters (WECs) and recent growth in both community and government support for wave energy projects in many countries (Clement et al. 2002, World Energy Council 2007). Several wave energy resource assessments have been published in preparation for the possible significant contribution by wave energy to national electricity production in some countries (e.g. Thorpe 1999, Henfridsson et al. 2007).

Previous studies of the wave climate in Australian waters have been focussed on the most energetic southwestern, southern and southeastern margins of the continent (Short and Trenaman 1992, Wright 1976, Lemm et al. 1994-96, Hemer et al. 2008). The information from these studies, however, is of limited value for a comprehensive assessment of the wave energy resource potential for all Australia. A first cut at assessing the potential resource would ideally (1) have national coverage; (2) have consistent temporal coverage that is of sufficient length to include important climatic cycles; and (3) be based on a consistent data type. The resource assessment reported here is based on predictions of wave conditions hindcast from the WAMmodel – a third generation ocean wave prediction model (Hasselmann and WAMDI Group 1988).

Data and methods

Implementation of the WAM model for the Australian region (AusWAM) was performed by the Australian Bureau of Meteorology using their high resolution atmospheric model on a 0.1° grid covering 110–156°longitude and 7–46° latitude (e.g. Greenslade 2001). The hindcast wave conditions are significant wave height H_s, mean wave period T_m and wave direction θ. The data set used here are 6-hourly time series of H_s, T_m and θ on the grid for the period 1 March 1997 to 29 February 2008 inclusive (11 years).

The WAM model integrates the basic transport equation describing the evolution of a two-dimensional ocean wave spectrum without any assumptions concerning the evolving spectral shape. Energy dissipation due to white-capping is included in the model, and energy dissipation due to bottom friction as well as refraction is included in the finite-depth version of the model (Folley and Whittaker 2009). Depth-induced wave breaking, however, is not included. For this reason and the limited grid resolution compared to the increased bathymetric complexity in shallow water, the AusWAM hindcasts are considered to be of limited value for water depths <25 m. Wave energy density E and power P were calculated from the AusWAM hindcast wave conditions using linear wave theory. This resource assessment is restricted to the wave energy present on Australia's continental shelf (<300 m).

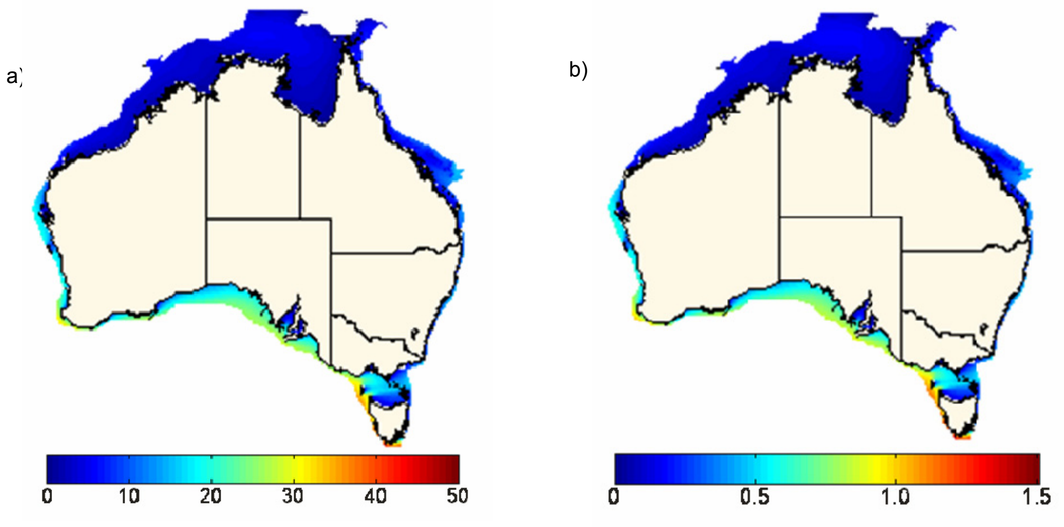

Fig. 1 a) Time averaged wave power (kW m-1); b) Total annual wave energy (TJ m-1).

Results

The time-averaged total wave energy on the entire Australian shelf is about 3.47 PJ (Fig. 1a; Table 1). Since the resource assessment is based on the same data source and includes the same time period for all locations, the resource can be compared from location to location without bias. The total amount of wave energy on the shelf is largest for Western Australia, followed by Queensland, South Australia, Tasmania/Victoria, Northern Territory and New South Wales. The spatial distribution of time-averaged wave power can be broadly separated into a northern and a southern region, separated at about 23°S (Fig. 1b). Wave power is greatest on the southern half of the Australian shelf. Over large areas of southern Australian shelf the mean wave power is >25 kW m^{-1} with 90th percentile values of >60 kWm^{-1} delivering >800 GJ m^{-1} of total annual energy in an average year, depending on location. Significantly, most of this energy is delivered in winter when there is greatest demand.

To provide an objective, straightforward comparison of the resource available for each state the maximum time-averaged wave power occurring on the shelf adjacent to each state are listed in Table 1, together with the total wave energy delivered annually. The values for water depths <50 m are also listed because the present generation of WEC's will be installed in this depth range. On the basis of this assessment the best resourced states are Tasmania/Victoria, Western Australia and South Australia.

By comparison, the Atlantic shelves of Portugal, France, and United Kingdom experience similar wave powers, however, the southern Australian margin extends for more than 3000 km and represents a world class wave resource.

Wave power over much of this area is persistently high and will pose significant challenges for engineering design and a failure analysis has been completed to help assess this. In addition to

the southern margin, large areas of the southern-mid Western Australia, New South Wales and southern-mid Queensland shelves have moderate wave power levels that are also potentially capable of contributing significantly to annual electricity production.
Although there is a large amount of energy on the northern half of the Australian shelf at any one time, due to the large shelf area, the energy density and power or rate that the energy is delivered is small (<10 kW m^{-1}) and unsuitable for harvesting with current technologies.

Table 1. Total wave energy and summary data for the most energetic site in ≤50m water depth for each state or territory.

			≤50 m water depth	
State	Total Energy (TJ)	Annual Total Energy (GJ m^{-1})	Mean Power (kW m^{-1})	Mean Energy (kJ m^{-2})
WA	1018.10	901.44	28.56	3.73
Qld	805.04	442.80	14.03	2.54
SA	631.62	885.13	28.04	3.51
Tas/Vic	485.49	1100.78	34.87	4.46
NT	458.20	167.90	5.32	1.23
NSW	69.53	391.04	12.39	1.89
Total	3467.98			

Summary

The data are sufficient to inform policy on energy resources at the national scale, as well as guiding industry to the most suitable regions for further assessment of the technically available energy resource. In the first instance the latter will require more refined assessment of the potential energy resource in nearshore (<25m depth) and coastal waters. To this end the data reported here can be used to drive wave transformation models to predict the delivery and redistribution of wave energy density over complex shallow water bathymetry (e.g. Folley and Whittaker 2009). The final steps of assessing the technically available resource will need to consider the efficiency of the WEC, transmission losses between the point of electricity generation and the grid, and various social and environmental factors (e.g. Thorpe 1999, Henfridsson et al. 2007).

References

Clement, A., McCullen, P., Falcao, A., Fiorentino, A., Gardner, F., Hammarlund, K., et al. 2002. Wave energy in Europe: current status and perspectives. *Renewable and Sustainable Energy Reviews*; 6:405–31.

Folley, M. and Whittaker, T.J.T. 2009. Analysis of the nearshore wave energy resource. *Renewable Energy*; 34:1709–1715.

Greenslade, D.J.M. 2001. The assimilation of the ERS-2 significant wave height data in the Australian region. *Journal of Marine Systems*; 28:141–60.

Hasselmann, K. and WAMDI Group. 1988. The WAM model – a third generation ocean wave prediction model. *Journal of Physical Oceanography*; 18:1775–810.

Hemer, M, Simmonds, I, and Keay, K. 2008. A classification of wave generation characteristics during large wave events on the southern Australian margin. *Continental Shelf Research*; 28:634–52.

Henfridsson, U., Neimane, V., Strand, K., Kapper, R., Bernhoff, H., Danielsson, O., et al. 2007. Wave energy potential in the Baltic Sea and the Danish part of the North Sea, with reflections on the Skagerrak. *Renewable Energy*; 32:2069–84.

Lemm, A.J., Hegge, B.J. and Masselink, G. 1999. Offshore wave climate, Perth (Western Australia), 1994–96. *Marine and Freshwater Research*; 50:95–102.

Short, A.D. and Trenaman, N.L. 1992. Wave climate of the Sydney region, an energetic and highly variable ocean wave regime. *Australian Journal of Marine and Freshwater Research*; 43:765–91.

Thorpe, T.W. 1999. *A brief review of wave energy*. UK Department of Trade and Industry. Report No. ETSU-R120.

World Energy Council. 2007. *2007 Survey of energy resources*. World Energy Council.

Wright, L.D. 1976. Nearshore wave-power dissipation and the coastal energy regime of the Sydney-Jervis Bay region, New South Wales: a comparison. *Australian Journal of Marine and Freshwater Research*; 27:633–40.

^ Taken from: Hughes, M.G. and Heap, A.D. 2020 National scale wave energy assessment for Australia. *Renewable Energy*; 35: 1783-1791.

Operational sea state forecasting

James Taylor
Bureau of Meteorology, Victorian Regional Office,
GPO Box 1636, Melbourne, VIC 3001, Australia

Introduction

Sea state forecasting within the Bureau of Meteorology (BoM) currently falls into two categories depending on whether or not a Regional Office (RO) is using the Graphical Forecast Editor (GFE) within the Next Generation Forecasting and Warning System (NexGenFWS).

The general process of sea state forecasting is similar with or without the GFE. However, the GFE provides a framework within which producing significant wave heights (Hsig) from forecasts of windsea (waves generated by local wind) and swell is relatively elementary. This allows the Meteorologist (Met) to more easily compare forecasts of Hsig with buoy data or numerical wave prediction model (NWPM) data.

One advantage with the NexGenFWS is the ability to produce graphical forecasts for the BoM website. Currently, graphical forecasts of elements such as wind, temperature and rainfall are produced for the Victorian region. Graphical forecasts of windsea, swell and/or Hsig have the potential to be included in this product suite.

The NexGenFWS was implemented in the Victorian RO in October 2008. It is planned that the system will be implemented in the New South Wales RO in September of this year. Implementations are scheduled for Tasmania and South Australia during 2011, Western Australia in 2012, and finally, the Northern Territory and Queensland by the end of 2013.

Pre-GFE sea state forecasting

Although finer details of the sea state forecast process will differ somewhat between ROs, certain elements of the process will be similar.

Initially a Met will generally follow a forecast funnel approach, considering hemispheric and synoptic scales before thinking in more detail about the meso scale. An analysis of satellite imagery and hemispheric long wave troughs helps to identify systems of concern at the synoptic scale.

An understanding of the current sea state can be obtained from observational data such as ship/buoy observations and remotely sensed marine winds and Hsig. However, the sparseness of observational data requires the Met to infer a lot about the current sea state.

As the BoM includes forecasts of both windsea and swell for coastal waters and high seas forecasts, the Met will often need to infer the proportion of windsea and swell that a Hsig observation represents. Some buoy observations partition windsea and swell from the wave spectrum, usually based on a separation frequency. Ship observations of windsea and swell can be useful in this regard but tend to be somewhat subjective.

Ground truthing of NWPM data to assess current model performance will play a role in the decision making process of which model data will produce the best guidance. The Met's appreciation of individual model performance (given a particular situation) can also play a role with this decision.

Forecasts of windsea and swell are written into coastal waters and high seas forecasts and warnings, taking into account any local effects, NWPM partitioning issues and perceived model bias.

As ROs issue many public weather, aviation, severe weather and marine forecast and warning products, Mets face considerable time pressures. Commonly 30-45 minutes may be required to accurately go through this process for a coastal waters outlook. However, often less than 20 minutes may be available if other operational pressures take priority.

Post-GFE sea state forecasting

As the GFE quickly calculates grids of Hsig given grids of windsea and swell, the sea state forecast process can be more focused on Hsig. The NexGenFWS also uses Hsig grids as a "combined sea and swell" forecast that is used within coastal waters warnings.

Another advantage of using the GFE is the ability to tune smart tools to ensure a higher level of consistency within the subjective part of windsea and swell partitioning. Pre-GFE, different windsea heights may be attributed to different wind speeds. This may be due to a particular RO policy or different Mets within a RO subjectively applying different windsea height.

As windseas from NWPM are derived from winds that are almost certainly different to Met derived wind grids within the GFE, it was recognised that model derived windsea could not be used directly without some post process editing. Within the GFE a smart tool was developed to ensure consistency between forecast GFE grid winds and windsea. A graphical approach was taken to derive equations of windsea given fetch and wind speed, and also given duration and wind speed. The equations were derived from the Groen-Dorrestein curves (Groen and Dorrestein 1976). Defaults of 150 km for maximum fetch and 7 hours for maximum duration are used within the smart tool as it is assumed that for fetches or durations greater than this, the sea state will have some swell component. Fig. 1 shows there is minimal error produced from the equations for low fetches and durations, such as those associated with windsea.

The process of forecasting the windsea component of sea state is essentially completed within the GFE when the forecast wind grids are completed. The Met simply needs to run the smart tool on the wind grids to obtain consistent windsea grids. There is the option to adjust the amount of energy assigned to windsea by adjusting the defaults of fetch and duration. This may occur in situations such as a deep low pressure system within coastal waters. However in the interest of maintaining consistency, the defaults will remain constant the vast majority of the time.

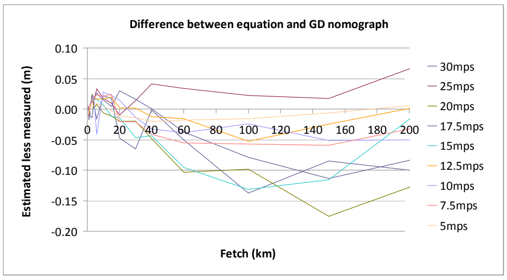

a)

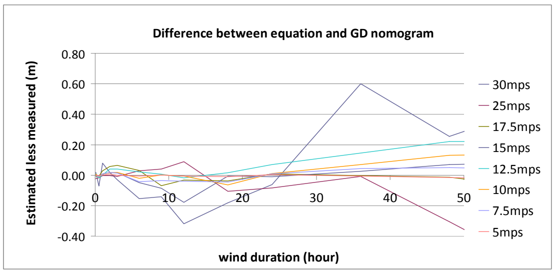

b)

Fig. 1 a) Estimated wave height from smart tool equation given wind speed and fetch minus wave height from GD curves; b) The same but with respect to duration.

Once the windsea component of the sea state is finalised the Met can make decisions about swell magnitude required for the desired Hsig forecast. Model swell guidance can be adjusted to the appropriate magnitude and direction. The Victorian RO also uses a smart tool that adjusts standard swell reference grids subjectively derived for Bass Strait.

Recently the BoM has implemented the full spectrum third generation wind wave model Wave Watch 3 (WW3) driven by the Australian Community and Climate and Earth-System Simulator (ACCESS) winds. The partitioning of windsea and swells by the WW3 is far superior to previous NWPMs run by the BoM. GFE will soon have grids of primary and secondary swell guidance available from the WW3. As this guidance has only become operationally available very recently there is still some question as to the best way to use it. There is potential for some problems around regions where primary and secondary swell have similar energy as different directions will be displayed in the one grid. There is also the issue of not partitioning any swell component when wind speeds approach gale force which results in large blank areas within the primary swell guidance corresponding to areas of near or above gale force wind speeds.

Future developments

A smart tool that calculates swell magnitude given windsea and Hsig would be highly useful. However, if a straight calculation of the magnitude was used this may result in swell grids displaying unrealistic swell magnitude gradients (such as near regions where the GFE wind grids differ significantly from the winds used within a NWPM to forecast Hsig). A better approach may be to develop a smart tool that does iterative adjustments to forecast swell magnitude to minimise the difference between forecast Hsig and NWPM Hsig. With a view to making GFE swell grids available on the BoM website, this approach may provide better guidance for marine forecast and warning service users.

Grids of wave trains rather than primary and secondary swell may prove to be more useful output from NWPMs for GFE. This sort of development work may well be underway within the National Oceanic and Atmospheric Administration (NOAA).

A more dynamically consistent approach to forecasting the windsea component of the sea state may be to send Met-derived GFE wind grids to a NWPM such as SWAN (2007) to provide forecast windsea. This approach is used in some offices in the United States National Weather Service (NWS) (Tracy et al. 2007). More interaction with the NWS GFE development team would be of benefit for the marine component of the NexGenFWS.

Conclusions

The sea state forecast process is going through some significant improvements with the NexGenFWS. The ability for Mets to quickly calculate forecast Hsig is a significant advantage over pre-GFE methods. Further developments such as making use of SWAN for windsea forecasts, or obtaining wave train grids directly from NWPMs, have the potential to provide considerable improvements to the sea state component of the NexGenFWS. Already, there is potential for graphical forecasts of windsea to be provided to the BoM website. With the implementation of some improvements to GFE swell forecasting, it is hoped that graphical swell and Hsig forecasts could also be provided.

References

Gröen, P. and Dorrestein, R. 1976. Zeegolven. KNMI Opstellen op Oceanografisch en Maritiem Meteorologisch: Gebied, 11, 124 pp.

SWAN – Technical documentation. Delft University of Technology, Environmental Fluid Mechanics Section, available from http://www.fluidmechanics.tudelft.nl/swan/index.htm (Version 40.51AB, August 2007).

Tracy, B., Devaliere, E., Hanson, J., Nicolini, T. and Tolman H. 2007. Wind Sea and Swell Delineation for Numerical Wave Modeling; 10th International Workshop on Wave Hindcasting and Forecasting & Coastal Hazard Symposium 2007; P13. http://oceanwavesystems.com/10th_wave_paper_tracy_dhnt.pdf

An examination of error sources in global wave models: the importance of the forcing winds

Tom H. Durrant and Diana J.M. Greenslade
Centre for Australian Weather and Climate Research, Bureau of Meteorology
GPO Box 1289, Melbourne, VIC, 3001, Australia

Introduction

The overall accuracy of a wave model forecast depends on the accuracy two models: the wave model itself, and that of the atmospheric model providing the forcing winds. A couple of decades ago, wave model development had reached a point where a significant proportion of the wave forecast error could be attributable to errors in the forcing winds, limiting gains that could be realised by improvements in the wave models themselves (Komen et al. 1994). The intervening period has seen great improvement in the atmospheric models (e.g. Janssen et al. 2002), resulting in a larger proportion of the error being attributable to the wave model, stimulating renewed vigour in wave model physics research.

The increasing availability of sea-state observations from satellite altimeters has allowed the large scale error characteristics typical of particular physics packages and model tunings to be investigated (e.g. Tolman et al. 2002; Bidlot et al. 2007). This information can then be used to refine and improve the models. However, a lack of knowledge of the comparable spatial error characteristics in the forcing wind fields can lead to uncertainty or misinterpretation of these results.

As part of the upgrade of the suite of numerical models at the Bureau of Meteorology, WaveWatchIII® (WW3) has been evaluated for operational implementation. Spatial error characteristics for both the forcing wind fields and the resulting wave fields have been determined, based on scatterometer and altimeter data respectively. The wave model results using several different physics packages are compared and contrasted in the context of known errors in the forcing winds.

Model

Model runs performed here use the latest version of the WW3 model, version 3.14 (Tolman et al 2002). This is a full-spectral third-generation wind wave model. Developed at the Marine Modeling and Analysis Branch (MMAB) of the Environmental Modeling Center (EMC) of the National Centers for Environmental Prediction (NCEP), this model was originally based on the widely used WAM model (Hasselmann 1988), but using the updated source terms of Tolman et al. (1996). This latest version of the model also includes source term packages similar to those available in the current and previous versions of WAM, namely that of WAM cycle 3 (Komen et al 1994) and WAM cycle 4 (Bidlot et al. 2007) (hereafter referred to as WAM4).

A number of hindcasts were performed using different combinations of wind forcing and source term packages. All runs were performed using a $1^o \times 1^o$ global grid. The wave spectrum was resolved into 24 azimuthal direction bins and 25 frequency bins logarithmically spaced from 0.04177 Hz to 0.4114 Hz. Blocking of wave energy due to islands that are unresolved by the grid were accounted for using artificial obstruction grids constructed using the automatic scheme of Chawla and Tolman 2008. No data assimilation is included.

Data

Spatial verification tools are constructed using altimeter data in the case of modelled significant wave height (H_s) and scatterometer data to verify the forcing winds (U_{10}). Altimeter data from both the Jason-1 (Menard et al. 2003; Carayon et al. 2003) and Envisat (Resti et al. 1999) satellites are combined to provide maximum spatial coverage. A small linear correction is applied to Envisat, as in Durrant et al. (2009). Scatterometer data from the QuikSCAT (Freilich et al. 1994) mission is used to assess the winds Fig. 1 shows the daily coverage of both Jason-1 and Envisat (Fig. 1a) and QuikSCAT (Fig. 1b).

In the case of both altimeter data and scatterometer data, for each observation, the model is interpolated in space and time to the observation location to give a single co-location. Co-locations are then accumulated within 3^o x 3^o boxes (for example) and statistics are calculated for each box over the globe.

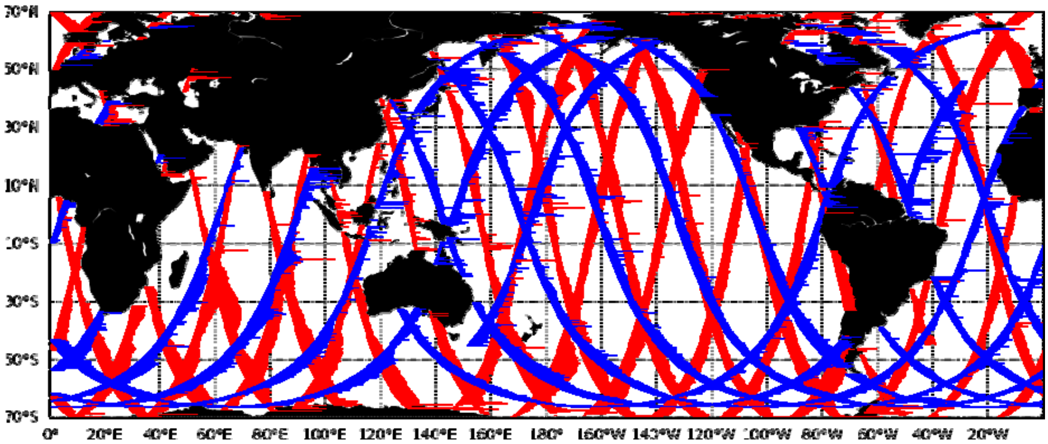

(a)

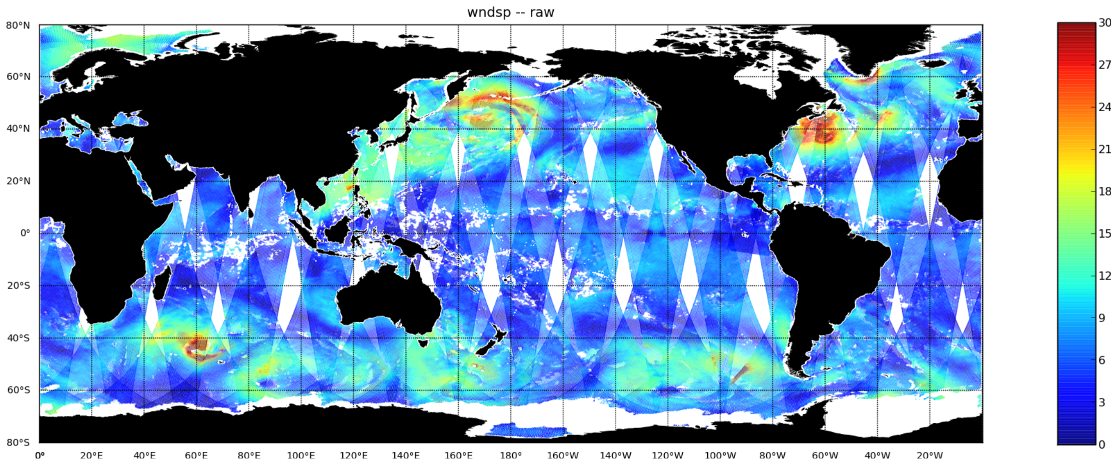

(b)

Fig. 1 24-hour coverage of (a) Jason-1 (blue) and Envisat (red) altimeter data and (b) QuikSCAT scatterometer data.

Results

Results are presented below for hindcasts performed over a four month period from July-October 2008. Spatial verification results were found to vary significantly with both the source term package used, and the winds used to force the model. Figure 2 shows, for example, the bias in the surface wind speed for both the GASP (Seaman et al. 1995) and ACCESS models, and the resulting bias in the Hs field produced by using the WAM4 source terms forced with these respective winds.

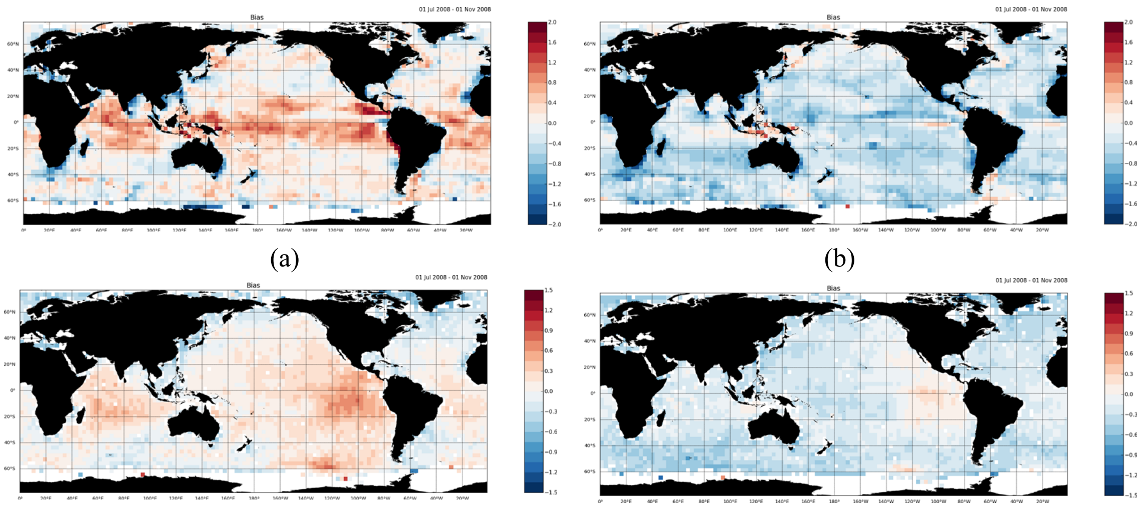

(a) (b) (c) (d)

Fig. 2 Spatial plots of (a) GASP U10 speed bias, (b) ACCESS U10 speed bias, (c) WAM4 Hs bias when forced with GASP winds and (d) WAM4 Hs bias when forced with ACCESS winds.

Conclusions

The combination of global altimeter and scatterometer data provides a powerful platform for wave model verification and diagnostics. When tuning the source terms in any wave model, it is important to know the structure to the errors in the forcing winds.

References

Bidlot, J.R., Janssen, P.A.E.M. and Abdalla, S. 2007. "A revised formulation of ocean wave dissipation and its model impact.," *ECMWF Tech. Rep.*

Chawla A. and Tolman, H. 2008. "Obstruction Grids for Spectral Wave Models," *Ocean Modelling*, **22**, pp. 12–25.

Carayon, G., Steunou, N., Courrin'ere, J.L. and Thibaut, P. 2003. "Poseidon-2 Radar Altimeter Design and Results of In-Flight Performances," *Mar. Geo.*, **26**, pp. 159–165.

Durrant, T.H., Greenslade, D.J.M. and Simmonds, I. 2009. "Validation of Jason-1 and Envisat Remotely Sensed Wave Heights," *J. Atmos. Oc. Tech.*, **26/1**.

Freilich, M.H., Long, D.G. and Spencer, M.W. 1994 "SeaWinds: a scanning scatterometer for ADEOS-II-science overview," in Geoscience and Remote Sensing Symposium, IGARSS'94. Surface and Atmospheric Remote Sensing: Technologies, Data Analysis and Interpretation., International, **2**.

Hasselmann, K. 1988. “The WAM model - a 3rd generation ocean wave prediction model,” *J. Phys. Oc*., **18**, pp. 1775–1810.

Janssen, P., Doyle, J.D., Bidlot, J., Hansen, B., Isaksen, L. and Viterbo, P. 2002. “Impact and Feedback of Ocean Waves on the Atmosphere,” in Advances in Fluid Mechanics (W.Perrie, ed.), **1**, pp. 155–197.

Komen, G.J., Hasselmann, S., Donelan, M., Cavaleri, L. and Janssen, P. 1994. Dynamics and Modelling of Ocean Waves.

Menard, Y., Fu, L.L., Escudier, P., Parisot, F., Perbos, J., Vincent, P., Desai, S., Haines, B. and Kunstmann, G. 2003. “The Jason-1 Mission,” *Mar. Geo*., **26**, pp. 131–146.

Resti, A., Benveniste, J., Roca, M., Levrini, G. and Johannessen, J. 1999. “The Envisat Radar Altimeter System(RA-2),” *ESA Bulletin*, **98**, pp. 94–101.

Seaman. R., Bourke, W., Steinle, P., Hart, T., Embery, G., Naughton, M. and Rikus, L. 1995. “Evolution of the Bureau of Meteorology’s Global Assimilation and Prediction system. Part 1: Analysis and initialisation,” *Aust. Met. Mag*, **44**, pp. 1–18.

Tolman, H.L., Balasubramaniyan, B., Burroughs, L.D., Chalikov, D.V., Chao, Y.Y., Chen, H.S. and Gerald, V.M. 2002. “Development and implementation of wind-generated ocean surface wave models at NCEP,” *Weather and Forecasting*, **17**, pp. 311–333.

Tolman H.L. and Chalikov, D. 1996. “Source Terms in a Third-Generation Wind Wave Model,” *J. Phys. Oc*., **26**, pp. 2497–2518.

Observation-based source functions for wave forecast models

Alexander V. Babanin and Ian R. Young
Swinburne University of Technology, PO Box 218, Hawthorn, VIC 3140, Australia

Introduction

Forecast of wind-generated waves is of primary importance across a broad range of applications such as naval exercises, marine transport, navigation, ship traffic control, ship design, coastal and offshore industries, maritime safety issues, coastal storm warnings, pollution control and mitigation, fishing, recreational activities at sea, among many others. The forecast is routinely conducted by meteorological centres of every country adjacent to significant water bodies, based on spectral wave models. The models operate by estimating evolution of wave spectra caused by energy sources/sinks.

Physics of two primary source/sink terms employed by the operational models, namely wave-breaking energy dissipation and wind-to-wave energy input have not been updated for decades. In the meantime, the new physics is available. For the first time under field conditions, in the course of ONR Lake George (Australia) project, estimates of the spectral distribution of the wave-breaking dissipation were obtained, and measurements of the wind input spectral function were conducted, including conditions of strong-to-extreme wind forcing. Corresponding outcomes were parameterised as source functions suitable for spectral wave models, and both exhibit a number of physical features presently not accounted for.

The source terms were tested, calibrated and validated on the basis of a research third-generation wave model. Physical constraints were imposed on the source functions in terms of the known experimental dependences for the total wind-wave momentum flux and for the ratio between the total input and total dissipation. Enforcing the constraints in the course of wave-spectrum evolution allowed calibration of the free experimental parameters of the new input and dissipation functions. The approach allows separate calibration of the source functions, before they are employed in the evolution tests. The evolution simulations were then conducted. The resulting time-limited development of integral, spectral and directional wave properties, based on implementation of the new physically-justified source/sink terms and constraints, is then analysed. Good agreement of the simulated evolution with known experimental dependences is demonstrated.

Observation-based source functions

Spectral evolution of the wind-generated wave field is commonly described by the radiative transfer equation (Hasselmann 1960):

$$\frac{dF(\omega,\mathbf{k})}{dt} = I(\omega,\mathbf{k}) + N(\omega,\mathbf{k}) + D(\omega,\mathbf{k}) + B(\omega,\mathbf{k}) \qquad (1)$$

where the total derivative of the frequency (ω) -wavenumber ($\mathbf{k}$) spectrum $F(\omega,\mathbf{k})$ on the left hand side is balanced by the sum of energy source I, sinks D and B, and spectral redistribution N terms on the right. Here, only energy terms for wind input I, dissipation in the water column D, bottom friction B, and four-wave non-linear interactions N are mentioned, as they are usually the dominant terms. Equation (1) is the basic equation used in most phase-average numerical wave prediction models.

A field experiment to study the spectral balance of the source terms for wind-generated waves in finite water depth was carried out in Lake George, Australia. The measurements were made from a shore-connected platform at varying water depths from 1.2 m down to 20 cm. Wind conditions and the geometry of the lake were such that fetch-limited conditions with fetches ranging from approximately 10 km down to 1 km prevailed. The resulting waves were intermediate-depth wind waves with inverse wave ages, measured by the ratio of wind speed at *10m* height above the sea level, U_{10} to the speed of the dominant (spectral peak) waves, c_p in the range of $1<U_{10} / c_p <8$. The range is very broad and atmospheric input, whitecap dissipation and bottom friction were measured directly and synchronously by an integrated measurement system (Young et al. 2005).

Wind input

Results of measurements of the wind input energy source *I* (1) are published in a three-part series by Donelan et al. (2005, 2006) and Babanin et al. (2007). Technology of direct field measurements of the wave-induced pressure in air flow over water waves is detailed in Donelan et al. (2005).

The dimensionless growth rate of wave due to wind is customarily expressed in terms of the fractional energy increase γ, which is a spectral function

$$\gamma(\omega) = \frac{\rho_w}{\rho_a} \frac{1}{\omega F(\omega)} \frac{\partial F(\omega)}{\partial t}. \tag{2}$$

Here, ρ_w and ρ_a are densities of water and air respectively. Once the growth rate function $\gamma(\omega)$ is known and the power spectrum $F(\omega)$ is available, the dimensional wind energy input is

$$I(\omega) = \rho a \omega g \gamma(\omega) F(\omega) \tag{3}$$

where g is the gravitational constant.

Previously reported measurements of the wave-induced air pressure were conducted in deep-water at conditions in which the level of forcing was rather weak: $U_{10} / c_p <3$. The data reported here, obtained during the Lake George experiment, have the much broader range of wind forcing as outlined above.

If translated into a form suitable for applications in spectral wave forecast models where information about steepness of individual waves is not available, the growth rate parameterisation, based on the Lake George observations, is

$$\gamma = G\sqrt{B_n}\left(\frac{U_{10}}{c} - 1\right)^2, \qquad \textit{(4)}$$
$$G = 2.80 - 1.00 \cdot \tanh\left(10\sqrt{B_n}\left(\frac{U_{10}}{c} - 1\right)^2 - 11\right).$$

Here $B_n(\omega) = \dfrac{\omega^5 F(\omega)}{2g^2} A(\omega)$ is the spectral saturation and $A(\omega)$ is the directional spreading function defined in Babanin and Soloviev (1998).

Whitecapping dissipation

As a result of Lake George experiment, spectral distribution of the wave energy dissipation was directly measured for the first time. Two different methodologies were used to investigate the dissipation function. The first employed the acoustic noise spectrograms to identify segments of breaking and non-breaking dominant wave trains (Babanin et al. 2001). As an independent second approach, a passive acoustic method of detecting individual bubble-formation events was developed. This method was found promising for obtaining both the rate of occurrence of breaking events at different wave scales and the severity of wave breaking (Manasseh et al. 2006). A combination of the two methods should lead to direct estimates of the spectral distribution of wave dissipation.

The following parameterisation of the dissipation term was suggested:

$$D(\omega) = -a_1 \rho_w g \omega ((F(\omega) - F_{thr}(\omega))A(\omega))^n - a_2 \rho_w g \int_{\omega_p}^{\omega} (F(q) - F_{thr}(q))A(q)dq \qquad (5)$$

where ωp is the spectral peak frequency, ai are experimental constants yet to be comprehensively obtained, $Fthr$ (ω) is the dimensional threshold (Young and Babanin 2006).

Discussion and conclusions

Tsagareli et al. (2010) and Babanin et al. (2010) tested and calibrated the new wind-input and dissipation function, respectively. The calibration was conducted on the basis of independent physical constraints, separately for the input and dissipation. The new source terms were then implemented in a research model with exact nonlinear-term computations and verified against measured integral, spectral and directional properties of wave field. The free parameters of the source-term shapes were not imposed, but allowed to evolve in the course of wave evolution. The resulting evolution yields results consistent with previously observed parameters.

References

Babanin, A.V., and Yu.P. Soloviev (1998) Variability of directional spectra of wind-generated waves, studied by means of wave staff arrays. *Marine & Freshwater Research*, Vol. 49 No. 2, 89-101.

Babanin, A.V., I.R. Young, and M.L. Banner (2001) Breaking probabilities for dominant surface waves on water of finite constant depth. *J. Geophys. Res.,* 106(C6), 11659-11676.

Babanin, A.V., M.L. Banner, I.R. Young, and M.A. Donelan (2007) Wave follower measurements of the wind input spectral function. Part 3. Parameterization of the wind input enhancement due to wave breaking. *J. Phys. Oceanogr.*, 37(11), doi: 10.1175/JPO3147.1, 2764–2775.

Babanin, A.V., K.N. Tsagareli, I.R Young, and D.J. Walker (2010) Numerical investigation of spectral evolution of wind waves. Part 2. Dissipation function and evolution tests. *J. Phys. Oceanogr.,* 40(4), 667-683.

Donelan, M.A., A.V. Babanin, I.R. Young, M.L. Banner, and C. McCormick (2005) Wave follower field measurements of the wind input spectral function. Part I. Measurements and calibrations, *J. Atmos. Oceanic Tech,* Vol. 22 No. 7, 799–813.

Donelan, M.A., A.V. Babanin, I.R.Young, and M.L. Banner (2006) Wave follower measurements of the wind input spectral function. Part 2. Parameterization of the wind input. *J. Phys. Oceanogr.*, Vol. 36 No. 8, 1672-1688.

Hasselmann, K. (1960) Grundleiehungen der Seegangsvoraussage. *Schiffstechnik*, Vol. 7, 191-195.

Manasseh, R., A.V. Babanin, C. Forbes, K. Rickards, I. Bobevski, and A. Ooi (2006) Passive acoustic determination of wave-breaking events and their severity across the spectrum, *J. Atmos. Oceanic Tech.,* Vol. 23 No. 4, 599–618.

Tsagareli, K.N., A.V. Babanin, D.J. Walker, and I.R. Young (2010) Numerical investigation of spectral evolution of wind waves. Part 1. Wind input source function. *J. Phys. Oceanogr.,* 40(4), 656-666.

Young, I.R., M.L. Banner, M.A. Donelan, A.V. Babanin, W.K. Melville, F. Veron and C. McCormic (2005) An integrated system for the study of wind wave source terms in finite depth water, *J. Atmos. Oceanic Tech,* Vol. 22, 814-828.

Young, I.R., and A.V. Babanin (2006) Spectral distribution of energy dissipation of wind-generated waves due to dominant wave breaking, *J. Phys.*

Application of an inertial coupling scheme in a global wave forecasting model

Malek Ghantous and John A. T. Bye
School of Earth Sciences, University of Melbourne, VIC 3010, Australia
Eric Schulz
Centre for Australian Weather and Climate Research,
GPO Box 1289, Melbourne, VIC 3001, Australia

Introduction

Most wave forecasting models employ air–sea coupling parameterisations based on wind and wave observations made at relatively low wind speeds, leading to unreliable predictions of the wave field at high wind speeds. With recent theoretical, experimental and field work we now have a much better idea of the behaviour of the wave field under extreme winds, such as those of a tropical cyclone. Using recent data, a model for air–sea interaction based on the inertial coupling of the air and water—that is, a model based on the physics of the interaction and not just the observations—has been developed. A refinement to the model involves the inclusion of an empirical parameter which represents the sea spray characterised by white capping.

According to one school of thought, the production of sea spray is largely responsible for the reduction of drag at high wind speeds, so the ability to represent it in models should allow for a more complete and accurate forecast. We have conducted numerical experiments using a modified version of the WAM wave model, where the standard coupling algorithm has been replaced with the new inertial coupling model, and compared the results against those using several other coupling schemes as well as against recently published field data.

Coupling model

The foundation of the air–sea coupling model is the inertial coupling model of Bye (1995) for fluids with greatly differing densities, where the stress at the surface due to inertial forces between the air and water (as opposed to viscous forces) is given by:

$$\tau_s = \rho_a K \left| u_a - u_0 - \frac{1}{\varepsilon}(u_w - u_0) \right| \times \left(u_a - u_0 - \frac{1}{\varepsilon}(u_w - u_0) \right)$$

Where $\varepsilon = \sqrt{\rho_a / \rho_w}$ and ρ_a and ρ_w are the densities of air and water respectively, u_a and u_W the velocities, and u_0 a reference velocity. K is the so-called inertial drag coefficient, not to be confused with the usual ten metre drag usually indicated by C_D. Deriving an expression for this latter value was one of the main aims of the analysis of Bye and Wolff (2008). To do this they appealed to a "similarity" condition for the boundary layer, by which it is meant that characteristic lengths above and below the interface are assumed to be the same. The relevant quantities are summarised in Fig. 1.

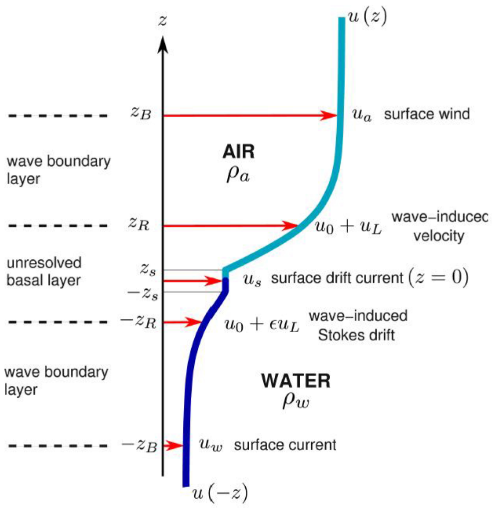

Fig. 1 Velocity structure of the wave boundary layer according to the inertial coupling model of Bye and Wolff. All quantities are measured relative to the surface at *z*=0.

The fundamental equation for the drag coefficient is:

$$\frac{1}{\sqrt{C_D}} = \frac{R}{\sqrt{K}} = \frac{1}{\kappa}\ln\left(\frac{(u_* BR)^2}{2Kz_{10}g}\right)$$

where z_{10} is the ten metre height, κ is von Kármán's constant, and u_* is the friction velocity. The parameter B is defined as the ratio between the wave peak phase speed and the air velocity, and R is a function of the ratio between the Eulerian and Stokes shears in the water. Various forms for these parameters were developed, including the addition of another parameter representing spray. They were tested against field measurements and further refinements were made as a result, leading, significantly, to the collapse of several parameters into one, and in particular the complete disappearance of the wave peak phase speed from the relation.

Conclusion

A new model for the interaction between wind and waves has been developed and tested within a third-generation wave prediction model. The results suggest that the drag does not depend on the peak waves at all, which is consistent with most of the stress being supported by the short waves. Bye et al. (2010)

References

Bye, J.A.T. 1995. Inertial coupling of fluids with large density contrast. *Physics Letters A*, 202(2-3):222–224.

Bye, J.A.T and Wolff, J.-O. 2008. Charnock dynamics: a model for the velocity structure in the wave boundary layer of the air–sea interface. *Ocean Dynamics*, 58(1):31–42.

Bye, J.A.T, Ghantous, M. and Wolff J.-O. 2010. On the variability of the Charnock constant and the functional dependence of the drag coefficient on wind speed. *Ocean Dynamics*, DOI: 10.1007/s10236-010-0300-8.

Incorporating Breaking Wave Predictions in Spectral Wave Forecast Models

Russel Morison and Michael Banner
School of Mathematics, The University of New South Wales, Sydney 2052, Australia

Introduction

Dissipation through wave breaking is a key process in the evolution of wind waves. Most of the wind input momentum and energy fluxes to the waves leave the wave field locally via wave breaking to drive currents and generate turbulence, respectively, in the upper ocean (Donelan, 1998).

Wave breaking underlies the very significant enhancement in surface layer turbulent kinetic energy (TKE) dissipation rate measurements over conventional rough wall levels (e.g. Terray et al. 1996, Gemmrich and Farmer, 2004). Wave breaking also enhances interfacial fluxes through enhanced overturning of the sea surface (e.g. Melville, 1994). Recent basin-wide theoretical model studies have demonstrated the potentially strong contributions from breaking waves to the circulation and mixing (e.g. Restrepo, 2007, among others).

Yet, in wave forecasting models, the dissipation rate remains the least well-understood source term relative to the other two source terms, wind input and nonlinear spectral transfer, and these models do not provide any breaking predictions.

While incompletely understood, evidence is building that wave breaking in deep water is a process with a generic threshold that reflects the convergence rate and geometrical steepening of the waves that break. From their innovative analysis of storm waves, Banner et al. (2002) reported that a parameter based on the wave spectral saturation (Phillips, 1985) provides a robust spectral breaking threshold, at least for waves in the energy-containing range. Background turbulence in the wave boundary layer, to which breaking waves of all scales contribute, also has a role in dissipating the energy of wind waves.

Modeling background

Phillips (1985) introduced $\Lambda(\mathbf{c})$, the spectral density of breaking crest length per unit sea surface area as a basic spectral measure of wave breaking, $\Lambda(c)\ d\mathbf{c}$ gives the crest length/unit sea surface area, of breaking crests travelling with velocities in ($\mathbf{c}$, $\mathbf{c}$+d$\mathbf{c}$). $\Lambda(\mathbf{c})$ is one of the primary breaking forecast parameters computed in this study. $\Lambda(\mathbf{c})$ can also be used to model breaking wave enhancements to the wind stress and allied air-sea fluxes such as sea spray based on the sea state, rather than the wind field.

A closely related major challenge is to be able to relate the geometric/kinematic measurements of $\Lambda(\mathbf{c})$ accurately to the underlying energy dissipation rate $\varepsilon(\mathbf{c})$. Phillips (1985, equation (6.3)) proposed the following connection between these two distributions, given below in scalar form:

$$\varepsilon(c)\ dc = b\, g^{-1} c^5 \Lambda(c)\ dc \tag{1}$$

where the non-dimensional coefficient b connects the energetics to the whitecap geometry and kinematics, and reflects the breaking strength.
Underlying (1) is the assumption that the mean wave energy dissipation rate at scale (c, c+dc) is dominated by wave breaking at that scale. This may have shortcomings, especially for shorter breaking waves due to the attenuation of short wave energy by the passage of longer breaking waves (e.g. Banner et al. 1989).

A less restrictive form for S_{ds} should have a local contribution from the given breaking wave scale, S_{ds}^{loc} , plus a background attenuation component, S_{ds}^{loc} , representing the background turbulence in the wave boundary layer and the cumulative attenuation of short waves by longer breaking waves sweeping through them. To account for these effects, we modeled the total dissipation rate as the sum of these two contributions: locdsSnlocdsS

$$S_{ds} = S_{ds}^{loc} + S_{ds}^{nloc} \tag{2}$$

and used S_{ds}^{loc} as the appropriate dissipation rate in (1).

Brief description of the methodology

The breaking probability $P_{br}(c)$ for wave scales c is defined as:

$$\mathrm{Pr}_{br}(\mathbf{c}) = \frac{\int \mathbf{c}\Lambda\, d\mathbf{c}}{\int \mathbf{c}\Pi\, d\mathbf{c}} \tag{3}$$

It is easily shown from the definition that

$$\Pi(c_p) = \chi\, g/(2\pi c_p^3) \tag{4}$$

where $\chi \sim 0.7$ is the measured crest intermittency factor at the in the +/- 30% relative speed bandwidth about the spectral peak.

Hence

$$\Lambda(c_p) = (\chi\, g/2\pi c_p^3) * \Pr(\tilde{\sigma}_p) \tag{5}$$

The sea state threshold variable used was the normalised spectral saturation

$$\tilde{\sigma}(k) = \sigma(k) \,/ < \theta(k) > \tag{6}$$

where $\sigma(k)$ is the azimuth-integrated spectral saturation given by

$$\sigma(k) = k^4 \Phi(k) = (2\pi)^4 f^5 G(f) / 2g^2 \tag{7}$$

and $<\theta(k)>$ is the mean spectral spreading width given by

$$< \theta(k) > = \int_{-\pi}^{\pi} (\theta - \bar{\theta})\, F(k,\theta)\, k\, d\theta \Big/ \int_{-\pi}^{\pi} F(k,\theta)\, k\, d\theta \tag{8}$$

Where $\bar{\theta}$ is the mean wave direction, and F(k), G(f) and F(k,θ) are, respectively, the spectra of wave height as a function of scalar wavenumber, frequency and vector wavenumber.

Banner, Gemmrich and Farmer (2002) showed evidence for a common threshold behaviour for the dissipation rate at different frequencies at and above the spectral peak

$$Pr_{br}(\tilde{\sigma}_p) = H(\tilde{\sigma} - \tilde{\sigma}_T) * \alpha_{br} * (\tilde{\sigma} - \tilde{\sigma}_T) \qquad (9)$$

where α_{br}~33. In our methodology, $\tilde{\sigma}(k)$ calculated from our spectral wave model is used to calculate the breaking probability at the spectral peak at any stage of wave development.

Spectral peak breaking strength coefficient b_p

We begin by recalling Phillips (1985) form:

$$S_{ds}^{loc}(c)\, dc = b\, g^{-2} c^5 \Lambda(c)\, dc \qquad (10)$$

This is term in (2) that is relevant to the local breaking strength and crest length properties. It should be noted that, a priori, b may vary across the spectrum. For the spectral peak, using the preceding result for $\Lambda(c)$ and transforming the local dissipation rate from **c** to **k** dependence to match with our wave model output, we obtain

$$\begin{aligned} b_p &= 2\, \frac{g^3}{c_p^8} \frac{S_{ds}^{loc}(k_p)}{\Lambda(c_p)} \\ &= \frac{4\pi}{\chi} \frac{g^2}{c_p^5} \frac{S_{ds}^{loc}(k_p)}{Pr_{br}(\tilde{\sigma}_p)} \end{aligned} \qquad (11)$$

Recalling (5):

$$\Lambda(c_p) = (\chi\, g/2\pi c_p^3) * Pr(\tilde{\sigma}_p) \qquad (12)$$

it is seen that with the wave model output for the spectrum (for $\tilde{\sigma}$) and the local component of the dissipation rate source term (S_{ds}^{loc}), equations (5) and (12) provide the breaking crest length spectral density and breaking strength at the spectral peak at any time step.

Results

The spectral wind wave model used to generate the present results is described in detail in Banner and Morison (2009). In Fig. 1 it can be seen that the modeled value of $\Lambda(c_p)$ agrees well with the measurements for Period 1. There was no breaking observed at the spectral peak for the mature sea (Period 3), which the model also reproduced.

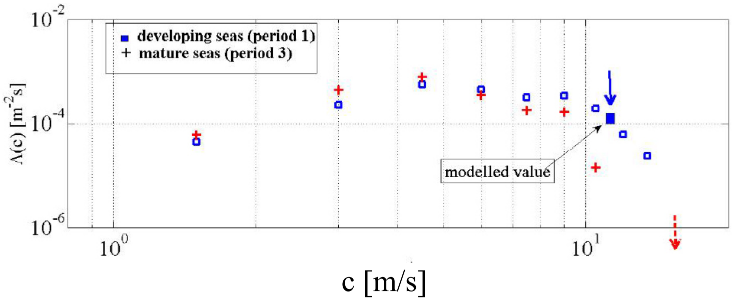

Fig. 1 Calculated $\Lambda(c_p)$ plotted on the measure $\Lambda(c)$ spectra for the developing (period 1) and mature (period 3) sea states in FAIRS. The corresponding wave ages were c_p/U_{10}~0.9 and 1.25 respectively, with the nominal wind speed U_{10}~12 m/s.

Figure 2 shows the modeled variation of the spectral peak lambda [Λ (cp)] and corresponding spectral peak breaking strength [bp] as the wave age c_p/U_{10} varies from young to old, for the wind speed U_{10}=12 m/s representative of FAIRS.

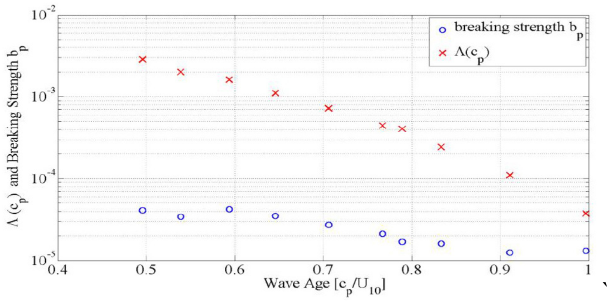

Fig. 2 Predicted variation of Λ(cp) and bp with wave age for the peak waves U_{10} = 12 m/s

More results were shown during the talk.

Summary

(i) our framework provides predictions of dominant wave breaking properties (crest length spectral density per unit area and breaking strength) using standard wave model output.

(ii) it provides accurate predictions for the limited breaking data available for developing and mature wind seas.

(iii) further validation against data will be made as suitable new breaking wave data sets becomes available.

(iv) after further validation, this methodology is easily added to existing spectral wave forecasting models. However, refinement of the nonlinear transfer source term beyond the DIA approximation is probably needed.

Acknowledgments

The authors gratefully acknowledge the support of ONR for their air-sea interaction studies under the CBLAST and RaDyO DRI programs.

References

Banner, M.L., Gemmrich, J.R. and Farmer, D.M. 2002. Multiscale measurements of ocean wave breaking probability. J. Phys. Oceanogr., 32, 3364-3375.

Banner, M.L. and Morison, R.P. 2009. Refined source terms in wind wave models with explicit wave breaking forecasts. Part I. Model framework and validation against field data. Ocean Modelling, Feb 2010.

Donelan, M.A. 1998. Air-water exchange processes. In Physical Processes in Oceans and Lakes (J. Imberger, Ed), AGU Coastal and Estuarine Studies 54, 19-36.

Gemmrich, J.R. and Farmer, D.M. 2004. Near-surface turbulence in the presence of breaking waves. J. Phys. Oceanogr., 34, 1067-1086.

Phillips, O.M. 1985. Spectral and statistical properties of the equilibrium range in wind-generated gravity waves. J. Fluid Mech., 156, 505-531.

Using smoothed particle hydrodynamics to model rogue waves, tsunamis, dam breaks and coastal inundation

Murray Rudman, Mahesh Prakash and Paul W. Cleary
CSIRO Mathematics, Informatics and Statistics

Introduction

Modelling flows with a free surface or interface, such as those occurring when a wave breaks, is a difficult computational task because the location of the interface is one of the unknowns in the problem. Because the interface determines the size and shape of the fluid domain and consequently the location where boundary conditions must be applied, the modelling procedure must be flexible and adaptable enough to consider this. For the general case (e.g. in wave breaking) fluid fragmentation and coalescence occurs and can be an important part of the process. Simplified numerical techniques such as the Boundary Element Method (BEM) cannot handle such flows. Three modelling techniques can be potentially used in the general case– Volume-of-Fluid (VOF), Level Set or Smoothed Particle Hydrodynamics (SPH). It is not our intention to describe the relative merits of each of these methods, rather to demonstrate the applicability of one of them – SPH.

As opposed to traditional, mesh-based (Eulerian) fluid modelling techniques, SPH is a mesh free, Lagrangian method. There is no underlying computational mesh and all of the fluid information (mass, momentum and energy) is stored and transported on "particles" that are advected through the computational domain with the local fluid velocity. Due to its Lagrangian nature, complex time-dependant flow domains and their associated boundary conditions are handled easily and naturally. Fluid coalescence and fragmentation are similarly automatically handled without complex algorithmic logic being required.

In the presentation I will provide a brief overview of the SPH method before discussing a number of examples where it has been applied to problems of practical significance.

Examples

Marine hydrodynamics

In the area of marine hydrodynamics e a range of different physical phenomena need to be captured including two termed "slamming" and "green water on deck" (see **Fig. 3**). When a ship is travelling at speed, slamming can arise when the combination of swell position and pitch of the vessel causes the bow (or stern) to lie completely above the sea surface. As the pitch and swell position change, the bow (stern) can slam into the sea surface, giving rise to high pressures and structural loads that can damage the vessel structure. Green water on deck occurs when the pitch of the vessel causes it to be below the top of the next wave in a swell, so that significant volumes of water are flow over its bow, endangering crew and deck infrastructure.

Rogue wave impact on an offshore structure

Rogue waves are open ocean water waves that were, for many years, considered to be the products of sailors' overactive imaginations. Even though evidence in support of the existence of rogue waves was increasingly found during the 20th century, it wasn't until the "Draupner" wave was measured at 26 m (peak to trough) on New years day 1995 in the North Sea, that their existence was confirmed. Even then, it was believed that these waves were exceptionally rare and unlikely to be of much risk. However in 2001, European Space Agency satellites monitoring the world's oceans picked up more than 10 giant waves over 25 metre high in a period of just three weeks, and rouge waves became identified as a new danger to offshore structures including oil and gas platforms. Fig. 4 shows the SPH simulation of the impact of a 25 m rogue wave on a floating semi-submersible offshore platform. The pitch and trajectory of the platform as well as the tension in the mooring lines can be determined from the simulation results.

Dam break

The fracture of a dam wall can result in significant destruction and death as a result of the ensuing surge of water that flows into the valley systems below. The dangers from such an event are significant and earth wall dams and dams in earthquake prone regions are particularly vulnerable. An example is the collapse of the St Francis Dam, when 450 lives were lost when the dam suddenly collapsed just before midnight on March 12th 1928. SPH simulation results are shown in **Fig. 5** where the digital terrain model has been rendered with texture from satellite images. The rate of the inundation has been verified by the arrival time at a down stream power station taken from the historical record.

Tsunami impact on a shore line

Tsunami's are long wavelength, low amplitude waves in the open ocean, but when they approach a shoreline can reach large heights and can inundate vast areas of the coastal region, causing destruction and death. SPH has been used to model the impact of a tsunami on real coastal topography in **Fig. 6**. The left image shows the wave just before it starts inundating the coastline and the right shows the water engulfing the valleys on the coastline. The incident wave travels as far as 1 km inland in approximately 1 minute along the central valley indicated by the red arrow in frame. A return wave that has been reflected off the shore line can also be seen at this time.

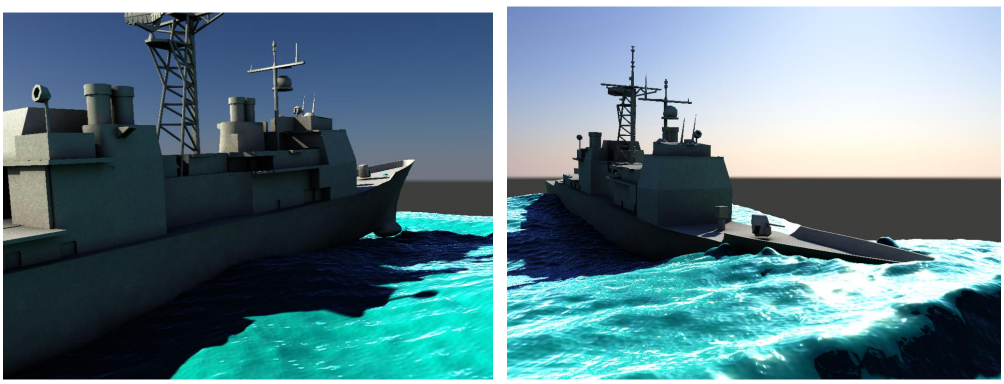

Fig. 3 Simulation of a cruiser travelling at 20 knots in a 6 m swell. The bow of the ship is about to "slam" into water (left) and has dipped significantly (right) after slamming and has dug into the next wave in the swell, leading to green water washing over the deck.

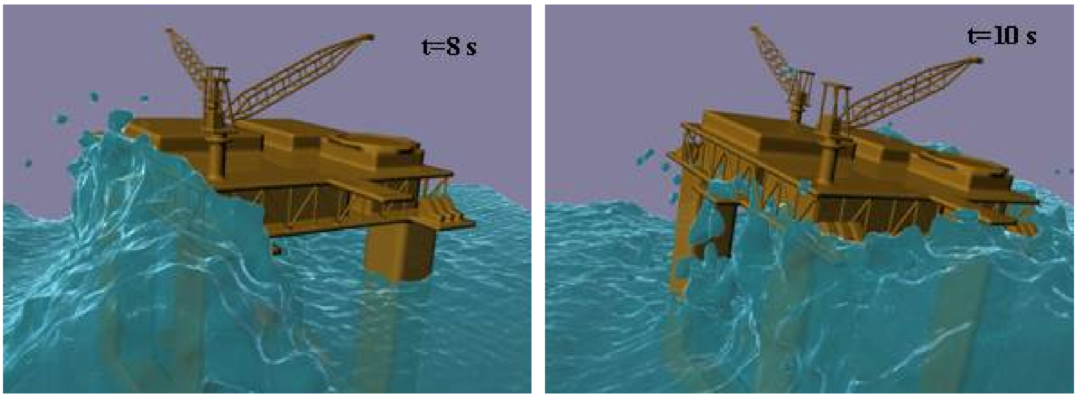

Fig. 4 Simulation of a rogue wave impacting a floating offshore gas platform that is tethered to the ocean floor. The pitch and trajectory of the mooring line tension are predicted from the simulation results.

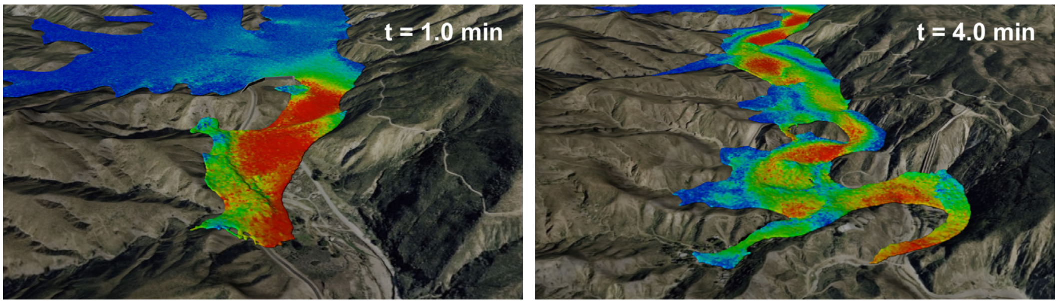

Fig. 5 Simulation of the collapse of the St Francis Dam in Southern California in 1928. The fluid colouring represents the speed of the water, with red high and blue low.

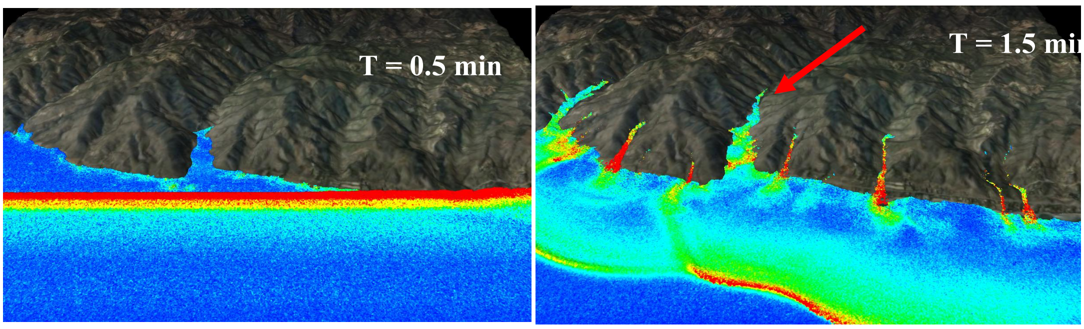

Fig. 6 Simulation of a very large (40 m) tsunami approaching coastline. The inundation pattern and timing of the surge front is predicted using the SPH technique.

The instability of wave trains propagating over an oblique current: a laboratory experiment in a directional wave basin

Alessandro Toffoli, Alexander V. Babanin
Swinburne University of Technology, P.O. Box 218, Hawthorn, VIC 3122, Australia
Fabrice Ardhuin
IFREMER, BP 70. Plouzané, 29280, France
Michel Benoit
Saint-Venant Laboratory, Univ. Paris-Est (EDF R&D-CETMEF-Ecole des Ponts)
6 quai Watier, BP 49 78401 Chatou,France
Elzbieta M. Bitner-Gregersen
Det Norske Veritas, Veritasveien 1, 1322 Hoevik, Norway
Luigi Cavaleri
Institute of Marine Science, Castello 1364/A, 30122 Venice, Italy
Jaak Monbaliu
K.U. Leuven, Kasteelpart Arenberg 40, 3001 Heverlee, Belgium
Miguel Onorato, Alfred R. Osborne
Università di Torino, Via P. Giuria 1, 10125 Torino, Italy
Carl-Trygve Stansberg
MARINTEK, P.o.Box 4125 Valentinlyst, N-7450 Trondheim, Norway

Introduction

Extreme waves represent a serious threat for marine structures and operations. Numerical and theoretical work has already demonstrated that the modulational instability plays a relevant role in the formation of extreme waves (Janssen 2003, Onorato et al. 2006, Onorato et al. 2001). However, strong deviations from Gaussian statistics can only be expected if waves are rather long crested i.e. the spectral energy is concentrated on a narrow range of directions (Onorato et al. 2002, Socquet-Juglard et al. 2005, Onorato et al. 2009). For more realistic short crested seas (i.e. broad directional distributions), the effect of modulational instability becomes less prominent and, as a result, the occurrence of extreme waves does not exceed predictions from second-order theory (e.g. Socquet_juglard et al. 2005). This transition between strongly to weakly non-Gaussian behavior is determined by a balance between nonlinearity (which promotes non-Gaussian behavior) and directionality (which suppresses non-Gaussian behavior). Thus, if there are circumstances when the nonlinearity is locally enhanced, we can expect that non-Gaussian behavior would persist also at broader directional spreads. In this respect, when waves propagates against an ambient current, wave steepness, and hence nonlinearity, increases as a consequence of the shortening of the wavelength, making nonlinear processes, such as the modulational instability mechanism, more likely. A number of laboratory experiments have been carried out to verify the behaviour of regular and irregular waves when opposing a strong current. Most experimental results until now have been obtained in wave flumes, where only one-dimensional propagation can be addressed. For the present study, we have accessed one of the largest directional wave tank in the world to address the more general two dimensional problem, where a multi directional wave field propagates obliquely over a uniform current in partial opposition. The aim is to explore the role of increasing wave steepness due to wave-current interaction on the modulational instability mechanism and the formation of large amplitude waves.

Laboratory experiments

The laboratory facility is a large rectangular wave basin with dimensions of 70 *m* X 50 *m*. The basin is fitted with a directional wave-maker along the 70 *m* side and a water circulation system along the 50 *m* side (see Stansberg 2008). For the present experiments the water depth was uniform over the basin and fixed at 3 *m*.

The methodology of the experiment was fairly simple. It consisted in monitoring the spatial evolution of regular and irregular wave fields as they propagate over an oblique current. In this respect, time series were recorded at a sampling frequency of 75 Hz along the mean wave direction. Regular fields were characterized by a monochromatic wave (carrier wave) and two side band perturbations. We used a carrier wave with period of 0.8 *s* and steepness ka=0.1, where k is the wavenumber of the carrier wave and a is its amplitude, while the two perturbations had amplitude equal to 0.25a and bandwidth Δk = 0.25. According to the instability diagram of Benjamin-Feir (see, e.g. Yuen and Lake 1982), this configuration is stable. Irregular waves were defined by a JONSWAP spectrum with peak period T_p=1 *s*, significant wave height H_s=0.08 *m* and peak enhancement factor γ=6. A frequency-independent $cos^N(\theta)$ directional function was then applied to describe the energy in the directional domain. A number of values of the spreading coefficient N were used, ranging from long to short crested conditions: N = 840; 200; 90; 50; and 24. At the wave-maker, waves were generated as an inverse Fourier transform with random amplitudes and phases approximation.

For both regular and irregular experiments, a uniform current was run at its maximum speed of 0.2 *m/s*. In the wave tank, the current flows in the longitudinal basin direction, so that it crosses directional wave fields. An angle of 110 *deg* was considered; this configuration generates a partial opposition, which is expected to increase the wave steepness of about 8-10%. For reference, tests were also performed in the absence of current.

For each random test, 30-minute time series were recorded. Experiments were also repeated four times with the same spectral configuration but different random amplitudes and phases to ensure a sufficiently large data set for statistical analysis.

Results

In Fig. 1, the evolution of the maximum amplitude of the wave packets is shown as a function of the dimensionless distance from the wave-maker. In the absence of an ambient current, the wave packets are basically stable, i.e., the amplitude does not change significantly as waves propagate along the tank.

However, when waves interact with a partial opposing current, the steepness of the carrier wave increases due to the shortening of the wavelength. This increase triggers effects related to the nonlinear dynamics of the wave packets. In this respect, we observed a robust increase of the maximum surface elevation along the tank; a peak is evident after about 23 wavelengths and it is almost twice the value of the initial wave train. Note that this behavior is expected from the evolution of unstable wave packets (see, for example, Yuen and lake 1982).

If the current is able to trigger the instability of wave packets and hence extreme waves, then it is feasible to suspect that in a random wave fields the percentage of extreme events can substantially increase. For irregular wave fields, the occurrence of extreme events can be summarized conveniently by the fourth order moment of the probability density function of the surface elevation, namely the kurtosis. For reference, we mention that the kurtosis of a Gaussian (linear) wave field is equal to 3.

In the absence of an ambient current, it is well established that random wave fields strongly deviate from Gaussian statistics, provided waves are sufficiently steep and narrow banded both in frequency and direction (Onorato et al. 2009). In a more realistic condition, however, wave fields are characterized by a broader directional distribution and, as a result, the percentage of extreme waves decreases substantially. The overall effect of directionality is highlighted in Fig. 2, where the maximum kurtosis detected in the tank is presented as a function of the directional spreading coefficient.

In the presence of an ambient current, extreme waves still remain less likely in directional wave fields rather than in long crested conditions (Fig. 2). Nonetheless, we observed a systematic enhancement of the kurtosis as a consequence of the wave-current interaction. It is interesting to note that this difference becomes a bit more prominent for broader directional sea states: the kurtosis is about 1.5% higher for $N > 90$, while it is about 3% higher for $N \leq 90$. This seems to suggest that the weak increase of steepness related to the wave-current interaction slightly compensates the suppression of non-Gaussian behavior due to directionality.

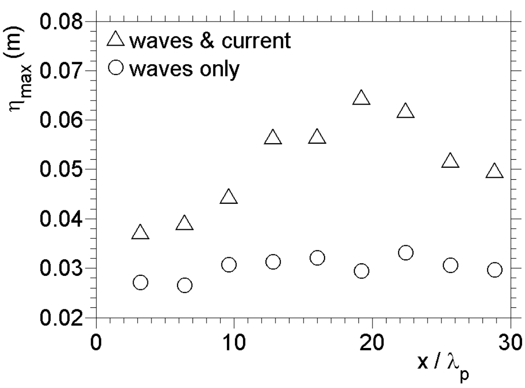

Fig. 1 Regular waves experiments evolution of wave amplitude.

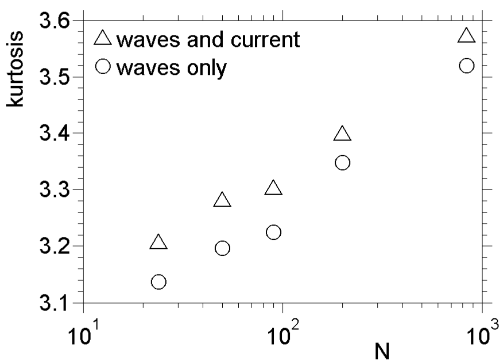

Fig. 2 irregular waves experiments: kurtosis as function of the directional spreading coefficient.

References

Janssen P.A.E.M. 2003. *J. Phys. Ocean.,* **33/4**.

Onorato, M., Osborne, A., Serio M. and Bertone. 2001. *Phys.Rev. Lett.,* **86/25**.

Onorato, M., Osborne, A., Serio, M., Cavaleri, L., Brandini C. and Stansberg C. 2006.*Europ. J. Mech. B/Fluids,***25**.

Onorato, M., Osborne, A.R. and Serio, M. 2002. *Physics of Fluids,* **14/4**.

Onorato, M., Waseda, T., Toffoli, A., Cavaleri, L., Gramdstad, O., Janssen, P.A.E.M., Kinoshita, T., Monbaliu, J., Mori, N., Osborne, A.R., Serio, M., Stansberg, C., Tamura H. and Trulsen K. 2009. *Phys. Rev. Lett.,***102**(114502).

Socquet-Juglard, H., Dysthe, K., Trulsen, K., Krogstad H. and Liu J. 2005. *J. Fluid Mech.,* **542**.

Stansberg, VC.T. 2008. In Proc. 27th Int. Conf. Offshore Mechanics and Artic Engineering OMAE, paper OMAE2008–57621.

Yuen, H.C. and Lake, B.M. 1982. *Advances in AppliedMechanics,* **22**.

Wave and Wind Parameters from HF Ocean Radar

Mal L. Heron, Jasmine B. D. Jaffrés
Australian Coastal Ocean Radar Network, Marine Geophysics Laboratory,
James Cook University, Townsville, QLD 4811

Andrew Middleditch
Seaview Sensing Ltd, Sheffield Technology Parks, Arundel Street, Sheffield S1 2NS, UK

Introduction

A sparse network of surface current and wave-capable HF radars is being established around the Australian coastline to produce quality controlled data into a public-domain archive under the umbrella of the Integrated Marine Observing System (IMOS). The phased array installations within the Australian Coastal Ocean Radar Network (ACORN) produce maps of significant wave heights, and wind directions, and under good signal-to-noise conditions, generate directional wave spectra.

The radar installations are always made in matched pairs, spatially separated so that the beams formed by the phased arrays cross at a non-acute angle in the primary area being mapped; this gives the 2-D capability of each radar pair. Phased-array stations are installed at the Capricorn/Bunker Groups, QLD (Tannum Sands, and Lady Elliot Island); the entrance to the South Australian Gulfs, SA (Cape Wiles, Eyre Peninsula and Cape Spencer, Yorke Peninsula); Rottnest Area, WA (Port Beach, Fremantle and Guilderton); and Coffs Harbour, NSW (Red Rock and North Nambucca).

Extraction of wave and wind parameters from HF radar

In order to make proper use of the data from HF radar, it is important to understand the methodology, the algorithms, and the limitations. This is a remote sensing method where the basic data are time series of radar echoes from a patch of ocean defined by the propagation time of the electromagnetic wave from the transmitter to the patch and back to the receiver, and the width of the beam formed by the phased-array. A power spectrum of the echoes from such a patch of ocean is shown in Fig. 1. The frequency range on the abscissa is ±1 Hz, which represents the Doppler shifts imposed by the dynamic sea surface. The dominant peaks near ± 0.298 Hz are the Bragg peaks for a radar frequency 8.5125 MHz. Essentially all other energy above the base noise level (near ± 1Hz) is due to second-order scatter from non-linear properties of the waves, or from double scatter of the electromagnetic wave. It is the double scatter which gives us information about the wave heights and the directional wave spectrum.

The two Bragg peaks (A and B) are from waves with the resonant wavelength which are propagating towards and away from the radar site. The frequency offset from the calculated position (dashed line) is proportional to the surface current component in the radial direction away from the radar station.

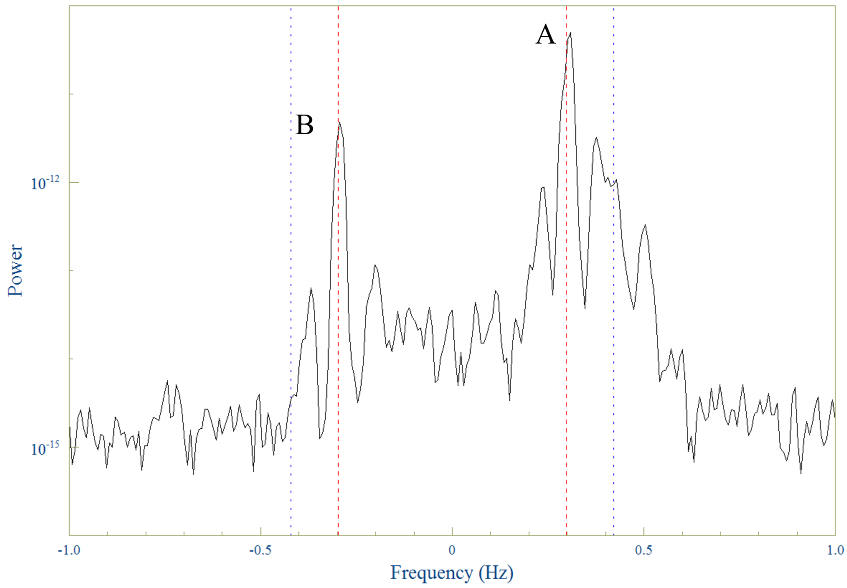

Fig. 1 Doppler spectrum of echoes from a defined patch of ocean. The dominant peaks, A and B, are from first-order Bragg scatter, and the surrounding energy is from second-order scatter due to hydrodynamical effects in the gravity waves, and a double-scatter effect.

Wind direction

The wind direction is determined from the relative energy in the two first-order Bragg lines. Because it is solely based on the first-order energy, wind directions (and surface currents) are available from the maximum working range of the radar at any time. The extraction of wind direction assumes a directional spreading function for the gravity waves at the Bragg wavelength. For a radar operating at 8.5125 MHz the Bragg wavelength is 17.62m, which is a short wind wave. We adopt the model of Longuet-Higgins et al. (1963) and assume the spreading function is

$$G(k,\theta) = A(k)\cos^{2S}(\theta - \theta_0) \tag{1}$$

where θ_0 is the wind direction, k is the wavenumber of the gravity wave, S is a spreading parameter, and $A(k)$ is a normalizing factor such that

$$\int_0^{2\pi} G(k,\theta) = 1. \tag{2}$$

In the routine algorithm for wind direction, we use equations (1) and (2) with S = 2, and the measured ratio, R, of the energy in the first-order Bragg peaks. Then, following Heron and Prytz, (2002):

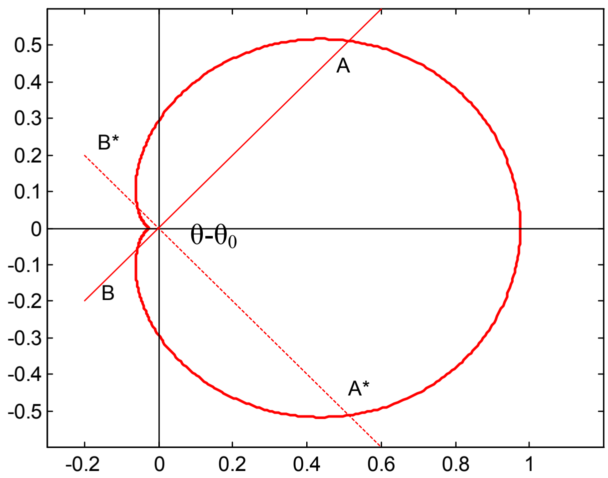

Fig. 2 The algorithm model for wind direction. A given ratio, R, has two solutions, A/B, and A*/B*.

$$\left|\theta - \theta_0\right| = \left|2\arctan\left(R^{\frac{1}{2S}}\right)\right| \quad . \tag{3}$$

There is an ambiguity between $\pm(\theta\text{-}\theta_0)$ which is resolved by using the same analysis procedure for the other station.

Significant wave height

Barrick (1977) derived a relationship for rms wave height as:

$$h_{rms}^2 = \frac{2\alpha^2 \int_{-\infty}^{+\infty} [\sigma_2(\omega_d) W(f_d)] df_d}{k_0^2 \int_{-\infty}^{+\infty} \sigma_1(f_d) df_d} \tag{4}$$

where f_d is the Doppler frequency, σ_1 and σ_2 are the first and second-order scattering cross sections respectively, k_0 is the radar wavenumber, and $W(f_d)$ is a weighting function which removes cusps in σ_2. The coefficient α is a scaling factor. Barrick noted the theoretical limitation which requires $k_0 h_s < 0.6$, where h_s is the significant wave height, because of the truncation of second-order expansions. Heron and Heron (1998) evaluated the empirical coefficients by comparing HF radar output with a wave gauge, and suggested $\alpha = 2.20$. They also pointed out that this algorithm is not reliable when the radar beam is within about 15 degrees of orthogonal to the wind direction. An improved algorithm is being developed to account for inaccuracies as the angle changes between the wind direction and the radar beam; and to account for higher-order expansion for high wave heights which breach the theoretical limitation suggested by Barrick (1977).

Directional wave spectra

$$\sigma_2(\omega) = 2^6 \pi k_0^4 \sum_{m,m'=\pm 1} \int_{-\infty}^{+\infty}\int_{-\infty}^{+\infty} |\Gamma|^2 S(m\tilde{k}) S(m'\tilde{k}') \delta(\omega - m\sqrt{gk} - m'\sqrt{gk'}) dpdq \qquad (5)$$

The expansion for the second-order scattering cross-section, σ_2 in equation (4) involves a double integral of $S(\tilde{k})S(\tilde{k}')$ (equation (5)) over wave- number space, where

$$\tilde{k} + \tilde{k}' = -2\tilde{k}_0 \qquad (6)$$

is required to satisfy the Bragg criterion for double scatter. Wyatt (1990) has developed an inversion which fits a Pierson-Moskowitz model for the wind waves, makes simplifying assumptions to reduce the kernel of the integral, and iteratively solves for the directional spectrum of the longer waves.

Acknowledgments

This work is supported by an Industry Linkage grant from the Australian Research Council in collaboration with Seaview Sensing Ltd (UK) and Helzel Messtechnik GmbH (Germany). Data were sourced from the Integrated Marine Observing System (IMOS), under the National Collaborative Research Infrastructure Strategy (NCRIS).

References

Barrick, D.E. Remote sensing of the sea state by radar, in Remote Sensing of the Troposphere,

Barrick, D.E. 1977. Extraction of wave parameters from measured HF radar sea-echo Doppler spectra, Radio Sci., 12, 415-424.

Derr, V.E. ed. 1972. NOAA/Environmental Research Laboratories, Boulder, CO, 12.1-12.6.

Heron, M.L. and Prytz, 2002. A. Wave height and wind direction from the HF coastal ocean surface radar, *Can. J. Remote Sensing*, 28, 385-393.

Heron, S.F. and Heron, M.L. 1998. A comparison of algorithms for extracting significant wave height from HF radar ocean backscatter spectra, J. Atmos. Ocean Tech., 15, 1157-1163.

Longuet-Higgins, M.S., Cartwright, D.E and Smith, N.D. 1963. Observations of the directional spectrum of sea waves using the motions of a floating buoy, in *Ocean Wave Spectra, Proceedings of a Conference.* Prentice-Hall Inc., Englewood Cliffs, N.J., pp. 111-136.

Wyatt, L.R. 1990. A relaxation method for integral inversion applied to HF radar measurement of the ocean wave directional spectrum, Int. J. Remote Sens. 11, 1481-1494.

Evaluation of ADCP wave, WAVEWATCH III and HF radar data on the GBR

Jasmine B. D. Jaffrés, Malcolm L. Heron
Marine Geophysical Laboratory, James Cook University, Townsville, Australia
Michael L. Banner
School of Mathematics, University of New South Wales, Sydney, Australia
Andrew Middleditch
Seaview Sensing Ltd, Sheffield, UK
Craig R. Steinberg
Australian Institute of Marine Science, Townsville, Australia
Tom H. Durrant
Centre for Australian Weather and Climate Research,
Bureau of Meteorology, Melbourne, Australia

Introduction

Wave climate can have a very significant impact on the dynamics of the near-coastal oceans, including geomorphology and currents. This study is a preliminary investigation of the suitability and compatibility of a wave-capable Acoustic Doppler Current Profiler (ADCP) mooring, an HF ocean radar system and the numerical model WAVEWATCH III (WW3), with the focus on the area of the Capricorn and Bunker Groups of reefs and islands, Australia.

Study site

The Capricorn and Bunker Groups of reefs and islands are located within the southern Great Barrier Reef (GBR), Australia. The study site is located on a continental shelf, which is characterised by a concave shape, facing into the prevailing southeasterly wind and dominant swell of the area (Fig. 1). This is a dynamic region for waves from the open ocean, encountering the continental shelf edge and propagating up onto the shelf.

WAVEWATCH III

WAVEWATCH III (WW3), developed by NOAA/NCEP, is a third generation wind-wave model that facilitates the modelling of directional wave spectra (Tolman 2009). In order to obtain both local wind waves and swells in the wave model output, WW3 has to be run on a Pacific-wide scale to allow for the primarily easterly-southeasterly swell to move into the southern GBR. WW3 has one- and two-way nesting capabilities, which reduces the computational expense by allowing for nests outside of the main area of interest to be run at lower resolutions.

Here, three nests have been set up, with the grid size and wind forcing characteristics being listed in Table 1. The largest (Pacific-wide) and the middle (Coral Sea) grids are being forced by Global Analysis and Spectral Prognosis (GASP) winds (Seaman et al. 1995). The forcing of the innermost grid (southern GBR), in turn, is provided by MesoLAPS winds – a mesoscale version of the Limited Area Prediction System (LAPS) (Weinzierl and Smith 2007).

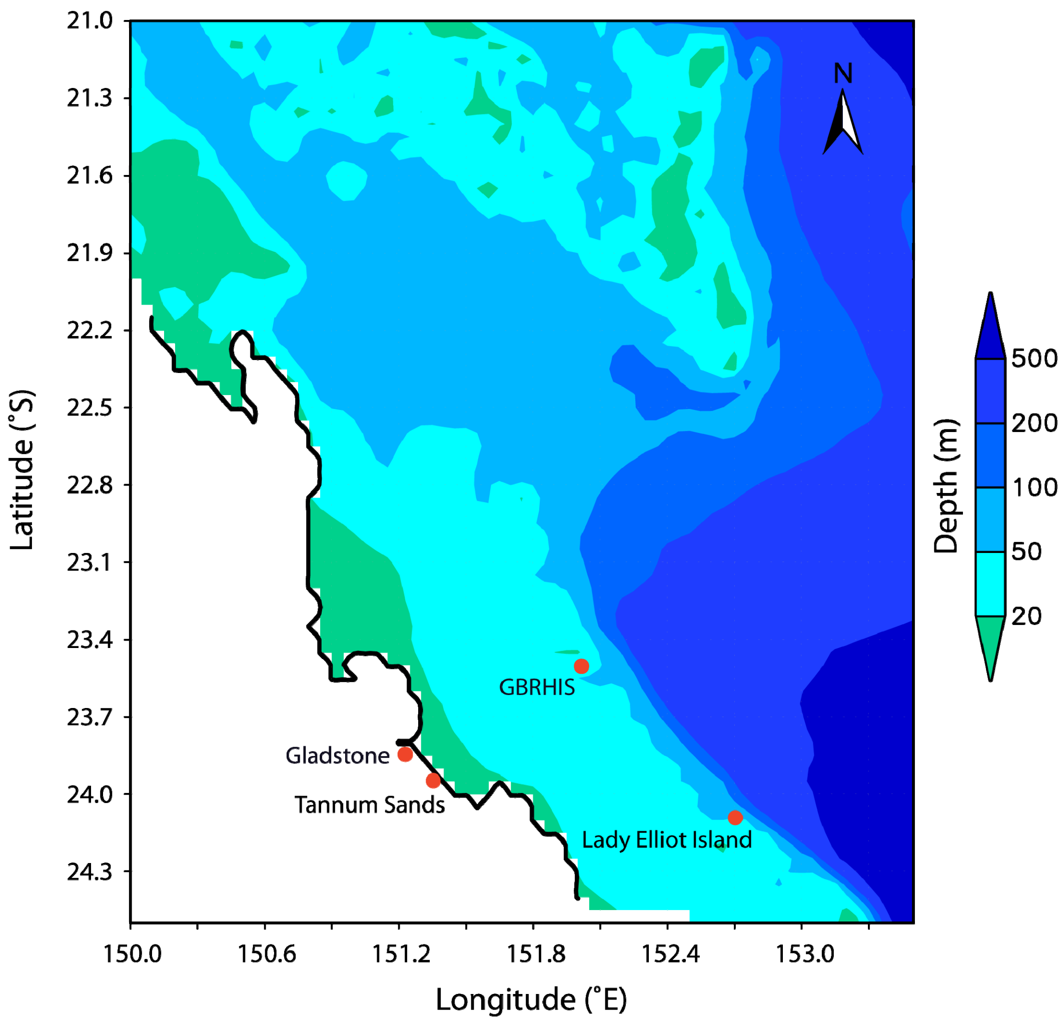

Fig. 1 Bathymetry of the southern Great Barrier Reef region, derived from DBDB2 (Digital Bathymetric Data Base), a 2-minute resolution grid. Also indicated are the locations of the Heron Island South (GBRHIS) ADCP mooring, as well as Lady Elliot Island and Tannum Sands.

Table 1. Grid characteristics of WAVEWATCH III.

nest name	Pacific	Coral	GBR
resolution (°)	1	1/2	1/20
min. latitude (°N)	-70	-35	-24.5
max. latitude (°N)	60	-8	-21
min. longitude (°E)	130	142	150
max. longitude (°E)	260	165	153.5
wind data	GASP	GASP	MesoLAPS
wind resolution (°)	1/2	1/2	1/8

HF ocean radars

Direct measurement of wave parameters can be obtained from the HF radars, stationed at Tannum Sands (23.94°S; 151.37°E) and Lady Elliot Island (24.11°S; 152.72°E) (Fig. 1). Maps of significant wave height are supplied on a 3 km grid independently from each station for ranges up to 75 km from the stations. The WERA radar system has been operational since November 2007 and is mainly used to map surface currents over the continental shelf in this area.

When wave data from the two HF radar stations are combined - and with some spatial and temporal averaging - the radars can generate directional wave spectra (Wyatt 2000, Wyatt 1990). The optimum temporal averaging period is one hour, while the optimal spatial averaging is approximately 10 km. Wind direction can be inferred from HF radar data over the full coverage of grid points by adopting a general form for the directional spread. Phased array HF radars have the capacity to map variations in the significant wave height field (Heron and Heron 1998). Causes for modifications in the significant wave height field include wave setup when the waves are propagating in the direction opposing strong currents, and refraction (Haus et al. 2006).

ADCP mooring

The Great Barrier Reef Ocean Observing System (GBROOS) Heron Island South (GBRHIS) ADCP mooring (23.51°S; 151.96°E) is situated to the south of Heron Island and west of One Tree Island (Fig. 1). GBRHIS is equipped with a Nortek Acoustic Doppler Wave and Current Profiler (AWAC). The AWAC includes a directional wave gauge, which employs Acoustic Surface Tracking (AST) to monitor surface waves. At GBRHIS, the AWAC is located 10 m below the surface on top of a mooring, at a total depth of 46 m. Output is generated every two hours. A typical directional wave spectrum from GBRHIS is shown in Fig. 2.

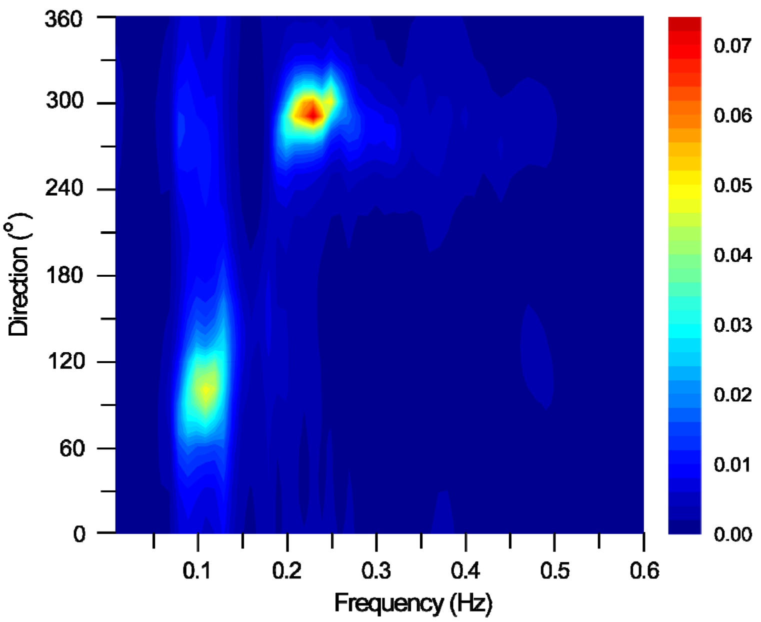

Fig. 2 Directional wave spectrum (m^2/s), from GBRHIS, derived with acoustic surface tracking by an AWAC. The waves, measured at 07:56, 22 February 2008 (UTC), display two distinct peaks. The local wind waves are predominantly from a west-northwesterly direction, whereas the lower frequency swell derives from the east-southeast.

Acknowledgments

Data were sourced as part of the Integrated Marine Observing System (IMOS) Ocean Data Portal www.imos.org.au. IMOS is supported by the Australian Government through the National Collaborative Research Infrastructure Strategy and the Super Science Initiative. The research project is funded through an Industry Linkage Grant from the Australian Research council in collaboration with Seaview Sensing Ltd (UK) and Helzel Messtechnik GmbH (Germany).

References

Haus, B.K., Ramos, R.J., Graber, H.C., Shay L.K. and Hallock Z.R. 2006. Remote observation of the spatial variability of surface waves interacting with an estuarine outflow. *IEEE J. Ocean. Eng.*, **31**/**4** 835-49

Heron, S.F. and Heron, M.L. 1998. A comparison of algorithms for extracting significant wave height from HF radar ocean backscatter spectra. *J. Atmos. Oceanic Technol.*, **15**, 1157-63.

Seaman, R., Bourke, W., Steinle, P., Hart, T., Embery, G., Naughton M. and Rikus L. 1995. Evolution of the Bureau of Meteorology's global assimilation and prediction system. Part I: Analysis and initialisation. *Aust. Met. Mag.*, **44**, 1-18.

Tolman, H. L. 2009. User manual and system documentation of WAVEWATCH III™ version 3.14: NOAA / NWS / NCEP / MMAB *Technical Note 276*.

Weinzierl, B., Smith, R.K., Reeder, M.J. and Jackson, G.E. 2007. MesoLAPS Predictions of Low-Level Convergence Lines over Northeastern Australia. *Wea. Forecasting*, **22**, 910-27.

Wyatt, L.R. 1990. A relaxation method for integral inversion applied to HF radar measurement of the ocean wave directional spectrum. *Int. J. Remote Sens.*, **11**/**8,** 1481 - 94.

Wyatt, L.R. 2000. Limits to the inversion of HF radar backscatter for ocean wave measurement. *J. Atmos. Oceanic Technol.*, **17,** 1651-66.

Detection and analysis of breaking wind-waves with passive acoustics

Richard Manasseh[1,2], Alexander V. Babanin[3] and Andrew Ooi[1]

*1: Department of Mechanical Engineering,
University of Melbourne, VIC 3010, Australia
2: Fluid Dynamics Group, CSIRO, PO Box 56, Highett, VIC 3190, Australia
3: Faculty of Engineering & Industrial Sciences,
Swinburne University of Technology Hawthorn, VIC 3122, Australia*

Introduction

The sounds emitted by breaking wind-waves have been measured and analysed for more than half a century (e.g. Knudsen et al. 1948, Terrill and Melville 2000). Breakers create bubbles ranging from centimetres to fractions of a millimeter and these bubbles in turn create sounds. Ocean-surface bubbles affect submarine sound propagation (Knudsen et al. 1948), remove CO_2 from the atmosphere (Sabine et al. 2004) and dissipate oceanic energy (Babanin et al. 2001), which is of fundamental importance to the physics of the upper ocean. This paper briefly reviews some issues and a method of analysing breakers using the sound they emit.

Passive bubble-acoustic physics

Frequencies of bubble sounds

A bubble is a gas, such as the air entrained by a breaking wave, surrounded by a liquid, such as seawater. Gases are much more compressible than liquids, while liquids are much denser. To an excellent first approximation first introduced by Rayleigh (1917), the bubble's dynamics can be modelled by the incompressible, spherically-symmetric momentum equation for the liquid, with the ideal gas law for the compressible gas providing an inner boundary condition. The linear solution of the resulting ordinary differential equation gives the natural frequency of the bubble's oscillation as

$$f_0 = \frac{1}{2\pi}\sqrt{\frac{3\kappa P_0}{\rho}}\,\frac{1}{R_0} \tag{1}$$

in which f_0 is the frequency in Hz, κ is the polytropic index for the gas, ρ is the density of the liquid, P_0 is the ambient pressure and R_0 is the spherically-equivalent radius of the bubble (Minnaert 1933). Since there is a relation between bubble size and natural frequency, it is possible in principle to measure the sounds (or spectrum of sounds) emitted by a complex bubbly flow and deduce the sizes of bubble present.

Issues in passive bubble-acoustic analysis

However, a naïve application of (1) runs into a number of issues, detailed elsewhere (Manasseh et al. 2001, Manasseh et al. 2008). Two of the most significant issues are: (i) groups of bubbles interact acoustically, generating coupled modes of oscillation that alter the frequency predicted by (1); and (ii) the relation between the fluid dynamics of the event generating the bubble and the amplitude of the sound produced remains complex and difficult to predict (Manasseh et al. 2008) recent progress in numerical calculations may lead to future amplitude predictions. Experimental work (Manasseh et al. 2001, Chanson and Manasseh 2003), explained by descriptive theory (Manasseh and Ooi 2009) has shown that (i) may be mitigated by capturing very brief pulses of sound and measuring their periods in the time domain. However, (ii) introduces a further uncertainty: an amplitude threshold must be chosen, above which pulses of sound are selected for analysis.

Detection of breaking wind-waves

The determination of when a wind-wave breaks by an objective, automated acoustic method would be a useful advance. However, this relied on an arbitrary parameter - the sound-amplitude threshold. Thus, an objective method of determining the optimal threshold was sought by Manasseh et al. (2006). This problem, logically identical to statistically optimizing a medical diagnostic test, requires a classification-accuracy analysis) in which the threshold is empirically optimised by a laborious ‘training’ comparison with an ‘absolute truth’ (Landis amd Koch 1977). The visual observation of a breaker was assumed to be absolute truth; wind-wave data obtained earlier (Babanin et al. 2001) had co-registered video and underwater-acoustic recordings. Values of the threshold were found that gave an optimum ‘diagnosis’ of breaking, with diagnostic metrics (Landis and Koch 1977) indicating ‘moderate’ to ‘substantially’ accurate diagnosis (Manasseh et al. 2006).

Analysis of breaking wind-waves

Once optimum thresholds were established, automated pulsewise analysis of data collected earlier (Babanin et al. 2001) showed an increase in average bubble size with wind speed (Fig. 1a). An increase in bubble production rate with wind speed can be seen in Fig. 1b. There is a clear ordering of the wind speeds with respect to both the bubble rate and the mean radius, with quite high correlation. Thus, higher wind speeds generate breaking events more frequently, and the bubbles at higher wind speeds are larger. Moreover, laboratory experiments (Manasseh and Babanin 2006) showed acoustically-estimated bubble size to be well correlated with breaking severity (energy lost during breaking). Similar trends of the mean bubble size with an independent variable related to the energetics of the flow have been found elsewhere (Manasseh et al. 2001, Chanson and Manasseh 2003)

Fig. 2 shows the wave power spectrum created from wave-height data (Babanin et al. 2001), and the breaking probability, bT, as a function of wave frequency for a 19.8 m s-1 wind speed. Here, bT is given by

$$bT(f)=n(f)/Nc(f), \qquad (2)$$

where Nc(f) is the number of waves in a small bandwidth about the wave frequency f (counted by a zero-crossing analysis of the wave-height data in (Babanin et al. 2001)) and n(f) is the number of breakers determined acoustically in the bandwidth about f . Details are given in (Manasseh and Babanin 2006). Although the bT curve only covers a fraction of the frequency spectrum, it is clear that there is a statistically-significant downward trend in breaking probability with wave frequency above the spectral peak.

Conclusions

Bubbles naturally emit sound on formation, and many bubble-formation events occur during the breaking of a wave. The acoustic frequencies of individual pulses of sound can be theoretically related to the bubble size, and empirically related to the severity of wave breaking. If individual pulses of sound are analysed in the time domain, two classes of data emerge: the frequency of each pulse; and the rate at which pulses are detected. These data are highly dependent of the threshold at which pulses of sound are selected for analysis. The amplitude of individual pulses depends on the energetics of each bubble-formation event, which remains difficult to predict, introducing uncertainty. It is possible to rigorously optimize the threshold by comparison with images that unambiguously identify breakers, with the result that breakers can be detected automatically. Once this is done, results show that both bubble size and bubble count rate rise with wind speed, and that breaking probability falls at wave frequencies above the spectral peak.

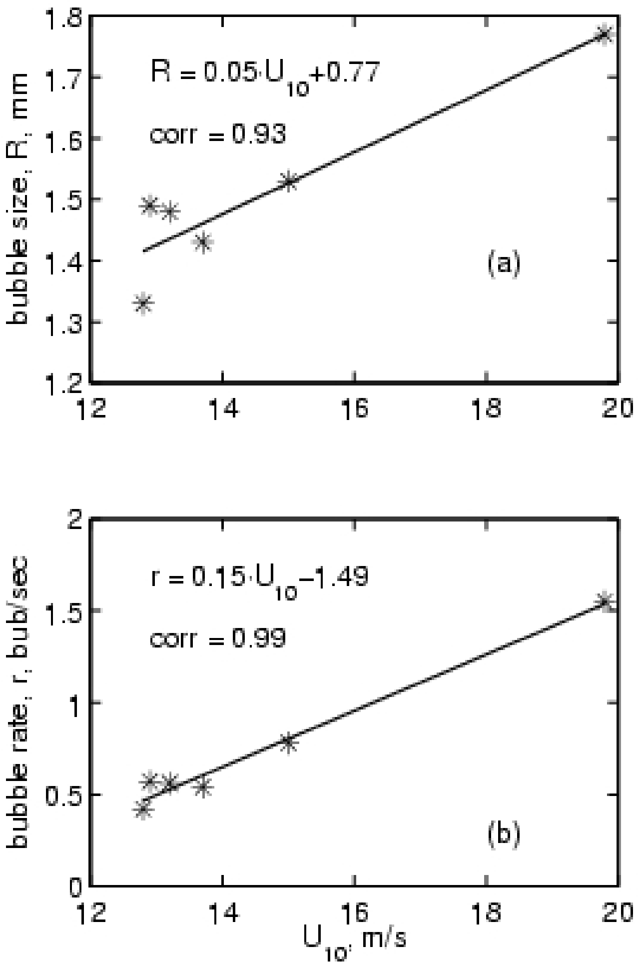

Fig. 1 Trends with wind speed at the optimal trigger level determined by the classification-accuracy analysis. a) mean bubble radius; b) bubble-detection count rate. From Manasseh et al. (2006).

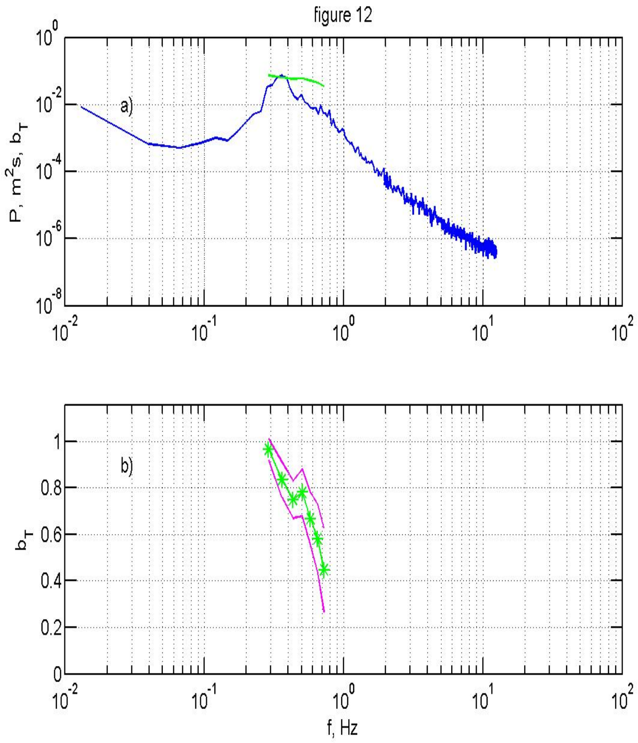

Fig. 2 Wave power spectrum and breaking probability vs. wave frequency f: (a) wave power spectrum P(f) and (b) wave breaking probability bT(f); pink lines show 95% confidence intervals. From Manasseh et al. (2006).

References

Babanin, A.V., Young, I.R. and Banner, M.L. 2001. *J. Geophys. Res.* **106** (C6), 11659–11676.

Chanson, H. and Manasseh, R. 2003. *J. Fluids Eng.* **125** (5), 910–921.

Knudsen, V., Alford, R.S. and Emling, J.W. 1948. *J. Marine Res*. **7**, 410–429.

Landis, J. R. and Koch G. G. 1977. The measurements of observer agreement for categorical data. *Biometrics* **33**, 159– 174.

Manasseh, R., Babanin, A., Forbes, C., Rickards, K., Bobevski, I. and Ooi, A. 2006. *J. Atmos. Ocean Technol.* **23**, (4), 599–618.

Manasseh, R., LaFontaine, R.F., Davy, J., Shepherd I.C. and Zhu Y. 2001. *Exp. Fluids* **30** (6), 672–682.

Manasseh, R. and Ooi, A. 2009. *J. Bub. Sci. Tech.* **1,** 58-74.

Manasseh, R., Riboux, G. and Risso, F. 2008. *Int. J. Multiphase Flows* **34**, 938–949.

Minnaert M. 1933. *Phil. Mag*. **16**, 235–248.

Rayleigh (Lord). 1917. *Phil. Mag*. **34**, 94–98.

Sabine, C.L., Feely, R.A., Gruber, N., Key, R.M., Lee, K., Bullister, J.L., Wanninkhof, R., Wong, C.S., Wallace, D.W.R., Tilbrook, B., Millero, F.J., Peng, T.-H., Kozyr, A., Ono, T. and Rios, A.F. 2004. *Science* **305**, 367–371.

Terrill E.J. and Melville, K.W. 2000. *J. Atmos. Oceanic Technol.* **17**, 220–239.

The Centre for Australian Weather and Climate Research is a partnership between CSIRO and the Bureau of Meteorology.